REVIEWS OF
MODERN PHYSICS

VOLUME 36, NUMBER 3 JULY 1964

Dynamical Diffraction of X Rays by Perfect Crystals

BORIS W. BATTERMAN

Bell Telephone Laboratories, Incorporated, Murray Hill, New Jersey

HENDERSON COLE

International Business Machines Corporation, Yorktown Heights, New York

CONTENTS

INTRODUCTION

There are two general theories which may be used to account for the intensities observed in x-ray diffraction studies. The better known one, the kinematical theory, treats the scattering from each volume element in the sample as being independent of that of other volume elements, except for incoherent power losses in reaching and leaving that particular volume element. The other theory, normally called the dynamical theory, takes into account all wave interactions within the crystalline particle, and must generally be used whenever diffraction from large perfect crystals is being considered. There has been a growing number of studies of diffraction from large perfect crystals within the last few years, due, in part, to the availability of such crystals as a by-product of semiconductor materials research. As a result of these studies, it was thought worthwhile to review the theory and bring out the explanations it offers of the observed effects.

The dynamical diffraction theory considers the total wave field inside a crystal while diffraction is taking

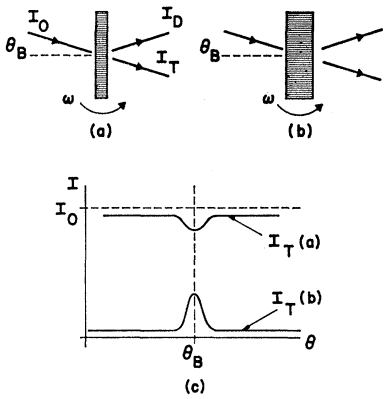

FIG. 1. Anomalous transmission. (a) Thin crystal Laue diffraction. (b) Thick crystal Laue diffraction. (c) Transmitted intensity for thin crystal case is shown in upper curve and thick crystal case in lower curve. The peaking of the lower curve at $\theta=\theta_B$ is the anomalous transmission.

place as a single entity. Although the wave field may be thought of, naïvely, in the beginning, as consisting of incident and diffracted beams, these beams are coherently coupled and the energy is swapped back and forth between them so that the total field must be considered as a unit. The conditions under which this coupling can be ignored and the kinematical formulas used can be derived quantitatively; but intuitively, if the size of the diffracting region and the weakness of the reflection are such that space does not permit multiple interplay of the beams, then the results predicted by the dynamical diffraction formulas are essentially the same as those predicted by the kinematical ones. Thus, for example, in general, for fine powders either theoretical approach leads to the same intensity expression. Even for small crystallites, however, the phenomenon of primary extinction, a dynamical diffraction effect, is often encountered when measuring a strong reflection, i.e., the integrated intensity is not as great as expected on the basis of the kinematical expression. Correcting for, or attempting to avoid this primary extinction, is probably the way most diffractionists become familiar with dynamical theory effects. A better example, however, for illustrative purposes, an effect which very clearly displays the properties of the total wave field, is the *anomalous transmission* of x rays through reasonably perfect single-crystal slabs when they are set for Laue diffraction. This effect was first observed by Borrmann in 1943, and is now generally called the Borrmann effect. (Campbell rediscovered the effect in 1950 and it is sometimes called the Borrmann–Campbell effect.) We use the explanation of the Borrmann effect to present the concepts that have emerged in the development of the dynamical theory of diffraction.

1.0 THE BORRMANN EFFECT

The basic features of the Borrmann effect are schematically represented in Figs. 1 and 2. In Fig. 1, a single crystal cut in the form of a parallel-sided slab with the planes to be used in the diffraction perpendicular to the slab faces is rotated through its diffracting position about an axis perpendicular to the plane of the figure. Although a monochromatic beam is not needed to observe the effect, it aids in the discussion to assume a monochromatic ray. We fix our attention on the transmitted beam only at this stage. When the crystal is well off the diffraction setting, i.e., when $\theta\neq\theta_B$ in Bragg's law $\lambda=2d\sin\theta_B$, the transmitted intensity is given by the usual expression for photoelectric absorption: $I_0\exp(-\mu_0 t)$. In case (a), $\mu_0 t$ is assumed $\ll 1$; in case (b), $\mu_0 t>10$. In case (a) as the crystal is rotated through $\theta=\theta_B$, there is a dip in I_T [upper curve in 1(c)] which would be expected from kinematical considerations, on the basis that additional energy is now removed from the transmitted beam by diffraction. For case (b), however, [the lower curve in 1(c)], if the crystal is perfect enough to be a single domain, a *peak* is observed in I_T at $\theta=\theta_B$.

The experiment shown in Fig. 2 demonstrates that this peak is clearly due to a diffraction effect. In this figure the thick crystal is set at $\theta=\theta_B$ and a film is placed on the far side to receive the beams emerging from the sample. When developed, the film usually shows three spots, spot (1) being the diffracted beam, spot (2) being a beam of about the same darkening as spot (1) and separated from it by a distance corresponding to the correct $2\theta_B$; and a weak spot, (3), which is actually in line with the incident beam and may be shown to consist of radiation which had not been involved in the diffraction (for example, possibly a hard component in the beam). The separation between the centers of spots (2) and (3) is proportional to the thickness of the sample. The peak shown in Fig. 1(c) is associated with spot (2). From the geometry shown in Fig. 2 it is clear that the radiation forming spots (1) and (2) emerged from the crystal at a point opposite to the point where the incident ray struck the crystal. We can thus conclude that the radiation apparently traveled along the atomic planes and that the *anomalous transmission* is really a diffraction phenomenon. We thus refer to this beam as the *forward diffracted* beam rather than the transmitted beam.

Even though the geometry shown in Fig. 2 may be straightforward, the startling thing about the Borrmann

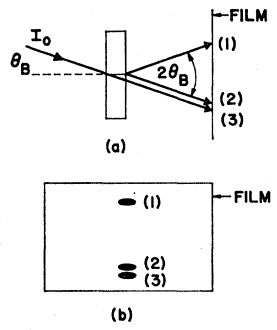

FIG. 2. Geometry of the beams when anomalous transmission is occurring. (a) Ray diagram required to explain spots on the film. (b) The energy in the diffracted beam (1) and forward diffracted beam (2) apparently flows along the atomic planes in the crystal.

effect is that *any energy at all* gets through a crystal for which the absorption factor is something like exp (−10). One would suppose that some mechanism must be operating which keeps the energy away from the absorbing atoms. The dynamical theory predicts that a standing-wave pattern should exist inside the crystal, shown schematically by the dark sine curve in Fig. 3 with nodal planes parallel to the atomic planes. Much the same thing happens when a light beam bounces back and forth between two parallel mirrors: interference fringes are set up in the region between the mirrors parallel to the mirrors, while the average energy flow is along the mirrors. In the x-ray case, if the crystal structure is simple enough, the nodes of the standing-wave pattern can coincide with the atomic sheets and so very little photoelectric absorption can take place. Thus, the peak in Fig. 1(c) results from an extinguishing of the normal photoelectric absorption; the dip in 1(c) occurs when the crystal is already so "thin" that little absorption was taking place.

A close analogy exists between the standing-wave pattern in the x-ray case and the electronic wavefunction at the edge of a Brillouin zone for free electrons moving in a periodic medium. From band theory, for the electron case, there are two permitted solutions; one which has nodes at the atoms, and one with antinodes at the atoms. The energy of the electron is different in the two cases, the difference essentially being the energy gap at the zone boundary. There are also two solutions in the x-ray case, one with nodal planes, in simple structures, passing through the atom sites, and another solution with antinodes at the atoms. This second field, of course, suffers *enhanced* absorption; this standing-wave pattern is shown dotted in Fig. 3. The existence of two standing-wave patterns for the x-ray case is consistent with the existence of two sets of incident and diffracted beams *inside* the crystal from a single ray incident from the outside. As a matter of fact, as we see, there are four sets of fields when one considers the two states of polarization of the electromagnetic radiation.

Most treatments of diffraction effects in crystals, for radiation whose wavelength is of the order of an angstrom or less, make use of Ewald's geometrical constructions in the reciprocal lattice in order to visualize the predictions based on Bragg's law or von Laue's formulas. The points in the reciprocal lattice each represent a set of planes in the real crystal lattice;

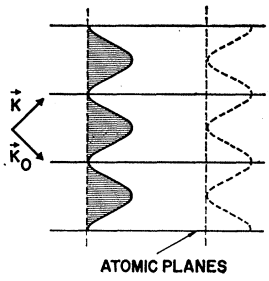

FIG. 3. Standing wave pattern produced by two coherent, traveling plane waves with wave vectors $\mathbf{K}_0$ and $\mathbf{K}$. Nodes of dotted curve coincide with antinodes of solid curve. When such a pattern exists relative to the atomic planes, the normal photoelectric absorption is radically altered.

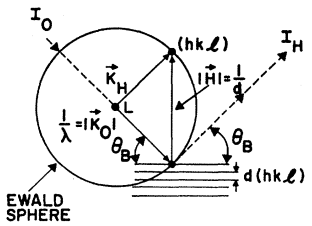

FIG. 4. Ewald sphere and Bragg's law. The incoming wave with wave vector $\mathbf{K}_0$ is diffracted by the atomic planes with interplanar spacing d. The diagram represents the situation in real space and in reciprocal space.

the position of the reciprocal lattice point indicating the orientation and reciprocal of the d spacing of the set of planes. Diffraction is generally expected to occur if a sphere of radius $1/\lambda$ (the Ewald sphere) passing through the origin of the reciprocal lattice and having its center back along the incident beam direction also passes through the particular reciprocal lattice point; at least, the geometrical conditions of Bragg's law, $\lambda=2d\sin\theta$ are satisfied: i.e., $1/d=1/\lambda(2\sin\theta)$ and $\theta_{\text{in}}=\theta_{\text{out}}$ (see Fig. 4). We also express most of the diffraction concepts in terms of the geometry of the reciprocal space.

Turning now to the dynamical diffraction theory, the crucial change is in the concept of the Ewald sphere. In reciprocal space, there is no longer a single Ewald sphere for a single monochromatic incident ray. Instead, the problem to be solved is to determine the loci of centers of permitted Ewald spheres, the so-called *dispersion surface.* Wave vectors drawn from points on this surface to reciprocal lattice points represent waves that are permitted solutions of Maxwell's equations in a periodic medium. The results of the formal theory present a wealth of detailed predictions with respect to these propagation vectors, energy flows, and absorption. The rest of the paper deals with this theory. The only general factor not explicitly considered in the theory is the effect of the thermal vibrations.

2.0 GENERAL THEORY

The original theoretical work done by Darwin,[1] Ewald,[2] and von Laue[3] has been ably summarized and extended in treatments by Zachariasen[4] and James.[5] Hirsch[6] has published two very necessary papers recasting the theory to bring out explanations of newer experimental results. Kato[7] has further extended the theory in both the x-ray and electron diffraction cases. Summaries of theory and experimental detail have

[1] C. G. Darwin, Phil. Mag. **27**, 315 (1914); **27**, 675 (1914).
[2] P. P. Ewald, Ann. Physik **49**, 1 (1916); **49**, 117 (1916); **54**, 519 (1917); Acta Cryst. **11**, 888 (1958).
[3] M. v. Laue, Ergeb. Exakt. Naturw. **10**, 133 (1931). A complete treatment of Laue's contributions is given in his book *Röntgenstrahl-Interferenzen* (Akademische Verlag, Frankfurt, 1960).
[4] W. H. Zachariasen, *Theory of X-Ray Diffraction in Crystals* (John Wiley & Sons, Inc., New York, 1945).
[5] R. W. James, *The Optical Principles of the Diffraction of X-Rays* (G. Bell and Sons, London, 1950), Chaps. II and VIII.
[6] P. B. Hirsch, Acta Cryst. **5**, 176 (1952); and P. B. Hirsch and G. N. Ramachandran, Acta Cryst. **3**, 187 (1950).
[7] N. Kato, J. Phys. Soc. Japan **7**, 397 (1952).

been prepared by Borrmann[8] (in German), Kohra[9] (in Japanese) and Authier[10] (in French). A very elegant approach to the basic theory is contained in an article by Slater[11] entitled, "Waves in Crystals."

The fundamental problem as pointed out by von Laue is to solve Maxwell's equations in a medium with a periodic complex dielectric constant. The formal steps employed follow in approach that used in discussing, for example, thermal diffuse x-ray scattering or any other characteristic value problem. Most of the mathematical steps can be found in Appendix A. We set down Maxwell's equations, use a periodic complex dielectric constant to describe the medium, assume wave solutions consistent with Bragg's law, obtain a set of homogeneous linear equations for the ratio of the field amplitudes, and write down a determinant whose value must be zero for nontrivial solutions of the equation to exist, which imposes certain conditions on the wave vectors. The loci of tips of permitted wave vectors in reciprocal space defines the *dispersion surface.* Once the properties of this surface in reciprocal space are understood, using constructions due to Ewald, the results of the dynamical theory of diffraction can be easily generated. The main body of the paper is concerned with understanding these properties.

In the material to follow, we mostly are concerned with a problem in classical electromagnetic wave theory. Fundamentally, the crystal is represented by a periodic, anisotropic, complex dielectric constant which depends explicitly on time. Being periodic in three dimensions, the dielectric constant can be represented by a Fourier series over the reciprocal lattice in exactly the same way that the periodic charge density is so represented in crystallographic work. In fact, in Sec. 2.1 to follow, we associate the Fourier coefficients of the dielectric constant with those of the charge density. A complex dielectric constant is used to handle the question of absorption, and an anisotropic one is required in the sense that waves propagating in different directions must have different indices of refraction. This difference becomes the important parameter in the whole problem.

2.1 THE PERIODIC, COMPLEX, DIELECTRIC CONSTANT

We recall that the electron density at any point in the crystal $\rho(\mathbf{r})$, can be expressed as a Fourier sum (for a sufficiently large crystal) over the reciprocal lattice. That is:

$$\rho(\mathbf{r})=(1/V)\sum_H F_H \exp(-2\pi i\mathbf{H}\cdot\mathbf{r}) \qquad (1)$$

where V is the volume of the unit cell and $\mathbf{H}$ is a reciprocal lattice vector. If $\mathbf{b}_1$, $\mathbf{b}_2$ and $\mathbf{b}_3$ are the reciprocal lattice vectors defining the unit cell in reciprocal space, then $\mathbf{H}=h\mathbf{b}_1+k\mathbf{b}_2+l\mathbf{b}_3$ where h, k, l are the Miller indices of the reflection described by the reciprocal lattice point. The sum over H signifies all possible values of h, k, l and F_H may be identified as the structure factor for the h, k, l reflection. Conversely:

$$F_H=\int_V \rho(\mathbf{r}) \exp(2\pi i\mathbf{H}\cdot\mathbf{r})\, dv. \qquad (2)$$

Within the assumption that the atoms behave as rigid spheres with respect to their charge densities and are not vibrating thermally, F_H can be written as

$$F_H=\sum_n f_n \exp(+2\pi i\mathbf{H}\cdot\mathbf{r}_n), \qquad (3)$$

where the sum over n is over the atoms in the unit cell. The atomic scattering factor of the nth atom is represented by f_n. In the kinematical treatment one includes thermal vibrations by replacing f_n by $f_n \exp(-M_n)$ where the exponential is the Debye–Waller factor. In a later section we discuss the corresponding situation in the dynamical treatment.

The connection between the Fourier Series which describes the electron density, Eq. (1), and a representation of the periodic dielectric constant can be made by performing essentially a dimensional analysis using the concept of electronic polarizability.

The electric displacement vector $\mathfrak{D}$ in the rationalized mks system can be written in terms of the electric field $\mathfrak{E}$, and polarization $\mathbf{P}$, as

$$\mathfrak{D}=\kappa\epsilon_0\mathfrak{E}=\epsilon_0\mathfrak{E}+\mathbf{P},$$

where κ is the dielectric constant and ϵ_0 is the permittivity of empty space; or more specifically

$$\kappa=1+\mathbf{P}/\epsilon_0\mathfrak{E}. \qquad (4)$$

If we consider a sinusoidal field of amplitude E_0, acting on a collection of electrons held by restoring forces such that they have a natural frequency of oscillation ω_0, then the amplitude of the induced electron motion is given by

$$x=(e/m)E_0/(\omega_0^2-\omega^2). \qquad (5)$$

If ω is much greater than ω_0, the polarization amplitude is $P=\rho ex$ and κ is now:

$$\kappa(r)=1-[(e^2/mc^2)\lambda^2/4\pi^2\epsilon_0]\rho(r). \qquad (6)$$

The quantity $(e^2/4\pi\epsilon_0 mc^2)$ is the classical electron radius r_e, and is equal to 2.818×10^{-13} cm. Thus, in any system of units we can write

$$\kappa(r)=1-r_e(\lambda^2/\pi)\rho(r).$$

[8] G. Borrmann, *Trends in Atomic Physics*, edited by O. R. Frisch, *et al.* (Interscience Publishers, Inc., New York, 1959).
[9] K. Kohra, *X-Ray Crystallography* (Maruzen Company Ltd. Japan, 1961), Vol. II 9, p. 849.
[10] A. Authier, Bull. Soc. Franc. Mineral Crist. 84, 51 (1961).
[11] J. C. Slater, Rev. Mod. Phys. **30**, 197 (1958).

If we define the symbol Γ:

$$\Gamma=\frac{r_e\lambda^2}{\pi V}=\left(\frac{e^2}{4\pi\epsilon_0 mc^2}\right)\frac{\lambda^2}{\pi V}$$

from Eq. (1) for $\rho(r)$ we have

$$\kappa(r)=1-\Gamma\sum_H F_H \exp(-2\pi i\mathbf{H}\cdot\mathbf{r}). \tag{7}$$

Naturally, if the x-ray frequency is near a resonant frequency for some of the electrons and also if absorption is present, the polarization is much more complicated than that given by the single expression in Eq. (5). As a matter of fact, the dielectric constant is generally taken to be a complex quantity with a complicated frequency dependence under such conditions. In x-ray work, this physical complexity is usually handled formally by considering the atomic scattering factors as complex and wavelength dependent. Thus, we now take for F_H

$$F_H=\sum_n(f+\Delta f'+i\Delta f'')_n \exp(+2\pi i\mathbf{H}\cdot\mathbf{r}_n). \tag{8}$$

The corrections to the atomic scattering factor f due to resonance and absorption, $\Delta f'$ and $\Delta f''$, are called the Hönl corrections. *All of the detailed physics of the scattering and absorption is thus included in these terms.* They have been investigated both theoretically and experimentally (see, for example, the chapters in James or von Laue), but even so, certain points regarding their dependence on scattering angle and temperature are still being worked out in detail.

F_H thus has a complex part, due to the physical scattering mechanisms. For convenience, in later sections we separate the contributions of the real parts of the atomic scattering factors $(f+\Delta f')$ and the imaginary parts $(\Delta f'')$ to F_H and write F_H as

$$F_H=F_H'+iF_H''. \tag{9}$$

Unfortunately, F_H' and F_H'' may still be complex quantities due to the spacial arrangement of the atoms or the choice of origin for the unit cell.

If we consider the $hkl=000$ term in the Fourier series for κ, Eq. (7), we can write in detail that

$$\kappa_0=1-\Gamma[F_0'+iF_0'']$$

where we see from Eq. (8) that F_0' and F_0'' are real quantities. That is,

$$\kappa_0=1-\Gamma\sum_n(f_0+\Delta f_0')_n-i\Gamma\sum_n(\Delta f_0'')_n. \tag{10}$$

Since these terms are of zeroth order, they are expressions for the average value of the dielectric constant. By using the methods in the sections to follow, we can show that for a beam traversing a slab of material without diffracting, the linear absorption coefficient is related to the imaginary part of the average dielectric constant. That is

$$\mu_0=(2\pi/\lambda)\Gamma F_0''. \tag{11}$$

From measured linear absorption coefficients, then, we can get a measure of $\Gamma F_0''$. For CuKα radiation passing through germanium, we have

$$\mu_0=350\ \text{cm}^{-1}, \qquad \lambda=1.54\times10^{-8}\ \text{cm},$$

and thus

$$\Gamma F_0''=0.86\times10^{-6}\ (\text{a pure number}). \tag{12}$$

From these considerations, we also see that κ differs only slightly from unity for x rays, a fact already well known from index of refraction measurements. The fact that κ differs from unity by, at most, one part in 10^4, and usually differs by the order of one part in 10^6, constitutes the main assumption in the development of the theory in the next sections.

2.2 WAVES WHICH SATISFY BRAGG'S LAW AND MAXWELL'S EQUATIONS

If we assume that the conductivity σ is zero at x-ray frequencies so that there is no resistive heat loss and that magnetically the crystal has the same behavior as empty space so that $\mu=\mu_0$, then Maxwell's equations can be used in the form[12]

$$\begin{aligned}&\text{(a)}\quad \nabla\times\mathcal{E}=-\frac{\partial\mathfrak{B}}{\partial t}=-\mu_0\frac{\partial\mathfrak{H}}{\partial t}\\ &\text{(b)}\quad \nabla\times\mathfrak{H}=\frac{\partial\mathfrak{D}}{\partial t}=\epsilon_0\frac{\partial(\kappa\mathcal{E})}{\partial t}.\end{aligned} \tag{13}$$

The magnetic vectors $\mathfrak{B}$ and $\mathfrak{H}$ are thus colinear and freely interchangeable. The dielectric constant κ is given by Eq. (7). Although κ is time dependent because of the lattice vibrations, we take its time derivative terms in (13b) to be negligible.

We now assume that the fields $\mathcal{E}$, $\mathfrak{D}$, and $\mathfrak{H}$ can be expressed as sums of plane waves. If now the wave vector of a wave is such that a diffracted wave is generated, that is, if the wave with wave vector $\mathbf{K}_0(|K_0|=1/\lambda)$ is scattered by the Fourier component of charge density with periodicity $\mathbf{H}$ ($|\mathbf{H}|=$ reciprocal d spacing) then the wave vector of the scattered wave is

$$\mathbf{K}_H=\mathbf{K}_0+\mathbf{H} \tag{14}$$

(see Fig. 4). This relationship between the two wave vectors may be taken as a statement of Bragg's law or as the conservation of momentum for the scattering of waves by waves. Although any wave may propagate in

[12] J. C. Slater and N. H. Frank, *Electromagnetism* (McGraw-Hill Book Company, Inc., New York, 1947), Chap. VII.

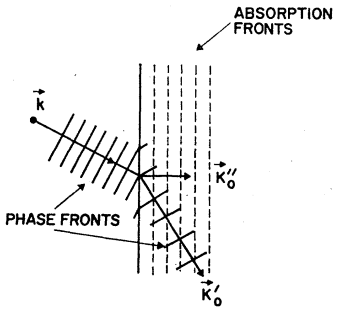

FIG. 5. The imaginary part of the wave vector $\mathbf{K}_0$ which represents absorption, is normal to the crystal surface. The real part of the wave vector $\mathbf{K}_0'$, describes the phase propagation.

the medium, it is only waves connected by (14) which are strongly coupled and of interest in diffraction.

We assume that the crystal is perfect in the sense that the reciprocal lattice vector $\mathbf{H}$, is independent of position in the crystal.[13]

In order to handle absorption with some ease, we take the wave vectors as complex, i.e.,

$$\mathbf{K}=\mathbf{K}'-i\mathbf{K}'', \tag{15}$$

where $\mathbf{K}'$ and $\mathbf{K}''$ are real. Note the negative sign.

For a wave described in complex exponential form, an imaginary term in $\mathbf{K}$ results in a real negative exponential damping term in the wave description, thus leading to absorption. The vector components of $\mathbf{K}$, $\mathbf{K}'$ and $\mathbf{K}''$ need not be collinear since planes of constant absorption which are perpendicular to $\mathbf{K}''$ need not be the same as planes of constant phase which are perpendicular to $\mathbf{K}'$. This is illustrated in Fig. 5. In all cases of interest in x-ray diffraction, as we saw in the last section, $|K''|/|K'|\approx 10^{-5}$ so that the direction of $\mathbf{K}$ is substantially that of its real part. We carry $\mathbf{K}$ along as complex, for absorption purposes, but when we refer to its directional properties we consider only its real part. This involves dropping a second-order term in taking cross products to get Poynting's vector for energy flow later on.

The substitution of plane-wave expressions into Maxwell's equations (13) with use of relations (7) and (14), are carried out in Appendix A. The result is Eq. (A12), which gives the fundamental set of equations describing the fields inside the crystal. Our primary interest is in the wave vectors which describe these permitted waves. However, from this point on, *we restrict our attention to the case of only one active reflection*, that is, where only one reciprocal lattice point is near enough to the Ewald sphere to give any appreciable diffraction. With this restriction, Eq. (A12) reduces to a pair of equations (A13) for the field amplitudes of the two waves; that is, for E_0 and E_H for each polarization state, which we reproduce here as Eq. (16).

$$[k^2(1-\Gamma F_0)-(\mathbf{K}_0\cdot\mathbf{K}_0)]E_0-k^2P\Gamma F_{\bar{H}}E_H=0,$$
$$-k^2P\Gamma F_H E_0+[k^2(1-\Gamma F_0)-(\mathbf{K}_H\cdot\mathbf{K}_H)]E_H=0. \tag{16}$$

The two polarization states have been handled in a combined form by use of the parameter P, which equals unity or $\cos 2\theta$, respectively, for the σ polarization state ($\mathbf{E}$ perpendicular to the plane of incidence, defined by $\mathbf{K}_0'$ and $\mathbf{K}_H'$) and for the π state ($\mathbf{E}$ in the plane of incidence), respectively. For these pairs of linear homogeneous equations in the field amplitudes to have a nontrivial solution, their determinant must equal zero, which restricts the permitted values of the wave vectors.

We set the determinant of Eq. (16) equal to zero:

$$\begin{vmatrix} k^2(1-\Gamma F_0)-\mathbf{K}_0\cdot\mathbf{K}_0 & -k^2P\Gamma F_{\bar{H}} \\ -k^2P\Gamma F_H & k^2(1-\Gamma F_0)-\mathbf{K}_H\cdot\mathbf{K}_H \end{vmatrix}=0, \tag{17}$$

where k is the vacuum value of the wave vector, $\mathbf{K}_0$ and $\mathbf{K}_H$ are the internal wave vectors, and F_0, F_H, $F_{\bar{H}}$ are the structure factors of the corresponding reflections. This determinant is free of approximations for the σ polarization state ($P=1$) but involves neglect of longitudinal components of $\mathbf{E}$ for the π state. This latter approximation, again, neglects terms of the order of 10^{-5} compared to unity.

The first and fourth terms above represent the difference between the square of the wave vectors $\mathbf{K}_0$ and $\mathbf{K}_H$ inside the crystal and the square of the vacuum value k^2, corrected for the average value of the dielectric constant $(1-\Gamma F_0)$. If there is no difference, there is no unique solution. Thus, the index of refraction for the $\mathbf{K}_0$ and $\mathbf{K}_H$ waves must be different from the average index of refraction. It is this difference which is the important parameter.

We can bring out this difference more clearly by defining new parameters, ξ_0 and ξ_H such that

$$\text{(a)}\quad 2k\xi_0\equiv\mathbf{K}_0\cdot\mathbf{K}_0-k^2(1-\Gamma F_0),$$
$$\text{(b)}\quad 2k\xi_H\equiv\mathbf{K}_H\cdot\mathbf{K}_H-k^2(1-\Gamma F_0). \tag{18}$$

That these parameters are fundamentally the needed difference parameters can be seen by writing the right-hand side, above, as the product of the sum and difference:

$$[(\mathbf{K}_0\cdot\mathbf{K}_0)^{\frac{1}{2}}+k(1-\Gamma F_0)^{\frac{1}{2}}][(\mathbf{K}_0\cdot\mathbf{K}_0)^{\frac{1}{2}}-k(1-\Gamma F_0)^{\frac{1}{2}}],$$

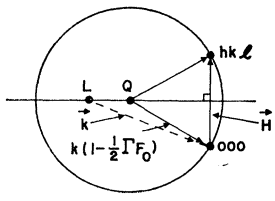

FIG. 6. Ewald sphere in reciprocal space corrected for the average index of refraction. L, the Laue point, would be the center in vacuum, Q is the center in the real crystal. $\mathbf{H}$ is the reciprocal lattice vector of the *hkl* reflection.

[13] P. Penning and D. Polder, Philips Res. Rept. **16**, 419 (1961); have treated the case where H is a slowly varying function of position in order to understand the behavior of elastically strained perfect crystals, also Philips Res. Rept. **18**, 82 (1963).

which reduces to

$$2k[(\mathbf{K}_0\cdot\mathbf{K}_0)^{\frac{1}{2}}-k(1-\tfrac{1}{2}\Gamma F_0)], \qquad (19)$$

where the approximation is extremely well justified, to terms of the order of the square of 10^{-5}. Thus

$$\text{(a)}\quad \xi_0=(\mathbf{K}_0\cdot\mathbf{K}_0)^{\frac{1}{2}}-k(1-\tfrac{1}{2}\Gamma F_0)$$

and similarly,

$$\text{(b)}\quad \xi_H=(\mathbf{K}_H\cdot\mathbf{K}_H)^{\frac{1}{2}}-k(1-\tfrac{1}{2}\Gamma F_0). \qquad (20)$$

ξ_0 represents the difference between the wave vector inside the crystal (still complex, since $\mathbf{K}_0\cdot\mathbf{K}_0$ is complex) and the vacuum value corrected by the average index of refraction. (The index of refraction n is the square root of the dielectric constant, κ).

In terms of ξ_0 and ξ_H, Eq. (17) reduces to the equation

$$\xi_0\xi_H=\tfrac{1}{4}k^2P^2\Gamma^2F_HF_{\bar{H}}. \qquad (21)$$

This is the fundamental equation describing the *dispersion surface.*

In the usual Ewald construction, Fig. 4, the center L of the sphere is determined such that the magnitude of the wave vectors to the origin and the (hkl) reciprocal lattice point is the vacuum value k. If the construction is now performed such that the distance to these points takes into account the average index of refraction of the medium, i.e., $\mathbf{K}$ (inside) $=k(1-\frac{1}{2}\Gamma F_0)$ the center of the Ewald sphere is now at point Q (Fig. 6). We have greatly exaggerated the distance from L to Q with respect to the radii of the spheres. Since we do not expect $\mathbf{K}_0$ or $\mathbf{K}_H$ to differ much from k or $k\kappa_0^{\frac{1}{2}}$, let us assume that the point A, somewhere in the neighborhood of L and Q in Fig. 7(a) is a proper point from which $\mathbf{K}_0$ and $\mathbf{K}_H$ can be drawn, such that Eq. (21) is satisfied.

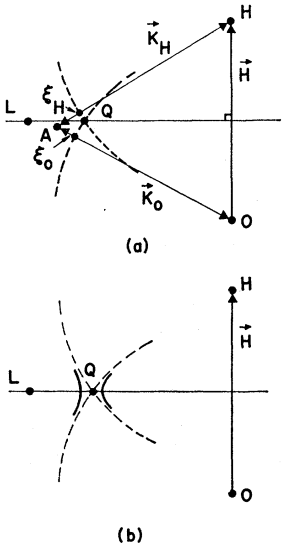

FIG. 7. (a) Geometrical representation of the parameters of the dispersion surface ξ_0 and ξ_H, where the point A, in the region of the center of the Ewald sphere is assumed to be a valid tie point from which wave vectors can be drawn to O and H to represent permitted solutions. (b) General nature of the dispersion surfaces. They are hyperbolic sheets which serve to join the spheres about O and H in the vicinity of Q, the center of the Ewald sphere.

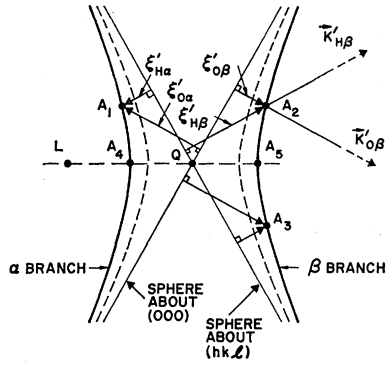

FIG. 8. More detailed view of the dispersion sheets in the region of the Q point. The spheres through Q centered on O and H form asymptotes for the hyperbola. Any point on the hyperbola represents a tie point, or a point from which wave vectors can be drawn to O and H. The dotted curve is for the π polarization state and the solid curve is for the σ state. The α branch is the designation for the branches closest to the Laue point.

Then, according to Eq. (20), ξ_0 represents the distance from the point A to the sphere of radius $k\kappa_0^{\frac{1}{2}}$ and ξ_H is the corresponding distance from A toward H. If the spheres are approximated as planes in the vicinity of Q, it follows from (21) that the locus of points A are hyperbolic sheets with the spheres from O and H as asymptotes. These hyperbolic sheets are the *dispersion surfaces* and are shown as heavy lines in Fig. 7(b).

2.3 THE DISPERSION SURFACES

In Eq. (21) which describes the dispersion surfaces, the right-hand side may be complex since $F_HF_{\bar{H}}$ is not necessarily real. Thus, ξ_0 and ξ_H are complex and in Eqs. (A12) and (16) the field amplitudes may be complex.

The structure factor for the $(\bar{h}\bar{k}\bar{l})$ reflection appears in Eq. (21) even though we assumed that only the (hkl) reflection was operative. This is reasonable since, in our coupled system, the wave with wave vector $\mathbf{K}_H$ is scattered by the backside of the atomic planes back into the $\mathbf{K}_0$ direction.

Since ξ_0 and ξ_H are complex, usually only their real parts are plotted in reciprocal space, as for instance, in Fig. 7. Generally, the real parts of the ξ's are related to the change of wavelength in the crystal (i.e., varying index of refraction) whereas the imaginary parts are related to absorption. If there is no absorption ($\Delta f''=0$) then, from Eq. (8) for the structure factors, we see that $F_HF_{\bar{H}}$ is real, and therefore, so are the ξ's.

Figure 8 shows a more detailed view of the region around the point Q. Since the distance between L and Q is proportional to the index of refraction for x rays which differs from unity by one part in 10^6, if the distance from L to Q is represented by 1 cm, the distance from Q to (000) or (hkl) is approximately 10^6 cm. On this scale then, the circles about (000) and

(*hkl*) which intersect at Q can be represented by straight lines. These straight lines form the asymptotes of the hyperbolas given by Eq. (21). The solid hyperbolas represent the σ polarization state ($P=1$) and the dotted ones the π state. We call the branch of the hyperbola closest to L the α branch and the other the β branch. The line LQ is part of the perpendicular bisector of **H** and is a symmetry axis for the dispersion surfaces. A point on one of the dispersion surface branches is called a *tie point*. Three tie points A_1, A_2, and A_3 have had their appropriate real ξ' values drawn in. Note from the definitions in Eq. (20) that ξ_0' and ξ_H' are both positive for the α branch and both negative for the β branch. Consider, for example, the tie point A_2. $\mathbf{K}_{0\beta}'$ and $\mathbf{K}_{H\beta}'$ are vectors drawn from A_2 to the origin and to (*hkl*), respectively, and represent a permitted pair of wave vectors. $\xi_{0\beta}'$ carries $K_{0\beta}'$ on out to the sphere of radius $k(1-\frac{1}{2}\Gamma F_0')$ and $\xi_{H\beta}'$ does the same for $K_{H\beta}'$. The tie points A_1 and A_3 are on opposite ends of a line through Q and their ξ_0' and ξ_H' values are equal in magnitude but opposite in sign. The wave vectors $\mathbf{K}_0'$ and $\mathbf{K}_H'$ for other tie points are not indicated in the figure. For the tie points on the hyperbolas and also lying on the line LQ, A_4 and A_5, we have that $\xi_0'=\xi_H'$. If $\mathfrak{D}$ is the distance between such a pair, from the geometry, and Eq. (21) with no absorption, we have that the diameter $\mathfrak{D}$ of the hyperbola is given by

$$\mathfrak{D}=k\Gamma \mid P \mid\mid F_H \mid \sec\theta_B. \tag{22}$$

This diameter, for reasons which we shall see, gives the width of the total reflection in Bragg diffraction from a perfect crystal, as derived by Darwin.

The general dispersion surface, given by Eq. (21) is, as we have seen, complex. We can justify our discussion of Fig. 8, however, by noting that if in Eq. (20) we take $\mathbf{K}_0\cdot\mathbf{K}_0=(K_0')^2-(K_0'')^2-2iK_0'K_0''\cos\beta$ and realize that $(K_0''/K_0')^2\ll 1$, (β is the angle between $\mathbf{K}_0'$ and $\mathbf{K}_0''$), then

$$\text{(a)}\quad \xi_0'\cong K_0'-k(1-\tfrac{1}{2}\Gamma F_0'),$$

$$\text{(b)}\quad \xi_0''\cong -K_0''\cos\beta+\tfrac{1}{2}k\Gamma F_0''. \tag{23}$$

Thus, indeed ξ_0' is very closely related to the real part of the wave vector, and ξ_0'' to the imaginary (or absorptive) part ($-K_0''$).

Now, in addition to describing the directional and absorptive properties of a wave, the tie points on the dispersion surface also characterize the ratio of the field amplitudes. From Eqs. (16), (A14), and (20) we obtain

$$E_H/E_0=-2\xi_0/kP\Gamma F_{\bar{H}}=-kP\Gamma F_H/2\xi_H, \tag{24}$$

where E_H and E_0 are the complex field amplitudes for a given state of polarization characterized by P. At the diameter points A_4 or A_5 in Fig. 8, the ratio E_H/E_0 tends toward ± 1. As we move up the hyperbola from A_4 towards A_1, ξ_0 increases and so $E_H>E_0$; as we move down from A_4, ξ_0 decreases and $E_0>E_H$.

Rather than, at this point, explicitly deriving detailed properties of the waves which are associated with each tie point, we first consider the incident boundary conditions which *select* the tie points characterizing a particular solution. That is, in any particular experiment, only certain of the tie points are chosen by the incident conditions, viz., the angle of incidence and orientation of the crystal surface with respect to the diffracting planes.

2.4 BOUNDARY CONDITIONS

We must consider the boundary conditions on the field vectors and on the wave vectors. For the field vectors, the conditions are usually that the tangential components $\mathfrak{E}$ and $\mathfrak{H}$ are continuous. However, since the index of refraction differs so little from unity, we can neglect any true reflection from the surface. Also, within the crystal, as we have seen in Appendix A, we can neglect any longitudinal components of the fields. Thus, with respect to field vectors, we say simply that the surface does not exist and all field vectors are continuous across any surface. This is not the case, however, with respect to the wave vectors.

We assume for the present that we can accurately treat the diffraction problem by assuming an incident plane wave. The limitations on this assumption, pointed out by Kato, is discussed in Sec. 2.9.

The mathematical matching of an incident and diffracted plane wave just outside the surface to the plane wave solutions which exist inside the crystal is carried out in some detail in Appendix B. The analysis results in conditions which seem quite reasonable. At the surface, the inside "incident" amplitudes, $\mathbf{E}_{0\alpha}$ plus $\mathbf{E}_{0\beta}$, add up to the outside incident wave amplitude $\mathbf{E}_0{}^i$. And the inside "diffracted" amplitudes, $\mathbf{E}_{H\alpha}$ plus $\mathbf{E}_{H\beta}$, add up to the outside diffracted amplitude, $\mathbf{E}_H{}^e$. In addition, in order to match phase fronts as is shown schematically in Fig. 5, the components of the inside wave vectors, $\mathbf{K}_{0\alpha}$ and $\mathbf{K}_{0\beta}$ along the surface must equal the surface component of the outside incident wave vector, $\mathbf{k}_0{}^i$. In Appendix B this condition is expressed the other way around, namely, that $\mathbf{K}_{0\alpha}$ and $\mathbf{K}_{0\beta}$ can differ from $\mathbf{k}_0{}^i$ *only by a vector along the surface normal* [see Eq. (B6)].

Since, without losing generality, we can assume that the outside incident wave is not being absorbed, then $\mathbf{k}_0{}^i$ is a real vector and the imaginary parts of $\mathbf{K}_{0\alpha}$ and $\mathbf{K}_{0\beta}$ then must lie along the surface normal. Thus, the absorption fronts in Fig. 5 are shown parallel to the physical surface.

In reciprocal space, the wave vector $\mathbf{k}_0{}^i$ starts at some point on the sphere which passes through the L point, say point P in Fig. 9 and ends at the origin. If it started at L, Bragg's equation would be exactly satisfied. If the line SS represents the physical entrance

surface, then from P we draw a line parallel to the inward surface normal until it cuts the dispersion sheets, generating tie points A and B. The tangential components of the internal vectors $\mathbf{K}_{0\alpha}'$ and $\mathbf{K}_{0\beta}'$ are equal to that of $\mathbf{k}_0{}^i$, which satisfies the boundary conditions on the wave vectors. Vectorially, we can write

$$\mathbf{K}_{0\alpha}=\mathbf{k}_0{}^i-\mathbf{PA}=\mathbf{k}_0{}^i-q_\alpha k\mathbf{n}, \qquad (25)$$

where $\mathbf{n}$ is a unit inward normal vector and we express the vector from P to A as $q_\alpha k\mathbf{n}$. A corresponding relationship holds for the B point. PA and q are complex. Using Bragg's law [as expressed in Eq. (14)] we have that

$$\text{(a)}\quad \mathbf{K}_{0\alpha}'=\mathbf{k}_0{}^i-q_\alpha' k\mathbf{n}, \qquad \mathbf{K}_{H\alpha}'=\mathbf{k}_0{}^i+\mathbf{H}-q_\alpha' k\mathbf{n};$$

$$\text{(b)}\quad \mathbf{K}_{0\alpha}''=q_\alpha'' k\mathbf{n}, \qquad \mathbf{K}_{H\alpha}''=q_\alpha'' k\mathbf{n}=\mathbf{K}_{0\alpha}''. \qquad (26)$$

Since the reciprocal lattice vector $\mathbf{H}$ is real, a consequence of Bragg's law is that the imaginary parts of $\mathbf{K}_0$ and $\mathbf{K}_H$ are equal, as shown above.

The geometrical construction shown in Fig. 9 gives us a quick way of determining the active tie points for an incident ray if we know how far off the Bragg angle it is (represented by the distance LP) and the relative orientation of the entrance surface and the diffracting planes.

Figure 9 has been drawn for the Laue case, that is, where $\mathbf{K}_{H\alpha}$ and $\mathbf{K}_{H\beta}$ (not shown on the figure) are directed into the crystal. For the Bragg case, SS is more nearly horizontal and the surface normal through P would cut only the α branch or β branch, or pass between the two branches of the hyperbola. If it passes between the branches, *only an exponentially attentuated field can exist in the crystal* and so total reflection results. This is why the diameter of the hyperbola is related to the angular width for total reflection in the Bragg case and is discussed in more detail in Sec. 3.0.

Boundary conditions similar to the ones above are imposed on the exit surface, but the entrance conditions are sufficient to select the particular tie points which are consistent with Maxwell's equations in the medium and which match the incident exciting wave. We see that there are *two* inside incident waves of *each* polarization state produced by the single outside incident ray.

The exit surface is generally taken to be a plane, usually parallel to the entrance surface so that the crystal is an infinite slab. However, the exit condition can be treated separately from the entrance one, and a separate exit wave vector matched to each of the interior wave vectors. Thus, for example, in the Borrmann effect for a single polarized incident ray, two forward diffracted beams and two diffracted beams emerge from the far side of the crystal slab. This is discussed in detail in Sec. 4.0. The intensities associated with these beams depend on the internal field amplitudes just at the exit surface.

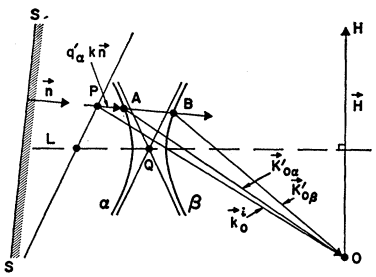

FIG. 9. Selection of the tie points by use of entrance point P and surface normal $\mathbf{n}$. **PO** represents the outside incident wave vector. The deviation from the correct Bragg angle, $\Delta\theta$, is given by LP/k. The real parts of each of the inside incident wave vectors $\mathbf{K}'_{0\alpha}$ and $\mathbf{K}'_{0\beta}$ thus have the same surface tangential component as has the outside incident wave vector $\mathbf{k}_0$.

2.5 FIELD AMPLITUDES

The field amplitudes at any point in the crystal depend on the *ratio* of the field amplitudes associated with the tie point describing the waves, the amount of energy assigned to the inside incident wave by the boundary conditions, and the absorptive losses in the medium. If we know ξ_0 for the tie point (both real and imaginary parts) Eqs. (23) and (14) would give us the wave vectors, and Eq. (24) the ratio of the field amplitudes, and then from the value of the fields at the entrance surface, we could evaluate the fields at every point in the crystal. *No matter how a certain tie point on the dispersion curve is selected, the properties of the waves associated with that point are invariant.* Nonetheless, since the incident conditions select the tie points, it is, perhaps, most useful to calculate ξ_0 [from Eq. (21)] for certain common experimental conditions. The two factors of importance in the incident conditions are: how far off the Bragg angle is the ray? At what angle does the ray strike the surface? We now derive expressions relating ξ_0 and ξ_H to these boundary conditions.

The real parts of ξ_0 and ξ_H, ξ_0' and ξ_H' are most conveniently handled geometrically.

In Fig. 10 the vectors from 0 to a point in the vicinity of the dispersion surface are parallel to within a few seconds of arc as is also the case for those vectors from H. Treating them as parallel, we see from the figure that

$$\text{(a)}\quad K_0'=k-q'k\mathbf{n}\cdot\mathbf{s}_0,$$

$$\text{(b)}\quad K_H'=PH-q'k\mathbf{n}\cdot\mathbf{s}, \qquad (27)$$

where $\mathbf{s}_0$ and $\mathbf{s}$ are unit vectors in the incident and diffraction beam directions and Eqs. (27) are the geometrical interpretation of Eq. (26a). $\mathbf{n}\cdot\mathbf{s}_0=\gamma_0$ and $\mathbf{n}\cdot\mathbf{s}=\gamma_H$, where γ_0 and γ_H are essentially the direction cosines of the incident and diffracted beams with respect to the incident surface.

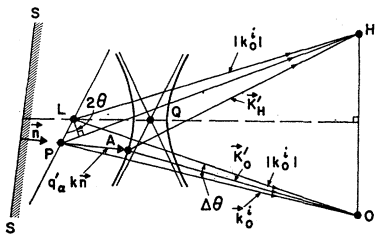

FIG. 10. Geometrical constructions used to derive expression for dispersion surface parameters ξ, in terms of entrance surface boundary conditions. See text.

Now, from Fig. 10,

$$PH=k+\mathrm{LP}\sin 2\theta=k-k\Delta\theta\sin 2\theta, \qquad (28)$$

where $\Delta\theta=LP/k$ and is negative in this figure. Combining (23), (27), and (28), we have for the real parts

$$\xi_0'=\tfrac{1}{2}k\Gamma F_0'-q'k\gamma_0,$$
$$\xi_H'=\tfrac{1}{2}k\Gamma F_0'-q'k\gamma_H-k\Delta\theta\sin 2\theta.$$

For the imaginary parts we need simply combine Eqs. (23b) and (26b) taking $\cos\beta=\gamma$ and obtain

$$\xi_0''=\tfrac{1}{2}k\Gamma F_0''-q''k\gamma_0,$$
$$\xi_H''=\tfrac{1}{2}k\Gamma F_0''-q''k\gamma_H.$$

Thus, we can write in combined (complex) form:

$$\text{(a)}\quad \xi_0=\tfrac{1}{2}k\Gamma F_0-qk\gamma_0$$
$$\text{(b)}\quad \xi_H=\tfrac{1}{2}k\Gamma F_0-qk\gamma_H-k\Delta\theta\sin 2\theta. \qquad (29)$$

We have thus, quite accurately, expressed ξ_0 and ξ_H in terms of $\Delta\theta$ and the entrance surface direction cosines, using the parametric variable q. Combining (29) with (21), eliminating q and solving for ξ_0 alone, we obtain

$$\xi_0^2+\xi_0(\gamma_0/\gamma_H)[\tfrac{1}{2}k\Gamma F_0(1-\gamma_H/\gamma_0)-k\Delta\theta\sin 2\theta]$$
$$-\tfrac{1}{4}(\gamma_0/\gamma_H)k^2P^2\Gamma^2F_HF_{\bar{H}}=0 \qquad (30)$$

or that

$$\text{(a)}\quad \xi_0=\tfrac{1}{2}k\mid P\mid\mid b\mid^{\frac{1}{2}}\Gamma[F_HF_{\bar{H}}]^{\frac{1}{2}}[\eta\pm(\eta^2+b/\mid b\mid)^{\frac{1}{2}}],$$
$$\text{(b)}\quad \xi_H=\tfrac{1}{2}k\mid P\mid(\Gamma/\mid b\mid^{\frac{1}{2}})[F_HF_{\bar{H}}]^{\frac{1}{2}}$$
$$\times[\eta\pm(\eta^2+b/\mid b\mid)^{\frac{1}{2}}]^{-1}, \qquad (31)$$

where,

$$b\equiv\gamma_0/\gamma_H$$

and

$$\eta=[b\Delta\theta\sin 2\theta+\tfrac{1}{2}\Gamma F_0(1-b)]/\Gamma\mid P\mid\mid b\mid^{\frac{1}{2}}[F_HF_{\bar{H}}]^{\frac{1}{2}}. \qquad (32)$$

Given $\Delta\theta$ and b, we can now, through the parameter η, calculate the real and imaginary parts of ξ_0 [Eq. (31)]. Now Eqs. (23) and (14) permit us to determine the real and imaginary parts of the wave vectors, and Eq. (24) the ratio of E_H to E_0. With these we can calculate the value of the fields anywhere in the crystal. Equation (31) is rather complicated since it is perfectly general, but simplifies a great deal if we consider symmetric cases. For the symmetric Bragg reflection, $b=-1$ and for the symmetric Laue case, $b=+1$. In fact, b negative indicates a Bragg reflection, entrance and exit beams through same surface, and b positive indicates a Laue case, entrance and exit beams through different faces. Note that for the Bragg case increasing glancing angle means decreasing η. Asymmetric reflections, $b\neq\pm1$ have many interesting properties[6]; and pathological cases, $b=0,\ \infty$ ($\mathbf{n}$ perpendicular to $\mathbf{k}_0^i$ or $\mathbf{k}_0^i+\mathbf{H}$) have to receive special treatment. However, we treat mostly the Laue case where $b=+1$. It really doesn't matter which case is treated, since once the properties of the waves associated with certain tie points on the dispersion curve are understood, the consequences of any incident conditions can be generated by determining which tie points they select. The symmetric Laue configuration, however, has an entrance geometry that selects tie points in a particularly simple fashion so that this case permits a straightforward discussion of the characteristics of the waves associated with particular tie points. Where appropriate, however, we write down the general expressions.

2.6 FIELDS AND TIE POINTS

As long as b is positive (Laue case) then $b/\mid b\mid=1$ and in Eq. (31) a convenient substitution for η is

$$\eta\equiv\tfrac{1}{2}(e^v-e^{-v})=\sinh v. \qquad (33)$$

With this definition, $\eta\pm(\eta^2+1)^{\frac{1}{2}}=\pm e^{\pm v}$ and we can write for ξ_0

$$\xi_0=\pm\tfrac{1}{2}k\mid P\mid\mid b\mid^{\frac{1}{2}}\Gamma[F_HF_{\bar{H}}]^{\frac{1}{2}}e^{\pm v}; \qquad (34)$$

and from Eq. (24)

$$\frac{E_H}{E_0}=\mp\left[\frac{\mid P\mid\mid b\mid^{\frac{1}{2}}}{P}\right]\frac{[F_HF_{\bar{H}}]^{\frac{1}{2}}}{F_{\bar{H}}}e^{\pm v}. \qquad (35)$$

For the *symmetric* Laue case ($b=+1$) these equations have the same form except that now Eq. (32) for η simplifies somewhat. Fundamentally, η is just a large constant (complex) times $\Delta\theta$. While $\Delta\theta$ may range over a few seconds of arc, η may vary between zero and plus or minus a small integer. Expressions (34) and (35) are then, through (33), functions of $\Delta\theta$ for this geometry. Figure 11 shows the relationship between the entrance points, the P's, and the tie points for the symmetric Laue case. The surface normal is parallel to LQ so that the entrance point P selects tie points on the line through P parallel to the line LQ. Any length, LP is, of course, proportional to $\Delta\theta$. When P coincides with L, the diameter points are selected; $\Delta\theta=0$, $\eta=0$,

and $v=0$. Thus, for the diameter points

$$\xi_0=\xi_H=\pm\tfrac{1}{2}k\mid P\mid\Gamma[F_HF_{\bar{H}}]^{\frac{1}{2}} \tag{36}$$

and

$$\frac{E_H}{E_0}=\mp\frac{\mid P\mid}{P}\frac{[F_HF_{\bar{H}}]^{\frac{1}{2}}}{F_{\bar{H}}}. \tag{37}$$

The positive sign is associated with the tie point on the α branch. Since ξ_0' is defined to be positive on the α branch, the positive sign indicates that *for the α branch points, one takes one of the square roots of the complex number $F_HF_{\bar{H}}$ such that its real part is positive.* With this choice, the determination of the actual phase of the ratio E_H/E_0 [Eq. (37)] depends on the polarization factor and $F_{\bar{H}}$ itself. If the crystal is centrosymmetric, then $F_H=F_{\bar{H}}$, for an origin at a symmetry center, and $\mid\mathbf{E}_H\mid=\mid\mathbf{E}_0\mid$. This result is very nearly true for any structure. Thus, for the diameter points, the field amplitude of the diffracted field is essentially equal to that of the inside incident field. From Eq. (37) we see that whatever the phase between $\mathbf{E}_0$ and $\mathbf{E}_H$ on the α branch, it changes by 180° for points on the β branch.

In Fig. 11, lines have been drawn along the wave vectors to represent the relative strength of the fields $\mathbf{E}_0$ and $\mathbf{E}_H$. For points such as P_1 or P_4 which are meant to be well off the Bragg condition, geometrically, we expect either ξ_0 or ξ_H to go to zero for the associated tie points. To show this behavior of ξ_0 more clearly, we set $b=+1$ in Eq. (30) and write out the step before Eq. (31), namely

$$\xi_0=\tfrac{1}{2}k\Delta\theta\sin 2\theta\pm\tfrac{1}{2}[k^2\Delta\theta^2\sin^2 2\theta+k^2P^2\Gamma F_HF_{\bar{H}}]^{\frac{1}{2}}. \tag{38}$$

In the limit that $\Delta\theta^2\sin^2 2\theta\gg P^2\Gamma F_HF_{\bar{H}}$, i.e., well off the Bragg angle: $\xi_0\rightarrow\frac{1}{2}k\Delta\theta\sin 2\theta\pm\frac{1}{2}k\mid\Delta\theta\mid\sin 2\theta$ or

$$\xi_0'\rightarrow 0,\qquad \pm k\mid\Delta\theta\mid\sin 2\theta,$$
$$\xi_0''\rightarrow 0.$$

Thus, for the tie points A_1 and B_4, $\xi_0\rightarrow 0$; therefore, $\mathbf{E}_H\rightarrow 0$ with respect to $\mathbf{E}_0$. That is, no diffracted wave is generated for these two tie points and only a single wave $\mathbf{E}_0$, propagates through the crystal. The real

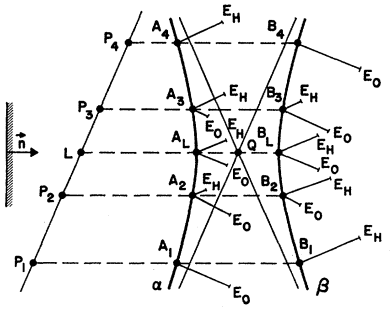

FIG. 11. Schematic representation of ratios of field strengths, E_H to E_0, for different tie points, using the symmetric Laue entrance conditions.

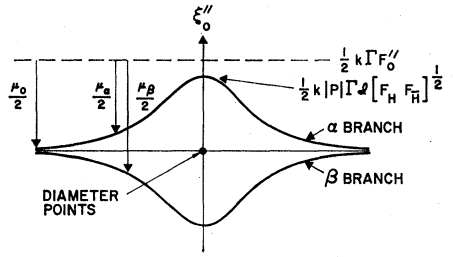

FIG. 12. Schematic representation of absorption associated with each tie point. The absorption depends on the difference between the solid curves and the upper dashed curve. The absorption is least for the α branch diameter point.

part of the wave vector for these single waves, from Eq. (23), is

$$K_0'=\xi_0'+k(1-\tfrac{1}{2}\Gamma F_0')\rightarrow k(1-\tfrac{1}{2}\Gamma F_0'),$$

which is just the vacuum value corrected for the average index of refraction; the imaginary part is, from Eq. (23)

$$K_0''\cos\beta=\tfrac{1}{2}k\Gamma F_0''-\xi_0''\rightarrow\tfrac{1}{2}k\Gamma F_0''.$$

The absorption factor for these waves then is

$$\exp(-2\pi\mathbf{K}_0''\cdot\mathbf{r})=\exp[-2\pi(\tfrac{1}{2}k\Gamma F_0'')t],$$

where t is the distance in the ray direction. Since the intensity loss goes as the square of the amplitude,

$$\exp(-2\pi k\Gamma F_0''t)\equiv\exp(-\mu_l t),$$

and the linear absorption coefficient then becomes

$$\mu_l=\mu_0=2\pi k\Gamma F_0''. \tag{39}$$

For the tie points B_1 and A_4, $\xi_H\rightarrow 0$, which implies that an infinitely large $\mathbf{E}_H$ would be excited by the presence of any $\mathbf{E}_0$, or essentially, that $\mathbf{E}_0\rightarrow 0$. That is, no incident wave can really excite these wave points. Thus, beginning at a point P_1, well off the Bragg angle, with $\Delta\theta$ negative, only tie points on the α branch are excited and only a transmitted beam exists. As we approach the center of the dispersion sheets, tie points on both branches become active, the diffracted beam grows in strength and $\mid\mathbf{E}_H\mid\approx\mid\mathbf{E}_0\mid$ at the diameter points. For points with $\Delta\theta$ large and positive, only wave points on the β branch are active, and again, only a transmitted beam exists.

From Eq. (38) we see that for the diameter points ($\Delta\theta=0$), ξ_0 is proportional to the square root of a complex constant, $[F_HF_{\bar{H}}]$. As we move away from the diameter points, a rapidly increasing real part is added to the complex constant before taking its square root. Thus, the imaginary part of ξ_0, ξ_0'' becomes increasingly less important until it essentially is zero, well off the Bragg angle. These conclusions are sketched out in Fig. 12 for the imaginary parts ξ_0''. For the diameter points $\xi_0''=\pm\frac{1}{2}k\mid P\mid\Gamma\mathcal{I}[F_HF_{\bar{H}}]^{\frac{1}{2}}$ (where $\mathcal{I}$ means imaginary part) and then it goes to zero well off the Bragg angle. A line equal in value to $\frac{1}{2}k\Gamma F_0''$ is sketched

in. From Eq. (23) we see that the effective absorption coefficient is proportional to the difference between this line and the corresponding ξ_0'' curve.

Since there is always absorption (and not amplification) of the waves in the crystal, $\frac{1}{2}k\Gamma F_0''$ is always larger than ξ_0''. It is possible, however, for them to be almost equal at the diameter points, giving very low absorption for the α branch.

We can now write down expressions for the fields in the Laue case in some detail. From the boundary conditions on amplitudes (details in Appendix B)

$$\mathbf{E}_0{}^i=\mathbf{E}_{0\alpha}+\mathbf{E}_{0\beta}, \qquad 0=\mathbf{E}_{H\alpha}+\mathbf{E}_{H\beta}. \tag{40}$$

For the variation of E_0 along the hyperbola in Fig. 11 we can write:

$$E_{0\alpha}=E_0{}^i(e^{-v}/2\cosh v); \qquad E_{0\beta}=E_0{}^i(e^{v}/2\cosh v) \tag{41}$$

where these results are separately true for each polarization state. Note that $E_{0\alpha}$ goes to zero for the points at high angle on the α branch, and goes to $E_0{}^i$ for points at low angle. The opposite is true for $E_{0\beta}$. The boundary conditions thus distribute the input energy to the various tie points and not every point on the dispersion surface is excited, even though selected. Thus, the complete expression for the separate fields can be written as

$$\text{(a)}\quad \mathfrak{E}_{0\alpha}=\mathbf{E}_0{}^i\frac{e^{-v}}{2\cosh v}\exp(2\pi i\nu t)\exp(-2\pi i\mathbf{K}_{0\alpha}'\cdot\mathbf{r})\times\exp(-2\pi\mathbf{K}_{0\alpha}''\cdot\mathbf{r}),$$

$$\text{(b)}\quad \mathfrak{E}_{H\alpha}=-\frac{\mathbf{E}_0{}^i}{2\cosh v}\frac{|P|}{P}|b|^{\frac{1}{2}}\frac{[F_HF_{\bar{H}}]^{\frac{1}{2}}}{F_H}\exp(2\pi i\nu t)\times\exp(-2\pi i\mathbf{K}_{H\alpha}'\cdot\mathbf{r})\exp(-2\pi\mathbf{K}_{H\alpha}''\cdot\mathbf{r}),$$

$$\text{(c)}\quad \mathfrak{E}_{0\beta}=\mathbf{E}_0{}^i\frac{e^{v}}{2\cosh v}\exp(2\pi i\nu t)\exp(-2\pi i\mathbf{K}_{0\beta}'\cdot\mathbf{r})\times\exp(-2\pi\mathbf{K}_{0\beta}''\cdot\mathbf{r}),$$

$$\text{(d)}\quad \mathfrak{E}_{H\beta}=\frac{\mathbf{E}_0{}^i}{2\cosh v}\frac{|P|}{P}|b|^{\frac{1}{2}}\frac{[F_HF_{\bar{H}}]^{\frac{1}{2}}}{F_H}\exp(2\pi i\nu t)\times\exp(-2\pi i\mathbf{K}_{H\beta}'\cdot\mathbf{r})\exp(-2\pi\mathbf{K}_{H\beta}''\cdot\mathbf{r}), \tag{42}$$

where the wave vectors can be related to the incident conditions and crystal structure through Eqs. (26), (29), (34) and (39).

2.7 DISCUSSION OF FIELDS

So far, plane wave solutions of Maxwell's equations in a medium of periodic dielectric constant related to the periodic electron density have led to permitted wave vectors differing little from the vacuum values, but described by the dispersion surfaces in reciprocal space, and to field amplitude ratios and absorption factors generally summarized in Figs. 11 and 12. Although the equations in the section above, for the Laue case, give the fields explicitly, the general nature of the fields associated with any tie point on the dispersion surface can be understood from Figs. 9, 11, and 12. For a ray entering the crystal well off the Bragg angle, a tie point close to the asymptote described by the sphere about the origin of the reciprocal lattice is selected and only one wave is excited. This wave travels substantially in the incident beam direction, which, as seen from Fig. 12, suffers the normal photoelectric absorption. On the other hand, for a field whose tie point is a diameter point on the α branch, two waves are excited; one in the "transmitted" direction and one in the "diffracted" direction. These are coherently related; that is, have essentially equal amplitude and wavelength, and suffer less than normal absorption. When two such waves exist in a common region, as we shall see more explicitly in Sec. 2.10B(2), the resulting pattern contains nodal planes of electric field intensity. These statements also hold for fields described by a diameter point in the β branch, except that this structured field now experiences even greater absorption (Fig. 12) than that of a single plane wave. Although a great deal more can be said about the structure of the resulting fields, in both the Laue and Bragg cases, a more fruitful line of questioning would be to first examine the energy flows. After all, diffraction is, in general, thought of as a transport problem. The absorption properties, which are the most interesting aspect, turn out to be most easily discussed in terms of the energy flows, or Poynting's vectors. In the next few sections, we consider these aspects before going on to calculate the diffracted-beam line shapes and integrated intensities.

2.8 ENERGY FLOW AND POYNTING'S VECTOR

The energy flow in the crystal is described in terms of the Poynting vector for the total wave field. We continue to work with infinite plane waves, such as given by Eq. (42); the limitations of this assumption is discussed in Sec. 2.9. The instantaneous Poynting vector of an electromagnetic field is given by $\mathbf{S}_0=\mathfrak{E}\times\mathfrak{H}$ and represents the energy flowing across a unit area perpendicular to $\mathbf{S}$ in a unit time. The instantaneous $\mathbf{S}$ at every point $\mathbf{r}$ may be quite complicated and is of little use; instead, we are more concerned with certain averages. The time average of $\mathbf{S}$, $\langle\mathbf{S}\rangle$ is averaged over the spatial unit cell and finally averaged over a volume related to the interchange of energy between two directions as a function of depth. In this section, we are mostly concerned with the directional properties of this *highly averaged* energy flow which are essentially independent of absorption, and in Sec. 2.10 consider the absorption as a function of flow direction.

The time average of $\mathbf{S}$ is given by[14]:

$$\langle\mathbf{S}\rangle=\tfrac{1}{2}\mathfrak{R}[\mathfrak{E}\times\mathfrak{H}^*], \tag{43}$$

[14] Reference 12, p. 103.

where $\Re(\mathfrak{E}\times\mathfrak{H}^*)$ represents the real part of this expression. $\mathfrak{E}$ and $\mathfrak{H}$ describe the total fields inside the crystal. We continue to use the field expressions for the Laue case, Eq. (42), to illustrate various points and thus $\mathfrak{E}$ and $\mathfrak{H}$ can be thought of as sums of the individual waves of (42) associated with all the tie points of the dispersion surfaces selected by the incident boundary conditions. If the index w describes the particular sheet of the dispersion surface, i.e., $w=\alpha$, β, etc., for the polarization σ or π state, then

$$\mathfrak{E}\times\mathfrak{H}^*=\sum_w\sum_{w'}\exp[-2\pi i(\mathbf{K}_{0w}'-\mathbf{K}_{0w'}')\cdot\mathbf{r}]\times\exp[-2\pi(\mathbf{K}_{0w}''+\mathbf{K}_{0w'}'')\cdot\mathbf{r}]\sum_H\sum_{H'}(\mathbf{E}_{Hw}\times\mathbf{H}_{H'w}^*)\times\exp[-2\pi i(\mathbf{H}-\mathbf{H}')\cdot\mathbf{r}],\quad(44)$$

where we have used the Bragg relation $\mathbf{K}_{Hw}=\mathbf{K}_{0w}+\mathbf{H}$ in (42).

This expression simplifies if we average over a unit cell. Although von Laue[15] carries out the averaging in detail, if one assumes that the absorption per cell is negligible, i.e., $\exp[-2\pi(\mathbf{K}_{0w}''+\mathbf{K}_{0w'}'')\cdot\mathbf{r}]$ is constant over the cell, then the variation of the first exponential of (44) over a cell, where $\mathbf{K}_{0w}'-\mathbf{K}_{0w'}'$ is the order of the diameter of the dispersion curves, is also negligible, and in integrating the last exponential over a cell we get zero contribution unless $\mathbf{H}=\mathbf{H}'$. Thus, the average over a cell of the time averaged Poynting's vector becomes

$$\langle\langle\mathbf{S}\rangle\rangle=\tfrac{1}{2}\Re\{\sum_w\sum_{w'}\exp[-2\pi i(\mathbf{K}_{0w}'-\mathbf{K}_{0w'}')\cdot\mathbf{R}]\times\exp[-2\pi(\mathbf{K}_{0w}''+\mathbf{K}_{0w'}'')\cdot\mathbf{R}]\sum_H(\mathbf{E}_{Hw}\times\mathbf{H}_{Hw'}^*)\},\quad(45)$$

where we have replaced $\mathbf{r}$ by $\mathbf{R}$ to signify that with respect to energy flow, variations of this term within a cell are negligible.

From the structure of the field as given in Appendix A, $\mathbf{E}_{Hw}\times\mathbf{H}_{Hw'}^*=0$ if w and w' refer to different polarization states, and we can, therefore, treat the energy flow of each polarization state separately. Also, we have, in general, that

$$\mathbf{E}_{Hw}\times\mathbf{H}_{Hw'}=[\epsilon_0/\mu_0]^{\frac{1}{2}}\,|\,\mathbf{E}_{Hw}\,||\,\mathbf{E}_{Hw'}^*\,|\,\mathbf{s}_H,\quad(46)$$

where we have used Eq. (A4) to relate the magnitudes of $|\,\mathbf{E}\,|$ and $|\,\mathbf{H}\,|$, taken $\mathbf{s}_H$ as a unit vector along $\mathbf{K}_H$, and made the following assumptions: (1) we neglect the imaginary parts of $\mathbf{K}_H$ when discussing directions and (2) we neglect the small correction to the magnitude of (46) due to the index of refraction, i.e., let $|\,\mathbf{K}_H'\,|$ be the vacuum value. Actually, we need only assume that the differences in the $|\,\mathbf{K}_H'\,|$'s are negligible so that we can factor out a $[\epsilon_0/\mu_0]^{\frac{1}{2}}$ in the equation to follow.

[15] M. v. Laue, Acta Cryst. **5**, 619 (1952).

From (45) and (46) we have, for the case of one active reciprocal lattice point and two tie points

$$[\mu_0/\epsilon_0]^{\frac{1}{2}}\langle\langle\mathbf{S}\rangle\rangle=\tfrac{1}{2}\exp(-4\pi\mathbf{K}_{0\alpha}''\cdot\mathbf{R})\times(|\,\mathbf{E}_{0\alpha}\,|^2\,\mathbf{s}_0+|\,\mathbf{E}_{H\alpha}\,|^2\,\mathbf{s}_H)+\tfrac{1}{2}\exp(-4\pi\mathbf{K}_{0\beta}''\cdot\mathbf{R})(|\,\mathbf{E}_{0\beta}\,|^2\,\mathbf{s}_0+|\,\mathbf{E}_{H\beta}\,|^2\,\mathbf{s}_H)+\exp[-2\pi(\mathbf{K}_{0\alpha}''+\mathbf{K}_{0\beta}'')\cdot\mathbf{R}]\times\{|\,\mathbf{E}_{0\alpha}\,||\,\mathbf{E}_{0\beta}\,|\,\mathbf{s}_0+|\,\mathbf{E}_{H\alpha}\,||\,\mathbf{E}_{H\beta}\,|\,\mathbf{s}_H\}\times\cos 2\pi[(\mathbf{K}_{0\alpha}'-\mathbf{K}_{0\beta}')\cdot\mathbf{R}],\quad(47)$$

which we write as

$$\mathbf{S}_T=[\mu_0/\epsilon_0]^{\frac{1}{2}}\langle\langle\mathbf{S}\rangle\rangle=\mathbf{S}_\alpha+\mathbf{S}_\beta+\mathbf{S}_{\alpha\beta}.\quad(48)$$

This quantity can be considered as the vector sum of the effective Poynting's vectors of three wave fields in the crystal. $\mathbf{S}_\alpha$ and $\mathbf{S}_\beta$ are the effective energy flows each with its own absorption, associated with a tie point on the α and β branches, respectively. $\mathbf{S}_{\alpha\beta}$ represents a coupling term between the two. We consider these terms in some detail again for the Laue case.

A. Pendellösung

The absorption factors for the three Poynting vectors in Eq. (48) do not, in general, affect the directional properties. At this point, for convenience of discussion, we assume that the crystal is nonabsorbing and consequently set $\mathbf{K}_{0\alpha}''=\mathbf{K}_{0\beta}''=0$. As a result of this, $\mathbf{S}_\alpha$ and $\mathbf{S}_\beta$ are independent of depth below the surface of the crystal while $\mathbf{S}_{\alpha\beta}$ has a sinusoidal dependence. The boundary conditions demand that the vector $(\mathbf{K}_{0\alpha}-\mathbf{K}_{0\beta})$ be perpendicular to the entrance surface of the crystal [this can be seen geometrically in Fig. (9)], and hence, $\mathbf{S}_{\alpha\beta}$ is constant in planes parallel to the crystal surface, varying sinusoidally with depth with period

$$P=1/(\mathbf{K}_{0\alpha}'-\mathbf{K}_{0\beta}').\quad(49)$$

For the symmetric Laue case at the center of the range of reflection, $(1/P)$ is simply the diameter of the hyperbola of the dispersion surface, so that P is the order of 10^{-3} cm. Equation (47) shows that $\mathbf{S}_{\alpha\beta}$ shifts the energy flow around the average direction $\mathbf{S}_\alpha+\mathbf{S}_\beta$ periodically with the depth beneath the crystal surface. This is the phenomenon of Pendellösung, a term used by Ewald because of the mathematical similarity between the variation of the energy flow of the wave field in the crystal and the energy transfer between two weakly coupled pendulums.

If the wave field inside the crystal described by Eq. (42) is substituted in Eq. (47) the explicit behavior of the coupling vector $\mathbf{S}_{\alpha\beta}$ is made clearer. Using the abbreviation $a=\frac{1}{2}\cosh(v)$ and for $F_H\approx F_{\bar{H}}$, grouping the terms as in (47) we have:

$$\mathbf{S}_T\approx\tfrac{1}{2}a^2\,|\,\mathbf{E}_0{}^i\,|^2|\,e^{-2v'}\mathbf{s}_0+b\mathbf{s}_H\,|+\tfrac{1}{2}a^2\,|\,\mathbf{E}_0{}^i\,|^2[e^{2v'}\mathbf{s}_0+b\mathbf{s}_H]+a^2\,|\,\mathbf{E}_0{}^i\,|^2[\mathbf{s}_0-b\mathbf{s}_H]\cos 2\pi(Z/P),\quad(50)$$

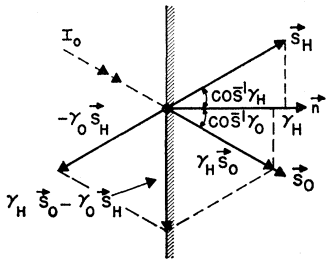

FIG. 13. Vector diagram used in discussing Pendellösung effect. See text.

where Z is the depth below the surface of the crystal. At the depth for which $\cos 2\pi(Z/P)=1$, the component of $\mathbf{S}_{\alpha\beta}$ in the diffracted beam direction just cancels the corresponding contributions from $\mathbf{S}_\alpha$ and $\mathbf{S}_\beta$ and all the energy flows in the primary beam direction $\mathbf{s}_0$. When the cosine term is -1, half a Pendellösung period further in Z, the beam in the diffracted direction is strong while in $\mathbf{s}_0$ the intensity is proportional to $\sinh^2 v/\cosh v$ which is zero when the incident beam exactly satisfies Bragg's law at the center of the range of reflection. Thus, the energy swaps back and forth as a function of depth, extinguishing completely in the $\mathbf{s}_H$ direction and very nearly in the $\mathbf{s}_0$ direction, with a period P. Note, however, that this swapping requires the excitation of a tie point on both the α and β branches.

From Eq. (50) it can be seen that $\mathbf{S}_{\alpha\beta}$ has the direction of the vector $\gamma_H\mathbf{s}_0-\gamma_0\mathbf{s}_H$. Figure 13 shows the vectors $\gamma_H\mathbf{s}_0$ and $-\gamma_0\mathbf{s}_H$ relative to the surface normal. It is evident that the vector $\mathbf{S}_{\alpha\beta}$ is parallel to the crystal surface and does not contribute to energy flow through the crystal.

B. Direction of Energy Flow

The net direction of energy flow, determined finally by averaging Poynting's vector over a Pendellösung period is, from Eq. (47)

$$\mathbf{S}_T=\mathbf{S}_\alpha+\mathbf{S}_\beta=(|\mathbf{E}_{0\alpha}|^2\mathbf{s}_0+|\mathbf{E}_{H\alpha}|^2\mathbf{s}_H)+(|\mathbf{E}_{0\beta}|^2\mathbf{s}_0+|\mathbf{E}_{H\beta}|^2\mathbf{s}_H), \quad (51)$$

where again the absorption does not significantly affect the directions. Equation (51) represents a complete decoupling of the four plane waves which comprise the two wave fields. The decoupling arises because $\mathbf{S}_T$ represents an averaging over the regions where interaction takes place. For example, the two plane waves of wave field α, $\mathbf{E}_{0\alpha}$ and $\mathbf{E}_{H\alpha}$ interact within regions the size of a unit cell, and this average has been taken in reaching Eq. (47). The two wave fields α and β interact over a Pendellösung period, and this has been averaged to obtain (51) so that the total Poynting's vector in (51) is just the sum of the *individual* Poynting's vectors associated with each of the four plane waves.

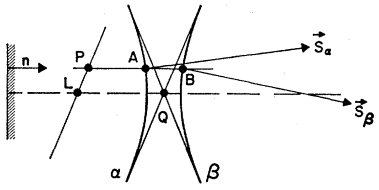

FIG. 14. Averaged energy flow associated with the points A and B. Poynting's vectors S_α and S_β for the flow of each tie point is perpendicular to the real part of the dispersion curve at that tie point.

A simple and elegant property of the energy flow $\mathbf{S}_T$ has been first proven in the general case by Kato[16]; namely, that the direction of energy flow corresponding to a tie point on a particular sheet of the dispersion surface is that of the *normal* to the surface at that point. This result can be obtained by deriving an expression for the normal to a point on the dispersion surface and showing that it agrees with the direction of $\mathbf{S}_\alpha$ or $\mathbf{S}_\beta$. Thus, $\mathbf{S}_\alpha$ is perpendicular to the hyperbola at A and $\mathbf{S}_\beta$ at B in Fig. 14. The energy flows *along the atomic planes* for the diameter tie points. This condition exists, for example, in the symmetric Laue case when L is the incident point. For any other incident point, there are two flows: $\mathbf{S}_\alpha$ and $\mathbf{S}_\beta$ (Fig. 14), one directed above the atomic planes and one below.

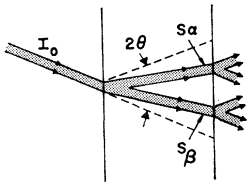

FIG. 15. Schematic representation of the separation of the energy flows in the crystal for a narrow beam off the Bragg angle but within the range of reflection.

In an actual experiment, where the incident beam has a cross section small compared to the thickness of the crystal, for a ray slightly off the Bragg angle, a decoupling can take place between the two wave fields because of a physical separation of the two flows within the crystal. This is shown schematically in Fig. 15. The only interaction between the fields occur near the entrance surface where the fields of $\mathbf{S}_\alpha$ and $\mathbf{S}_\beta$ actually overlap. Outside of that region the energy flows independently along paths determined by the Poynting vectors associated with the tie points on each branch of the dispersion surface.

The direction of $\mathbf{S}_\alpha$ depends upon $|\mathbf{E}_{0\alpha}|$ and $|\mathbf{E}_{H\alpha}|$ which in turn, by Eq. (35) depends on the deviation of the angle of incidence from the exact Bragg conditions. It can be seen from Eq. (47) that the direction of each $\mathbf{S}_\alpha$ depends only upon the ratios of intensities in the primary and diffracted beam directions. This result is true irrespective of whether the crystal is or is not absorbing.

2.9 LIMITATIONS OF THE PLANE WAVE THEORY

The treatment thus far has assumed that the incident beam can be considered an infinite plane wave.

[16] N. Kato, Acta Cryst. 11, 885 (1958).

Kato[17] in a series of papers has investigated the validity of this assumption. We only sketch his arguments and present the conclusions pertinent to the present treatment.

One of the conditions for a plane-wave approximation to be valid is that the angular width Ω, of a coherent incident wave at the entrance surface must be smaller than $\Delta\theta$, the angular width of the reflection. $\Delta\theta$ is usually the order of 10^{-5} rad while Ω, for fairly typical experimental conditions (source to crystal distance of 10 cm and beam width at the crystal of 10^{-3} cm) is greater than 10^{-4}. It follows that the basic condition for a plane-wave approximation is usually not satisfied, and one cannot consider different tie points to be independently excited. In a typical experiment the entire dispersion surface is, in a sense, illuminated with coherent radiation, and in principle, interference is possible between waves arising from any pair of points on the dispersion surface whose fields are superposed in the crystal. The usual incident beams then produce wave fields which fill the full 2θ range between $\mathbf{s}_H$ and $\mathbf{s}_0$. This region is called the "x-ray fan." A range of incident angles the order of a few seconds of arc produces an angular spread of 2θ within the crystal.

Kato shows that the true incident beam can be represented as a superposition of plane waves each of which produces a set of waves in the crystal which can be calculated from the plane-wave treatment we have been considering. These plane waves superpose to create wave bundles within the crystal. The wave bundle associated with the vectors terminating in the region $d\tau$ of the dispersion surface in the neighborhood of point A (Fig. 16) can be shown to propagate in a direction normal to $d\tau$ and consequently perpendicular to the dispersion surface at A. This is in agreement with the results in Sec. 2.8. The basic difference between the spherical or wave-bundle approach and the plane wave treatment shows up when one considers the angular range and lateral width of the coherent bundles emanating from the region $d\tau$. These are, in typical cases, small enough so that, except for regions of the crystal quite close to the incident surface, the bundles from regions adjacent to $d\tau$ are separated physically in space, and, as a result, propagate independently of one another. For this reason, the Pendellösung phenomenon described in the previous section between points A and B does not often exist because the wave bundles from these points do not superpose in a common volume of crystal. However, since the normals to the dispersion surface of points A and A′ are parallel, Pendellösung interference is observed between these points. This has been experimentally verified by Kato and Lang.[18] A direct proof of the separation of the energy propagation has been demonstrated in an ingenious experiment by Authier.[19]

[17] N. Kato, Acta Cryst. **13**, 349 (1960).
[18] N. Kato and A. R. Lang, Acta Cryst. **12**, 787 (1959).
[19] A. Authier, Compt. Rend. **251**, 2003 (1960).

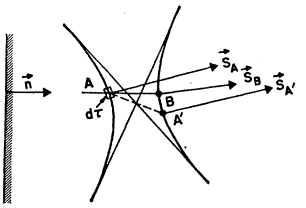

FIG. 16. Energy flows important in the discussion of a spherical entrance wave front.

Concerning integrated intensities the spherical wave treatment gives results essentially identical to that calculated from the plane wave theory.

2.10 ABSORPTION

The most interesting aspects of the dynamical diffraction theory are those dealing with the effective absorption. For this reason, we treat the absorption phenomena in some detail and from several points of view. In Sec. 2.10A we deal with the formal expressions relating the absorption to the direction of energy flow and in 2.10B a physical interpretation of the results are discussed in terms of the nodes of the field patterns and the distribution of absorbing matter in the crystal.

A. Formal Absorption Factors

The absorption factor for each wave within the crystal is expressed through the imaginary part of the wave vector, $-K''$ and is explicitly indicated in Eqs. (42) and (47). As expressed in Eq. (42), the absorption is a function of the incident condition which selects a tie point on the dispersion surface. As we saw in the last section, however, the direction of energy flow depends only on the ratio of the field amplitudes which, according to (24), depends only on the tie point on the dispersion surface. Intuitively, we would expect the absorption for a given flow direction to depend only on that direction and not on how the direction was established. Thus, the absorption of each of the internal beams corresponding to a given tie point should be independent of how that point is selected by the external parameters of angle of incidence and orientation of the crystal surface. We derive the absorption coefficients on this basis from the dispersion surface properties in terms of the complex variables ξ_0 and ξ_H.

From Eq. (42) the absorption factor for the intensity (the square of that for the amplitude) is given by

$$\exp(-4\pi\mathbf{K}_0''\cdot\mathbf{R}). \tag{52}$$

$\mathbf{K}_0''$, as we have seen, is directed along the surface normal. The planes of constant absorption are parallel to the physical surface, and the absorption coefficient for distance along this normal is

$$\mu_n = 4\pi K_0''. \tag{53}$$

If we consider absorption along some other direction the absorption coefficient is smaller since the absorption itself only depends on depth from the surface. Thus,

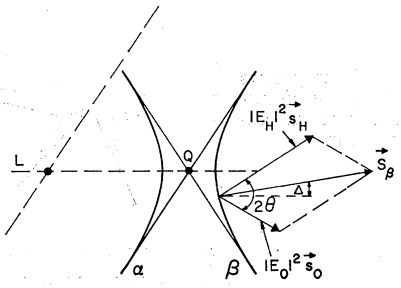

FIG. 17. Geometry used in derivation of energy flow as a function of angle Δ, between flow direction and atomic planes. The Poynting's vector is the vector sum of the individual flows.

the absorption coefficient along any direction $\mathbf{x}$ is given by

$$\mu_x=\mu_n\cos(\mathbf{n},\mathbf{x}), \tag{54}$$

where $(\mathbf{n},\mathbf{x})$ is the angle between $\mathbf{n}$ and $\mathbf{x}$.

We must now evaluate K_0''. From the definition of ξ_0 and ξ_H [Eq. (23)]:

$$\begin{aligned}&\text{(a)}\quad \xi_0'=K_0'-k(1-\tfrac{1}{2}\Gamma F_0'),\\ &\qquad \xi_H'=K_H'-k(1-\tfrac{1}{2}\Gamma F_0'),\\ &\text{(b)}\quad \xi_0''=-K_0''\gamma_0+\tfrac{1}{2}k\Gamma F_0'',\\ &\qquad \xi_H''=-K_H''\gamma_H+\tfrac{1}{2}k\Gamma F_0''.\end{aligned} \tag{55}$$

We have discussed the absorption qualitatively in Fig. 12 using (55b). The salient point of the formal development to be presented here is that we can express ξ_0'' and the ratio of the field amplitudes, in terms of ξ_0' which is uniquely associated with a point on the dispersion surface. That is, we can express the imaginary part of the ξ in terms of the real parts and express the ratio of the field amplitudes in these terms also. This implies physically that the absorption is determined inherently by the field strength, which in turn, is fixed by the tie point through Eq. (24), and so the absorption also must be fixed solely by the tie point. Writing the fundamental equation of the dispersion surface (21) in terms of real and imaginary parts, we have

$$\begin{aligned}&\text{(a)}\quad \xi_0'\xi_H'-\xi_0''\xi_H''=C^2\mathcal{R}_H\\ &\text{(b)}\quad \xi_0'\xi_H''+\xi_0''\xi_H'=C^2\mathcal{I}_H,\end{aligned} \tag{56}$$

where $C=\frac{1}{2}|P|k\Gamma$ and $\mathcal{R}_H$ and $\mathcal{I}_H$ are the real and imaginary parts of $F_H F_{\bar{H}}$.

It can be shown from (55) that $\xi_0''\xi_H''$ is small compared with $\xi_0'\xi_H'$, to second order in (F_0''/F_0') and it is neglected. With this approximation and since $K_0''=K_H''$, inserting Eqs. (55) in (56) gives

$$\begin{aligned}&\text{(a)}\qquad \xi_0'\xi_H'=C^2\mathcal{R}_H,\\ &\text{(b)}\quad -K_0''(\xi_0'\gamma_H+\xi_H'\gamma_0)=C^2\mathcal{I}_H-(\xi_0'+\xi_H')\tfrac{1}{2}k\Gamma F_0'',\end{aligned} \tag{57}$$

We have thus expressed K_0'' in terms of ξ_0' and the structure factors. The direction cosines, γ_0 and γ_H are still in the expression but these drop out later.

Turning now to Eq. (24) for the ratio of the field amplitudes, multiplying each term by its complex conjugate to get absolute values and then multiplying the terms together, we obtain

$$|\mathbf{E}_H/\mathbf{E}_0|^4=(\xi_0\xi_0^*/\xi_H\xi_H^*)(F_HF_H^*/F_{\bar{H}}F_{\bar{H}}^*). \tag{58}$$

The ratio of the structure factors is unity for centrosymmetric crystals and departs slightly from unity for polar crystals, and then only if the radiation is close to an absorption edge. Taking this term as unity and using the same approximation on ξ_0''/ξ_0' as we did before, we have

$$|\mathbf{E}_H/\mathbf{E}_0|^2=\xi_0'/\xi_H'. \tag{59}$$

Now combining Eqs. (57) and (59), setting $\mu_0=2\pi k\Gamma F_0''$ we can express $\mu_n=4\pi K_0''$ as

$$\mu_n=\mu_0\left(\frac{\mathbf{E}_H^2+\mathbf{E}_0^2}{\gamma_H\mathbf{E}_H^2+\gamma_0\mathbf{E}_0^2}\right)\left[1\mp\left(\frac{|P|\mathcal{I}_H}{F_0''\mathcal{R}_H^{\frac{1}{2}}}\right)\frac{|\mathbf{E}_0||\mathbf{E}_H|}{|\mathbf{E}_0|^2+|\mathbf{E}_H|^2}\right]. \tag{60}$$

This is an intermediate expression for μ_n in terms of the field strengths. The absorption coefficient is more conveniently expressed if one uses a coefficient μ_s, taken with respect to the direction of the energy flow $\mathbf{S}$. That is, from expression (54)

$$\mu_S=\mu_n\cos(\mathbf{n},\mathbf{S}). \tag{61}$$

From (48) we have that $\mathbf{S}=|\mathbf{E}_0|^2\mathbf{s}_0+|\mathbf{E}_H|^2\mathbf{s}_H$ (Fig. 17) and the dot product of $\mathbf{S}$ with $\mathbf{n}$ gives

$$\mathbf{S}\cdot\mathbf{n}=|\mathbf{E}_0|^2\gamma_0+|\mathbf{E}_H|^2\gamma_H=|\mathbf{S}|\cos(\mathbf{n},\mathbf{S}). \tag{62}$$

The dot product of $\mathbf{S}$ with a unit vector $(\mathbf{u})$ lying in the diffracting planes, gives

$$\mathbf{S}\cdot\mathbf{u}=(|\mathbf{E}_0|^2+|\mathbf{E}_H|^2)\cos\theta=|\mathbf{S}|\cos\Delta, \tag{63}$$

where Δ is the angle between $\mathbf{S}$ and lattice planes. From (62) and (63) we have that

$$\cos(\mathbf{n},\mathbf{S})=\left(\frac{\gamma_0E_0^2+\gamma_HE_H^2}{E_0^2+E_H^2}\right)\frac{\cos\Delta}{\cos\theta}. \tag{64}$$

Substituting this into expression (61) and comparing with (60) for μ_n, we see that the direction cosines drop out giving

$$\mu_S=\mu_0\frac{\cos\Delta}{\cos\theta}\left(1\mp\frac{|P|\mathcal{I}_H}{F_0''\mathcal{R}_H^{\frac{1}{2}}}\frac{|E_0||E_H|}{|E_0|^2+|E_H|^2}\right). \tag{65}$$

A further simplification results if we introduce the parameter p, given by

$$p=(\tan\Delta)/(\tan\theta), \tag{66}$$

which is zero for the diameter points and goes to plus or minus one at the wings of the dispersion surface. From the geometry shown in Fig. 17 we see that

$$p=(|E_H|^2-|E_0|^2)/(|E_H|^2+|E_0|^2). \tag{67}$$

Substituting (67) into (65) we have

$$\mu_S=\mu_0\frac{\cos\Delta}{\cos\theta}\left(1\mp\frac{P\vartheta_H}{2F_0''\mathfrak{R}_H^{\frac{1}{2}}}\right)(1-p^2)^{\frac{1}{2}}. \qquad (68)$$

We see from (68) that the absorption coefficient of the wave field is indeed independent of incident conditions and is a function only of the angle Δ, between the direction of energy flow and the net planes. Since **S** is perpendicular to the real part of the dispersion surface at the tie point [Sec. 2.8B] this angle Δ is solely a property of the dispersion surface which is determined by the internal crystal structure.

We define a quantity ϵ as

$$\epsilon=\vartheta_H/2F_0''\mathfrak{R}_H^{\frac{1}{2}}. \qquad (69)$$

In order to reduce expression (69) to somewhat simpler terms, we recall that $F_H=F_H'+iF_H''$ where the primed quantity refers to the contribution from the real part of the *atomic* scattering factor, and the double primed to the contribution from the imaginary part. Since the structure factor may also be complex from the geometrical arrangement of the atoms and/or choice of origin, we have in detail that

$$\begin{aligned}F_H&=F_H'+iF_H''\\&=(F_H')_r+i(F_H')_i+i[(F_H'')_r+i(F_H'')_i],\\F_{\bar H}&=F_H'+iF_{\bar H}''\\&=(F_H')_r-i(F_H')_i+i[(F_H'')_r-i(F_H'')_i],\end{aligned}$$

and

$$\begin{aligned}F_HF_{\bar H}&=\mathfrak{R}_H+i\vartheta_H\\&=|F_H'|^2-|F_H''|^2+2i[(F_H')_r(F_H'')_r\\&\qquad+(F_H')_i(F_H'')_i].\end{aligned}$$

If the crystal structure is centrosymmetric and the origin for the structure factor is taken at a center of symmetry, then $(F_H')_i=(F_H'')_i=0$, and

$$F_H=(F_H')_r+i(F_H'')_r=F_{\bar H}=F_H'+iF_H'',$$

or

$$F_HF_{\bar H}=(F_H')^2[1-(F_H'')^2/(F_H')^2+2iF_H''/F_H'].$$

Generally, $F_H''<0.1F_H'$; therefore, neglecting the square, we have

$$\mathfrak{R}_H=(F_H')^2, \qquad \vartheta_H=2F_H'F_H''.$$

Making the same assumption for the general case gives

$$\mathfrak{R}_H=|F_H'|^2, \qquad \vartheta_H=2[(F_H')_r(F_H'')_r+(F_H')_i(F_H'')_i].$$

Hence, we have for the centrosymmetric case

$$\epsilon=F_H''/F_0'', \qquad (69a)$$

an expression which is also quite accurate for the general case.

Returning now to the symmetric Laue case, the effective absorption coefficient in the primary beam direction is given by $\mu_0(\text{eff})=\mu_s\cos\theta/\cos\Delta$ or

$$\mu_0(\text{eff})=\mu_0[1\pm|P|\epsilon(1-p^2)^{\frac{1}{2}}]. \qquad (70)$$

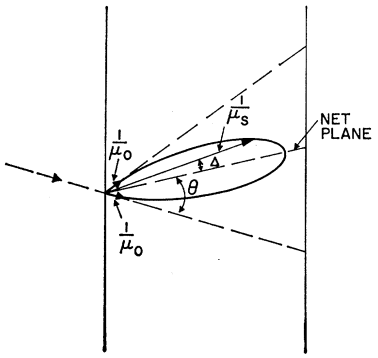

FIG. 18. Schematic representation of absorption associated with the points in the α branch as a function of the angle Δ, that the energy flow makes with respect to the atomic planes. The smallest absorption coefficient is for flow parallel to the net planes.

Equation (70) formally explains the Borrmann effect. For those reflections where all atoms scatter in phase, ϵ reduces to $[\Delta f''(2\theta)/\Delta f''(0)]$, the ratio of the imaginary part of the atomic scattering factor at diffracting angle 2θ to the value for forward scattering (we assume one atom type). This quantity usually departs only slightly from unity so that $\mu_0(\text{eff})$ for the σ polarization state ($P=1$) becomes zero or $2\mu_0$, for energy flow along the net planes ($p=0$). The wave field of the α branch (upper sign) thus traverses the crystal along the net planes with very low absorption. As the energy flows at greater angles to the net planes, the absorption coefficient increases arriving at the normal value, μ_0, when $p=\pm1$ and the energy flows either in the primary or diffracted beam directions. A schematic representation of absorption of the α branch in the general case [Eq. (68)] is given in Fig. 18 where the vectors in the x-ray fan are inversely proportional to the absorption coefficient. If the crystal is sufficiently thick, only those rays traveling parallel to net planes will survive and exit from the back face of the crystal.

We can now relate the absorption coefficient within the x-ray fan to the incident conditions. For simplicity, we restrict ourselves to the symmetric Laue case, ($b=+1$) and a centrosymmetric crystal. From (35) we have

$$|\mathbf{E}_H|/|\mathbf{E}_0|=e^{+v'}. \qquad (71)$$

From the definition of η for the symmetric Laue case (with $F_H''\ll F_H'$), Eq. (32) becomes

$$\eta=\sinh v=\frac{\Delta\theta\sin 2\theta}{\Gamma|P|F_H'}-i\frac{\Delta\theta\sin 2\theta F_H''}{\Gamma|P|F_H'}. \qquad (72)$$

Since $v=v'+iv''$,

$$\eta=\sinh v=\sinh v'\cos v''+i\cosh v'\sin v''. \qquad (73)$$

If we compare the imaginary parts of (72) and (73) we see that $\sin v''$ and hence, v'', are small quantities,

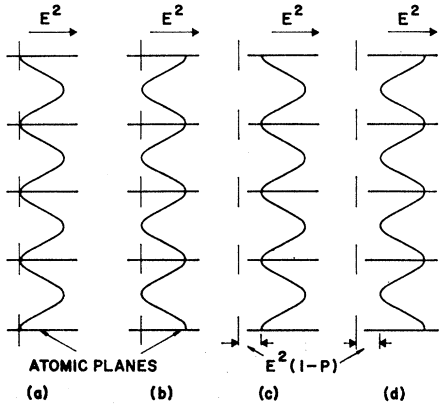

FIG. 19. Possible configurations of the standing wave patterns, assuming that the nodes of the α branch pattern, σ polarization, coincide with the atomic planes. (a) α branch, σ polarization (b) β branch, σ (c) α branch, π state (d) β branch, π state.

and to second order, $\cos v''$ is unity. We have, then

$$\eta' = (\sinh v)' = \sinh v' = (\Delta\theta \sin 2\theta)/\Gamma \mid P \mid F_{H'} \mid . \quad (74)$$

Comparing (71) with (65) we have

$$\frac{\mid \mathbf{E}_0 \mid\mid \mathbf{E}_H \mid}{\mathbf{E}_0^2+\mathbf{E}_H^2} = \frac{1}{e^{-v'}+e^{+v'}} = \frac{1}{2\cosh v'} = \frac{1}{2[1+(\eta')^2]^{\frac{1}{2}}},$$

and from (65), (67), (70), and (74)

$$\mu_0(\text{eff}) = \mu_0\{1 \mp \mid P \mid \epsilon/[1+(\eta')^2]^{\frac{1}{2}}\}. \quad (75)$$

From (74) we see that η' is a function of the angle between the incident beam and the exact Bragg angle. At the Bragg angle ($\Delta\theta=0$), (75) reduces to its extremal values and the energy flows along the net planes; while for $\mid \Delta\theta \mid$ large, the energy flows at the edges of the fan with the normal absorption coefficient. Comparing Eqs. (75) and (70) we see that as $\Delta\theta$ varies over the range of reflection (the order of seconds of arc), the energy flow direction varies through 2θ (the order of several degrees).

B. Physical Interpretation of Anomalous Absorption

(1) *Special Case*

The results of the formal derivation of the effective absorption coefficients for the different wave fields and different polarization states have a relatively simple explanation in terms of the positional dependence of the electric field intensity in the unit cells of the crystal. First, we show physically how the extremal values for the absorption coefficients arise. These values are those obtained formally from Eqs. (70) or (75) with $\eta'=\Delta=p=0$. In this case, for $F_H=F_{\bar{H}}$, the two coherent plane waves from a diameter point on a branch of the dispersion surface have amplitudes equal in magnitude, which for illustration are considered as real quantities. The total electric field is then the sum of the two coherent plane waves:

$$\mathfrak{E} = \exp(2\pi i\nu t)\mathbf{E}_0 \exp(-2\pi i\mathbf{K}_0\cdot\mathbf{r}) + \exp(2\pi i\nu t)\mathbf{E}_H \exp(-2\pi i\mathbf{K}_H\cdot\mathbf{r}). \quad (76)$$

These two waves add together to give a traveling wave moving along the bisector of the angle between $\mathbf{K}_0$ and $\mathbf{K}_H$, and a standing wave at right angles to this direction.

The field intensity, $\mathfrak{E}\cdot\mathfrak{E}^*$ is

$$\text{(a)} \quad \mid \mathfrak{E} \mid^2 = \mid \mathbf{E}_0 \mid^2 + \mid \mathbf{E}_H \mid^2 + 2\mathbf{E}_0\cdot\mathbf{E}_H \cos 2\pi\mathbf{H}\cdot\mathbf{r}$$

$$\text{(b)} \quad = 2 \mid \mathbf{E}_0 \mid^2 (1 \pm P \cos 2\pi\mathbf{H}\cdot\mathbf{r}), \quad (77)$$

where we have set $\mathbf{K}_0+\mathbf{H}=\mathbf{K}_H$ and $\mathbf{E}_0\cdot\mathbf{E}_H = P \mid \mathbf{E}_0 \mid^2$ and where $P=1$ for the σ and $\cos 2\theta$ for the π states of polarization. The ($\pm$) sign takes into account the two cases where the two plane waves have relative phases of zero or π.

We see from (77) that planes of constant intensity, i.e., the standing-wave pattern, occur when $\mathbf{H}\cdot\mathbf{r}=$ const, and hence, are parallel to the diffracting planes and are spaced $d_{hkl} = \mid H \mid^{-1}$ apart. From the field intensity we can see simply why anomalous absorption can occur. The photoelectric absorption of an atom is proportional to the electric field intensity at the atom. If nodal planes of the electric field are coincident with the atoms of the diffracting planes, much smaller than normal absorption occur. On the other hand, if the antinodal planes are at the atom sites an anomalously high absorption takes place. In Fig. 19 we give a schematic representation of the distribution of electric field intensity for the four possible cases described by (77). Figure 19a represents the σ polarization state ($P=1$), for the situation where true nodal planes of the field from one branch of the dispersion surface coincide with the planes of atoms and (b) is the field from the other branch where antinodes are at the atoms. (a) is then the case of minimum and (b) that of maximum absorption. In (c) and (d), the corresponding situations for the π polarization are shown.

Note that the $P=\cos 2\theta$ term prevents the electric field from going to zero at the atomic planes. We can see then, in terms of the field distribution, that even for the branch which produces nodes at the atoms, there is a higher absorption for the π state of polarization than for the σ state.

For both states of polarization the Poynting's vector, $\mathfrak{E}\times\mathfrak{K}^*$ has true nodal planes, so that the average energy flow in all the cases depicted in Fig. 19 is along the atomic planes. Of course, the nodal pattern aspects of the two coherent waves of equal amplitude and frequency are perfectly general, and are not the result just of the dynamical diffraction theory.

(2) *Relation Between Atomic Planes and Nodal Planes of the Wave Field*

In the section above, we merely assumed that the nodal planes were coincident with the atom planes and

that all the planes of atoms were also nodal planes of the electric field intensity. In this section, we investigate this in more detail. In the general case, the electric field associated with each tie point again is the sum of two plane waves with complex phase relationships between them. The field for a single point can be written, from Eq. (42) as

$$\mathfrak{E}=\exp(2\pi ivt)\exp(-2\pi i\mathbf{K}_0\cdot\mathbf{r})\mathbf{E}_0 \times[1+(E_H/E_0)\exp(2\pi i\mathbf{H}\cdot\mathbf{r})], \quad (78)$$

where E_H and E_0 are complex amplitudes.

The field intensity from (78) is proportional to a quantity R, defined as

$$R=|1+(E_H/E_0)\exp(2\pi i\mathbf{H}\cdot\mathbf{r})|^2. \quad (79)$$

As before, we see that planes of constant intensity, $R=$ const, are parallel to the diffracting planes and periodic in the d spacing of the (hkl) reflection involved.

It is obvious that the relationship between the position of the nodal planes and the atomic planes must be invariant with respect to the choice of origin for the position vector $\mathbf{r}$. We see from (79) that $\mathbf{r}$ appears directly in the exponential and indirectly in the ratio E_H/E_0, since the latter by (24) depends on the structure factor, which is affected by the choice of origin.

We can conveniently arrive at the position of any nodal planes, $R=0$, by making use of the invariance with respect to choice of origin. First assume that a nodal plane exists, then let the origin of $\mathbf{r}$ be in this plane and see what restrictions are imposed on E_H/E_0, and the structure factor, to make $R=0$. From (79) it follows that we must have $E_H/E_0=-1$ for R to have a zero value when $\mathbf{r}=0$. Unless a choice of origin can be found for the structure factor such that $E_H/E_0=-1$, no nodal planes exist. For the Laue case ($b=+1$) the ratio of field amplitudes (35) is

$$\frac{E_H}{E_0}=\mp\frac{|P|}{P}\frac{[F_HF_{\bar{H}}]^{\frac{1}{2}}}{F_{\mathrm{H}}}e^{\pm v}. \quad (80)$$

If the crystal has a center of symmetry then $F_H=F_{\bar{H}}$, if the origin is chosen at a symmetry center. Under these conditions, (80) equals unity only when the exact Bragg conditions are satisfied ($v=0$). R equals zero for one branch and has a maximum value for the other. The sign of E_H/E_0 determines which branch produces the nodal or antinodal plane passing through the center of symmetry; although the minimum absorption is always associated with the α branch. For example, for the (220) type of reflection in the diamond structures, $F_{220}=-8f$ and the α branch [upper sign in (80)] has an antinodal plane at the center of symmetry while the β field produces a node. For the (440) reflection $F_{440}=+8f$ and the α branch has the node. In both cases, reference to the actual structure shows that the α branch suffers the least absorption.

Generally, the strongest anomalous transmission occurs when all of the atoms in the crystal lie on nodal planes of the electric field intensity. Since the spacing of the nodal planes is $d(hkl)$ it follows that only those reflections for which *all* the atoms scatter in phase, and hence lie in the planes of the set (hkl) can satisfy this condition. We call these reflections *full* reflections. Invoking the invariance with respect to choice of origin, we now let $\mathbf{r}=0$ at an atom position and, as before, a node occurs at the atom if $E_H/E_0=-1$. Because all atoms are in phase in full reflections, $F_H=F_{\bar{H}}$ when the origin for the structure factor is taken at an atom, and F_{H} is positive. According to (79), only the α branch has nodal planes through the origin atom, and hence, through all the atoms of the crystal. The wave field of the β branch produces antinodes at all the atoms of the crystal and thus is highly absorbed.

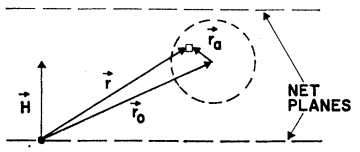

FIG. 20. Geometry used to calculate the absorption of an atom in a standing-wave pattern.

We can sum up these results as follows:

(a) Regardless of crystal symmetry, the maximum anomalous transmission occurs for those reflections where all the atoms scatter in phase.

(b) The wave field with least absorption is described by a point on the branch of the dispersion curve nearest the Laue point (L). This condition was first pointed out by Ewald.

(c) For centrosymmetric crystals, the symmetry center is on a nodal plane with the nodes of the other field $\frac{1}{2}d(hkl)$ away. The branch of the dispersion surface producing the node at the center of symmetry depends upon the reflection involved.

(3) *Calculation of the Absorption Coefficient in the General Case and the Physical Significance of* ϵ

We now generalize our qualitative treatment for the case where the energy flow is not parallel to the diffracting planes and see how the actual absorption coefficient of an atom depends upon its position in the wave field.

The wave field is again assumed to be the sum of two coherent plane waves of real amplitude $\mathbf{E}_0$ and $\mathbf{E}_H$ which are not necessarily equal. $\mathbf{E}^2$ is still given by (77a) or (78) since $\mathbf{K}_0+\mathbf{H}=\mathbf{K}_H$. For convenience in calculation we use complex notation (remembering that we are only concerned with the real part) and (77a) becomes

$$|\mathfrak{E}|^2=|\mathbf{E}_0|^2+|\mathbf{E}_H|^2+2\mathbf{E}_0\cdot\mathbf{E}_H\exp(-2\pi i\mathbf{H}\cdot\mathbf{r}). \quad (81)$$

In Fig. 20 let $\mathbf{r}_0$ be the position of the nucleus of an atom in the wave field and $\mathbf{r}$ the vector to the volume dv. Let $'\mu(\mathbf{r}_a)\,dv$ be the contribution to the average absorption coefficient of the volume dv of the atom, i.e., $\mu_0=\int\mu(\mathbf{r}_a)\,dv$. Assuming that the absorption co-

efficient at any point in the wave field is proportional to $|\mathfrak{E}|^2$, the absorption coefficient of the atom at $\mathbf{r}_0$ in the field is

$$\begin{aligned}
&(a)\quad \mu(\mathbf{r}_0) = T\int \mathfrak{E}^2(\mathbf{r})\mu(\mathbf{r}_a)\,dv \\
&(b)\quad = T\{(\mathbf{E}_0^2+\mathbf{E}_H^2)\int \mu(\mathbf{r}_a)\,dv \\
&\qquad +2\mathbf{E}_0\cdot\mathbf{E}_H\int \exp(-2\pi i\mathbf{H}\cdot\mathbf{r})\mu(\mathbf{r}_a)\,dv\} \\
&(c)\quad = T\{(\mathbf{E}_0^2+\mathbf{E}_H^2)\mu_0+2\mathbf{E}_0\cdot\mathbf{E}_H \exp(2\pi i\mathbf{H}\cdot\mathbf{r}_0) \\
&\qquad \times\int \exp(2\pi i\mathbf{H}\cdot\mathbf{r}_a)\mu(r_a)\,dv\} \qquad (82)
\end{aligned}$$

where the integral is over the volume of the atom and T is a proportionality constant. The average of $\mu(\mathbf{r}_0)$ taken over all positions in the field gives the average absorption coefficient of the atom μ_0, and the proportionality constant becomes $T=(E_0^2+E_H^2)^{-1}$. If the last integral in (82c) is abbreviated as μ_{0H} and we take the atom in the plane $\mathbf{H}\cdot\mathbf{r}_0=0$, (82c) gives the absorption coefficient in the field of (81):

$$\mu=\mu_0\left(1\pm P\frac{2|\mathbf{E}_0||\mathbf{E}_H|}{\mathbf{E}_0^2+\mathbf{E}_H^2}\frac{\mu_{0H}}{\mu_0}\right) \qquad (83)$$

where we have set $\mathbf{E}_0\cdot\mathbf{E}_H=\pm P|\mathbf{E}_0||\mathbf{E}_H|$.

We now make a comparison of the formal results in Sec. 2.10A. Combining (70) and (67) of that section, we have

$$\mu=\mu_0\left(1\mp|P|\frac{2|\mathbf{E}_0||\mathbf{E}_H|}{\mathbf{E}_0^2+\mathbf{E}_H^2}\epsilon\right) \qquad (84)$$

from the formal theory.

We see that (84) has the identical functional form as (83) which was derived simply from the absorption of a pair of coherent plane waves by an atom. Thus, the variation of absorption coefficient with the angle of propagation of energy flow in the x-ray fan can be explained in the same way as the extremal values obtained when the energy flow is parallel to the net planes. As the energy flows at greater angles from the net plane, $|E_H|/|E_0|$ departs further from unity, and the electric field at the atom will increase from zero for the α branch while it decreases from its maximum for the β branch. When the deviation of $|E_H|/|E_0|$ from unity is very large, the energy flows in either the primary or diffracted beam directions and μ approaches μ_0 for either branch.

Comparing (83) and (84) also gives us a feeling for the physical significance of ϵ. We see that our semiquantitative treatment relates ϵ with the quantity μ_{0H}/μ_0 which, defined in (82c) is related to the weighted distribution of absorbing power within the atom.

(4) *Effect of Thermal Vibrations*

It is apparent from the above treatment that the effective value of ϵ depends on the thermal vibrations of the atoms. Very simply, the larger the amplitude of vibration the more deeply the atom penetrates into the higher field intensities and the greater is the absorption. At the present time, however, no rigorous theoretical treatment is available to describe quantitatively the effect of thermal vibrations on ϵ.

Experiments have recently been performed to obtain the temperature dependence in anomalous transmission.[20,21] Okerse[21] has shown the temperature dependence behaves simply as the Debye–Waller factor, i.e.,

$$\epsilon=\epsilon_0 e^{-M}, \qquad (85)$$

where M is the usual factor related to the mean square amplitude of vibration. This is suggested by the expression $\epsilon=F_H''/F_0''$ if one naively assigns a Debye–Waller factor to F irrespective of where it appears.

Batterman has shown[20] that such a form for ϵ can be obtained from a derivation similar to that in the above section, by allowing $\mathbf{r}_0$, the position of the center of the atom, (Fig. 20) to vary periodically as in thermal motion. The derivation however, is not rigorous. There is also the question whether the nodal planes of the wave fields are themselves vibrating with respect to the static lattice.

If one treats the evaluation of ϵ_0 classically[22] one can readily show that ϵ_0 is related to the distribution of absorbing power in the atom [as in the physical interpretation of (83)] directly through the form factor of those electrons in the atom which photoelectrically absorb the x rays. However, experiment indicated that the variation of ϵ_0 with $\sin\theta/\lambda$ is much less than one would expect from the form factor and implied that a quantum mechanical treatment was necessary. Such a calculation was made by Wagenfeld[23] who extended Hönl's original treatment of anomalous dispersion. The new theoretical results were in much better agreement with experiment than that obtained classically. We thus have direct experimental and theoretical verification that the imaginary part of the atomic scattering factor has only a small variation with scattering angle. We give a more detailed discussion of this variation in Appendix C.

2.11 EXIT BEAMS

A. Boundary Conditions on Exit Surface

The wave vectors of those rays which exit the crystal must have exit points on the spheres which pass through the L point. The entrance condition of continuity of wave fronts selected the active tie points on the dispersion surface. In a similar manner, the tie points of the exit beams are selected to maintain equal tangential components of the wave vectors of the internal and external beams. This is illustrated in Fig. 21.

For simplicity, we have indicated only one of the polarizations of the α branch.

---

[20] B. W. Batterman, Phys. Rev. **126**, 1461 (1962).
[21] B. Okkerse, Philips Res. Rept. **17**, 464 (1962).
[22] B. W. Batterman, J. Appl. Phys. **32**, 998 (1961).
[23] H. Wagenfeld, J. Appl. Phys. **33**, 2907 (1962).

The tie point A was selected by the incident wave vector $\mathbf{k}_0{}^i$, by constructing from the entrance point P, a line along the normal $\mathbf{n}$ to the entrance surface. The intersection of the exit surface normal $\mathbf{n}_e$ through A with the spheres about (000) and (*hkl*) define termini of the exit beam wave vectors; viz: a forward diffracted wave $\mathbf{k}_0{}^e$ and a diffracted wave $\mathbf{k}_H{}^e$. It follows then that, in general, each branch of the dispersion surface produces two exit waves and that, in general, eight exit waves are produced, four of each polarization. For the case of Laue diffraction where the exit surface is taken to be a plane parallel to the entrance surface, $\mathbf{k}_0{}^e$ (exit) are the same as $\mathbf{k}_0{}^i$ (entrance), since the exit point for the forward diffracted beam coincides with the entrance point P.

The choice of boundary conditions on the field amplitudes depends on whether or not the outgoing beams overlap physically at the exit Laue surface. For the practical cases usually encountered in Laue diffraction, the incident beam cross section is small compared to the path length in the crystal so that the internal waves do indeed travel separately in the crystal and do not overlap at the exit surface. This is a departure from the infinite plane wave we have heretofore considered. It allows us now to treat each internal wave separately so that intensities rather than amplitudes are added for the exit beams.

A generalized ray diagram is shown in Fig. 22 for a reasonably symmetric Laue case, for a parallel-sided crystal slab. The incident ray $\mathbf{k}_0{}^i$ is assumed slightly off the Bragg angle but within the range of reflection $(\Delta\theta)_w$. This ray produces the two flows, $\mathbf{S}_\alpha$ and $\mathbf{S}_\beta$ which, if not completely absorbed, arrive at the exit surface and split into the diffracted beam and the forward diffracted beam. We thus see that the intensity of each exit beam is composed of the sum of the intensities for the two associated interior wave fields, if the fields do not overlap. That is, again assuming that the fields just inside the boundary equal the fields just outside, we have for the diffracted beam intensity

$$|\mathbf{E}_H{}^e|^2 = |\mathbf{E}_{H\alpha}|^2 + |\mathbf{E}_{H\beta}|^2 \qquad (86)$$

evaluated over the exit surface. A corresponding expression holds for the forward diffracted beam and each

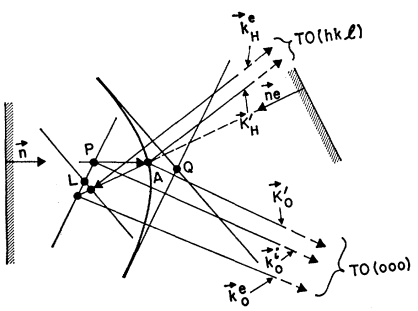

FIG. 21. Determination of exit wave vectors $\mathbf{k}_0{}^e\mathbf{k}_H{}^e$ in the Laue case.

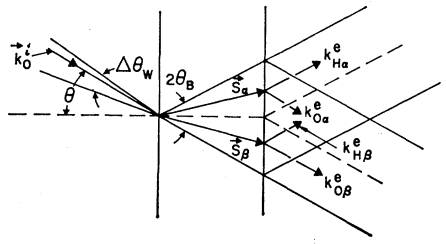

FIG. 22. Ray diagram of energy flows for small cross section, divergent, input beam.

polarization state. If the fields do overlap, then

$$|\mathbf{E}_H{}^e|^2 = |\mathbf{E}_{H\alpha}+\mathbf{E}_{H\beta}|^2. \qquad (87)$$

The evaluation of this expression is essentially the same as that encountered in discussing Pendellösung, and its value varies with crystal thickness, as is discussed in the section to follow.

B. Field Amplitudes at Exit Face

We discuss qualitatively the nature of the fields at the exit surface, using again, the symmetric Laue case for illustration. The Bragg case is considered in Sec. 3.0.

Since the ratios of the field amplitudes are fixed by the tie points selected, and their relative values are set by the entrance conditions on the field amplitudes, the only way the fields at the exit surface can differ from those at the entrance surface is through absorption losses or Pendellösung effects. That is, the diffracted beams exist at the entrance surface and then suffer some changes or attenuation in passing through the crystal.

If the crystal is very thin with respect to a Pendellösung period, then, using the entrance conditions (40), and the exit conditions (87), we see that there is no diffracted beam. As the crystal thickens until it is one-half of a Pendellösung period thick, as we have seen in Sec. 2.8A, all of the energy for the ray making the exact Bragg angle is flowing in the *diffracted* beam direction. This energy flow becomes progressively smaller with greater deviation from the exact Bragg angle. There thus is an intense, narrow (angle-wise) diffracted beam giving a certain integrated intensity. When the crystal gets to be a full Pendellösung period thick, there again is no diffracted beam. This oscillation in diffracted intensity with thickness keeps up until absorption kills the β field, or the fields separate physically, or irregularities in the thickness produces an averaging effect. The averaging effect of the thickness irregularities, mathematically, is equivalent to separation of the flows. Thus one goes, as the crystal thickens, from exit condition (87) to exit condition (86), where the diffracted beam intensity is made up of the sum of the intensities of the α field and the β field.

Because of the absorption factor, all fields eventually die out with increasing thickness. Thus, physically,

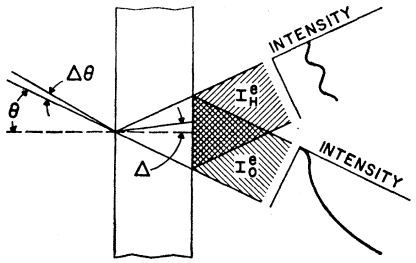

FIG. 23. Energy distribution, as calculated by Kato, across exit beams for small cross section, divergent, input beam. ($\mu_0 t \approx 2$).

there is some thickness at which the experimentally observed diffracted intensity is maximum. Zachariasen shows that the expressions for the integrated intensity in this physically thin region agree with those of the kinematical theory. Since, in the kinematical theory, the crystal thickness for maximum diffracted intensity is the reciprocal of the linear absorption coefficient ($t_m = 1/\mu_0$), which generally speaking, is ten or so Pendellösung periods, we would expect that normally the kinematical theory is still applicable up to about this thickness. We treat, however, in detail, the case where the product $\mu_0 t$ is indeed zero; but we assume in the next sections that t itself is large enough to permit use of exit condition (86).

With respect to the exit beams, we are interested in three aspects, namely: (1) what is the spatial intensity distribution across the beams within the 2θ fan of Fig. 22; (2) what is the shape of the rocking curve, i.e., intensity vs rocking angle; and (3) what is the integrated intensity. We consider these points in the above order.

C. Intensity Distribution Along Exit Face (Special Case)

The energy distribution along the exit face for the case of small incident beam cross section has been considered in detail by Kato.[24] We qualitatively discuss some interesting aspects of his results. The essential parameters are given in Fig. 23.

The incident beam is assumed to have uniform power per increment of $\Delta\theta$ within the incident angular range for reflection. The parameter along the exit surface is given by $p = \tan\Delta/\tan\theta$ such that $p = \pm 1$ corresponds to either end of the x-ray fan. The distribution of energy at the exit surface for different values of $\mu_0 t$ calculated for the forward diffracted and diffracted beams is given in detail in Fig. 24, but we have schematically shown the distribution in Fig. 23 for $\mu_0 t \approx 2$. The forward diffracted beam is most intense along the edge closest to the incident direction, and its intensity falls off in the direction of the diffracted beam. The diffracted beam has "hot edges."

In Fig. 24 we see the diffracted beam distribution in more detail. For thin crystals ($\mu_0 t \approx 0$) the edges of the beam have greater intensity than the center. The reason for this can be seen qualitatively by referring to Fig. 11. If we have a uniform distribution of incident points P we have a "pile up" of Poynting vectors $\mathbf{S}$ (which are normal to the curve) in the $\mathbf{s}_0$ and $\mathbf{s}_H$ directions because of the curvature of the dispersion surface. Since for thin crystals there is little absorption to attenuate this flow near the edges of the fan, the power is predominantly shifted to the beam edges. As the crystal gets thicker and absorption becomes more important, we see from the variation of absorption coefficient in the fan (Fig. 18) that the central region remains strong but the wings die out and in Fig. 24(a) the distribution for $\mu_0 t = 10$ is peaked in the central region. This explains the phenomenon of "double Laue spots" that has puzzled investigators for some 30 years. In a transmission Laue photograph of a relatively thin crystal it had been observed that some of the diffraction spots appeared double. It was originally thought that the effect was due to mosaic layers on the faces of the crystal giving enhanced diffraction. We can see now that this is a dynamical effect due to the curvature of the dispersion surface producing enhanced diffracted intensity at the edges of the x-ray fan.

In Fig. 24(b) we see that the transmitted or forward diffracted beam is asymmetric even for crystals as thick as $\mu_0 t = 10$. It is only for considerably thicker crystals that the diffracted and forward diffracted beams are of identical shape and intensity.

D. Diffracted Intensities: Laue Case

Using the boundary conditions (86) where the exit fields are separated, the intensity of the waves described by Eqs. (42) at the exit surface ($\mathbf{r} = \mathbf{r}_e$) is given by:

$$\text{(a)}\quad \frac{I_{0w}{}^e}{I_0} = \frac{|\mathbf{E}_{0w}|^2}{|\mathbf{E}_0{}^i|^2} = \frac{1}{4}\frac{e^{-2v'}}{|\cosh v|^2}\exp(-4\pi\mathbf{K}_{0w}''\cdot\mathbf{r}_e)$$

$$\text{(b)}\quad \frac{I_{Hw}}{I_0} = \frac{|\mathbf{E}_{Hw}|^2}{|\mathbf{E}_0{}^i|^2} = \frac{1}{4}\frac{|b|}{|\cosh v|^2}\exp(-4\pi\mathbf{K}_{Hw}''\cdot\mathbf{r}_e) \qquad (88)$$

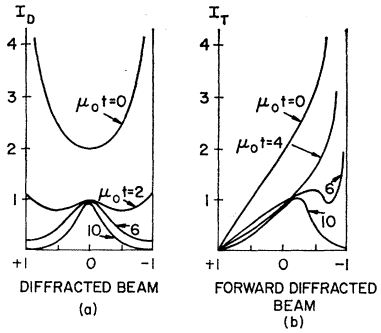

FIG. 24. After Kato. Energy distribution across diffracted beam (a) and forward diffracted beam (b) for the situation of Fig. 22, with respect to $\mu_0 t$. Note that for small $\mu_0 t$, the diffracted beam has "hot edges," a result of the curvature of the dispersion surface.

[24] N. Kato, Acta Cryst. **13**, 349 (1960).

where w represents a particular polarization of either the α or β branch, I_0 the corresponding incident intensity associated with that polarization and where for the diffracted beam we have set $|[F_H F_{\bar{H}}]^{\frac{1}{2}}/F_{\bar{H}}|=1$.

For the *symmetric* Laue case which we discuss in some detail, these can be expressed in terms of the incident conditions through η' using the approximations discussed in Eq. (73). The absorption coefficient, $4\pi K_{0w}''$, is also given in terms of η' by expression (75). Thus:

$$\text{(a)}\quad \frac{I_{0w}^{e}}{I_0}=\frac{1}{4}\left(1\mp\frac{\eta'}{[1+(\eta')^2]^{\frac{1}{2}}}\right)^2 \times \exp\left[-\frac{\mu_0 t_0}{\gamma_0}\left(1\mp\frac{|P|\epsilon}{[1+(\eta')^2]^{\frac{1}{2}}}\right)\right],$$

$$\text{(b)}\quad \frac{I_{Hw}}{I_0}=\frac{1}{4}\frac{1}{1+(\eta')^2}\exp\left[-\frac{\mu_0 t_0}{\gamma_0}\left(1\mp\frac{|P|\epsilon}{[1+(\eta')^2]^{\frac{1}{2}}}\right)\right], \quad (89)$$

where t_0 is the thickness of the crystal, the negative sign refers to the α field and η' is related to the relative angle of incidence, $\Delta\theta$ by

$$\eta'=(\Delta\theta\sin 2\theta)/|P|\Gamma|F_{H'}|. \quad (90)$$

Expressions (89) give the theoretical rocking curve line shapes on an η' scale. Conversion to the usual θ scale is made through (90); this is a linear relationship. The integrated intensity is the area under the curves given by (89). We discuss the line shapes first. A more complete discussion of the effect of the various parameters on the line shape and integrated intensities is to be found in the article by Hirsch.[6]

(1) *Rocking Curve Line Shape: Symmetric Laue Case*

Diffracted beam. From Eq. (89) we see that if $\mu_0 t \ll 1$, the so-called thin crystal case, then radiation from both the α and β branches is present in the diffracted beam, and on the η' scale, the peak shape is given by the simple expression:

$$I_H(\alpha+\beta)/I_0(\sigma \text{ or } \pi)=\tfrac{1}{2}\{1/[1+(\eta')^2]\}. \quad (91)$$

This is shown as the upper curve in Fig. 25. For radiation making the correct Bragg angle ($\eta'=0$; $\Delta\theta=0$), $I_H/I_0=\frac{1}{2}$, and all the crystal does is act as a beam splitter, for each polarization state, diverting one-half of the incident beam into the diffracted beam. This is true independent of the structure factor or strength of the reflection, but like all peak height effects, it is difficult to observe. It should be noted that this limiting form for $\mu_0 t \ll 1$ is not reached by allowing $t\to 0$. Obviously, as $t\to 0$, $I_H\to 0$ since there is no crystal to do any diffracting. Equations (88) are valid only when the crystal is large enough so that physical separation of the wave fields can take place. The limit $\mu_0 t\to 0$ is arrived at by keeping t sufficiently large and allowing the absorption to approach zero.

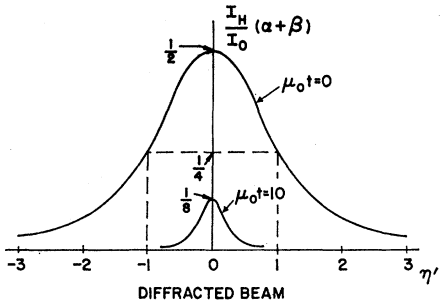

FIG. 25. Peak shape on an η' scale, for the diffracted beam in the symmetric Laue case as a function of $\mu_0 t$. Since η' is a linear function of $\Delta\theta$, this is also essentially a plot as a function of $\Delta\theta$.

The integrated intensity (the observable) does depend on F_H through the peak width. The half-width Ω on the η' scale is $\Omega=2$ or on the θ scale

$$(\Delta\theta)_\Omega=2|P|\Gamma|F_{H'}|/\sin 2\theta. \quad (92)$$

We see from (89b) that as $\mu_0 t$ gets very large, that is, $\mu_0 t>10$, radiation associated with the β branch of both polarization states generally is completely absorbed and for the α branch the π polarization state ($P=\cos 2\theta$) usually also is completely absorbed, so, at most, for an *unpolarized* I_0, $\frac{1}{8}$ of I_0 appears in I_H at the peak height. For $\mu_0 t>10$, the thick crystal case, (89b) thus reduces to

$$\frac{I_H(\alpha,\sigma)}{I_0}=\frac{1}{8}\frac{1}{1+(\eta')^2}\exp\left[-\frac{\mu_0 t_0}{\gamma_0}\left(1-\frac{\epsilon}{[1+(\eta')^2]^{\frac{1}{2}}}\right)\right]. \quad (93)$$

This is represented by the lower curve in Fig. 25 where we have assumed $\epsilon\approx 1$ so that $I_H/I_0=\frac{1}{8}$ at $\Delta\theta=0$. The absorption term in (93) sharpens up the peak. If (93) or the more general expression (89b) has appreciable value only for $(\eta')^2\ll 1$, then for an unpolarized I_0, for either polarization state it may be approximated by

$$\frac{I_H(\alpha)}{I_0}=\frac{1}{4}\exp\left[-\frac{\mu_0 t_0}{\gamma_0}(1-|P|\epsilon)\right] \times \exp\left[-\frac{\mu_0 t_0}{\epsilon_0}|P|\epsilon\frac{(\eta')^2}{2}\right]. \quad (94)$$

The peak drops to half its value when

$$\tfrac{1}{2}(\mu_0 t_0/\gamma_0)|P|\epsilon(\eta')^2=\ln 2,$$

and so the half-width, on the θ scale, is given by

$$(\Delta\theta)_\Omega=\frac{2|P|\Gamma|F_{H'}|}{\sin 2\theta}\left[\frac{2\ln 2}{|P|\epsilon(\mu_0 t_0/\gamma_0)}\right]^{\frac{1}{2}}. \quad (95)$$

Forward-diffracted beam. The line shape of the forward-diffracted beam is best understood by considering the α and β branch contributions separately. For the thin crystal case where $\mu t\to 0$ (89a) may be written

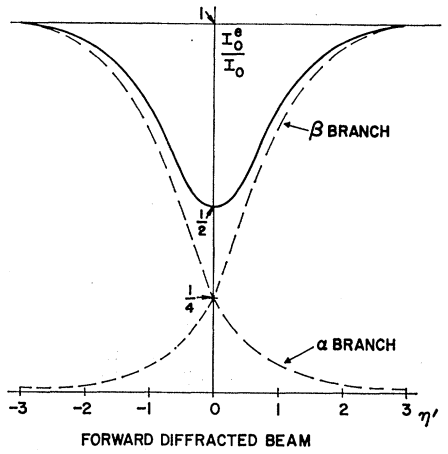

FIG. 26. Peak shape, on an η' scale, for the forward diffracted beam, symmetric Laue case, for zero absorption. The contribution from the points on the individual branches of the dispersion surface are shown dotted.

for each polarization state, as

$$\frac{I_0^e(\sigma \text{ or } \pi)}{I_0}=\frac{1}{4}\left(1-\frac{\eta'}{[1+(\eta')^2]^{\frac{1}{2}}}\right)^2 +\frac{1}{4}\left(1+\frac{\eta'}{[1+(\eta')^2]^{\frac{1}{2}}}\right)^2. \quad (96)$$

The first term on the right represents the α branch and the second the β branch. The behavior of these terms as a function of (η') is shown dotted in Fig. 26. The solid curve is the sum. For η' large and negative, we get 100% transmission described by a tie point on the α branch. At $\eta'=0$, ($\Delta\theta=0$), the forward-diffracted beam is $(\frac{1}{2})I_0$, one-quarter contributed by each branch. For η' large and positive, the point on the β branch describes the whole process. The solid curve of Fig. 26, the sum of the dotted curves, is merely the equivalent curve ($\mu_0 t \ll 1$) of Fig. 25 turned upside down.

As $\mu_0 t$ increases, (89a) goes through an interesting sequence. The β contribution dies out faster than the α contribution, and the wings of Fig. 26 die out faster than the middle. The result is shown schematically in Fig. 27. At intermediate values of $\mu_0 t$, there is an asymmetrical sum curve as shown by the middle curve in Fig. 27.

As $\mu_0 t$ becomes larger than 10, the thick crystal case, only the σ polarization state of the α branch remains, and

$$\frac{I_0^e(\alpha,\sigma)}{I_0}=\frac{1}{8}\left(1-\frac{\eta'}{[1+(\eta')^2]^{\frac{1}{2}}}\right)^2 \times \exp\left[-\frac{\mu_0 t_0}{\gamma_0}\left(1-\frac{\epsilon}{[1+(\eta')^2]^{\frac{1}{2}}}\right)\right]. \quad (97)$$

which is the same as (93) for I_H/I_0, except for a slight asymmetry with respect to η' due to the coefficient before the exponential. That is, the forward diffracted beam peaks at a slightly negative value of η'. As $\mu_0 t$ increases, the values of η' for which (97) has appreciable values become much less than unity, so that the forward-diffracted beam and the diffracted beam become equivalent.

(2) *Integrated Intensities*

The integrated intensity is usually measured by rocking through θ. On the θ scale, this quantity ρ_H is given by

$$\rho_H=\int\frac{I_H A}{I_0 A_0}\,d\theta, \quad (98)$$

where A, A_0 are cross sections of the beams. For the symmetric Laue case, the cross sections are equal. Converting the intensity ratios on the η' scale to a θ scale is more difficult than changing the integration parameter in (98) from θ to η'. We thus calculate ρ_H using

$$\rho_H=\int\frac{I(\eta')}{I_0'}\frac{d\theta}{d\eta'}\,d\eta'=\left(\frac{d\theta}{d\eta'}\right)\int\frac{I(\eta')}{I_0}\,d\eta',$$

where, from (90),

$$d\theta/d\eta'=|P|\Gamma|F_H'|/\sin 2\theta. \quad (99)$$

Diffracted beam: symmetric Laue case. For the thin crystal case, integration of (89b) with respect to η', (the area under the upper curve in Fig. 25) gives $\rho_H(\eta')=\frac{1}{4}\pi$ for each polarization state; then from (99)

$$\rho_H=(|P|\Gamma|F_H'|/\sin 2\theta)\tfrac{1}{4}\pi. \quad (100)$$

This is the integrated intensity for a perfect nonabsorbing crystal for the stated polarization state, in symmetric Laue diffraction, and it corresponds to the Darwin expression for the Bragg case. It is equal in value to one-half the integrated intensity in the Bragg case.

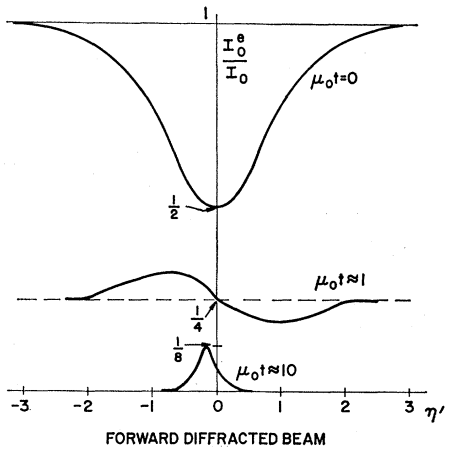

FIG. 27. Peak shape, on an η' scale, for the forward diffracted beam, symmetric Laue case, as a function of $\mu_0 t$. The lower curve is the anomalous transmission.

For the thick crystal, numerical integration of (89b) should be carried out for precision results. However, using the approximate expression, Eq. (94) which can be integrated directly, we have for each polarization state

$$\rho_H = \frac{|P|\Gamma|F_H|}{4\sin 2\theta}\left[\frac{2\pi}{|P|\epsilon(\mu_0 t_0/\gamma_0)}\right]^{\frac{1}{2}} \times \exp\left[-\frac{\mu_0 t_0}{\gamma_0}(1-|P|\epsilon)\right]. \quad (101)$$

This expression is usually quite adequate for survey studies of the Borrmann effect and applies to the forward-diffracted beam as well as to the diffracted beam. Although the effective absorption coefficient in (101) may be zero for the σ polarization state and α branch, the integrated intensity for this state does differ from that of the true no-absorption case, expression (100). As long as $\mu_0 t$ is finite, the peak shape is sharpened by an exponential dependence on η'.

Forward-diffracted beam. For the thick crystal, Eq. (101) usually satisfactorily indicates the values obtainable from a numerical integration of (89a). It should be noted from Fig. 27 for thinner crystals, that if exp $(-\mu_0 t)$ is measurable, a uniform contribution of this amount should be subtracted, otherwise the integral is infinitely large. Thus, for the thin crystal case, the integrated intensity for the forward-diffracted beam is the "negative" of that of the diffracted beam.

A detailed discussion concerning the numerical evaluation of both diffracted and forward diffracted beams is given in the Appendix.

3.0 THE BRAGG CASE

For the Bragg case of reflection, the diffracted beam exits from the same face that the incident beam enters. This is the classic case, picked by Darwin in 1914, who was the first to investigate scattering from a perfect crystal. His treatment was geometrical in that he considered partial scattering and transmission through a plane of atoms and took into account the fact that rays Bragg-scattered from lower planes satisfied the reflection condition for backscattering from the upper planes. He therefore did consider the dynamical problem simply and clearly, and his results are correct. However, the dynamical theory, as subsequently developed by Ewald and von Laue, gives not only Darwin's results but develops a description of the distribution of x-ray energy inside the crystal and permits inclusion of the effects of absorption in a straightforward way.

Although the Bragg case was treated historically before the Laue case, we approach it in terms of the dispersion surfaces and the point of view developed in the previous sections primarily for the Laue geometry. In Fig. 28, the vertical surface on the left represents the familiar symmetric Laue entrance surface, and the

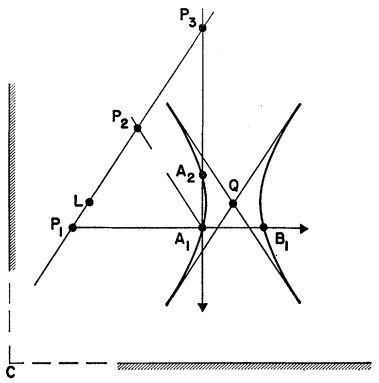

FIG. 28. Boundary conditions for the symmetric Laue case and for the symmetric Bragg case. Note that the tie points selected by a given set of incident conditions in the Bragg case lie on only one branch of the dispersion surface.

tie point A_1 is selected by the entrance point P_1. (Also the tie point B_1.) If one imagines the entrance surface pivoting clockwise about the point C, then an inward surface normal passing through A_2 would require entrance points P moving up the Ewald sphere through the Laue point. As soon as we pass the entrance point P_2, which represents the condition that P_2A_1 is essentially perpendicular to K_H, we enter the Bragg region, since now, for the first time, one of the wave vectors points back out the entrance surface. As the entrance surface becomes horizontal, in Fig. (28), we have the symmetric Bragg case. One of the important differences between the nearly symmetric Bragg case and the Laue case is that an incident point in the Bragg case selects two tie points on the *same branch* of the hyperbola, for a given polarization state, as opposed to one tie point on each branch.

In Fig. 29, for the symmetric Bragg case, we also note that there is a range of incident points, P_2 through P_3, which produce no intersections with the dispersion surface. That is, over this range of incident angles, no propagating solutions would be expected to exist. This is the region of "total" reflection. The incident point P_1, ($\Delta\theta = LP_1/k$) selects the tie points T_2 and T_1 on the α branch. The incident vector $\mathbf{k}_0{}^i$ and the diffracted exit vector $\mathbf{k}_H{}^e$ are indicated. Not only does the exit vector $\mathbf{k}_H{}^e$ intersect the entrance (and exit) surface, but the whole energy flow $\mathbf{S}_2$, perpendicular to the dispersion surface at T_2, flows outward across the surface. This is a general situation; for any Bragg case the flow of one tie point is into the crystal and the other tie point will have its Poynting vector pointing out of the crystal. This outward flow is *not* the generator of the diffracted beam. In fact, Kohler[25] has proven that only one of the two tie points gives a physically meaningful solution, and that is the one associated with the internal flow. Thus the tie point T_2 is not excited. $\mathbf{S}_2$ signifies an energy flow taking place in the entire crystal, ir-

[25] M. Kohler, Ann. Physik 18, 265 (1933).

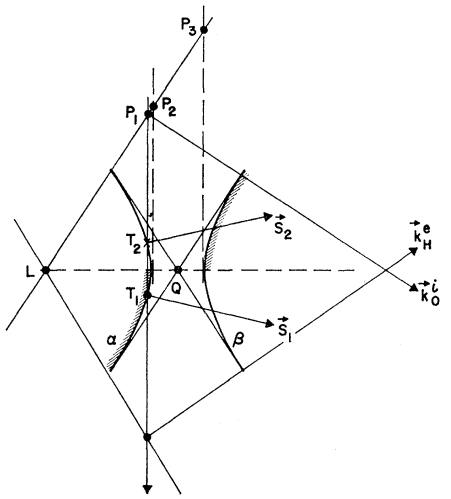

FIG. 29. Detailed selection of tie points in the symmetric Bragg case. Only tie points on the hatched region correspond to permitted solutions. The entrance conditions between entrance points P_2 and P_3 correspond to the region of "total reflection."

respective of depth, directed toward the outside. In order to have a finite $\mathbf{S}_2$ at the entrance surface of the crystal, we require deep within the crystal a very large $\mathbf{S}_2$ because the wave field loses energy by absorption as it flows toward the surface. This would require, as we let the crystal become infinitely thick, an infinitely strong field to give a finite field at the entrance surface. This, of course, is physically unreasonable, and, hence, the field associated with the tie point T_2 cannot be excited. This qualitative proof of the excitation of only one tie point in the Bragg case is due to Authier[26] and the argument is interesting from an historical point of view. As the dynamical theory advanced, stimulated to a large extent by the experimental discovery of the Borrmann effect, more emphasis was placed upon the direction of energy flow, and many of the features of the wave field interactions in the crystal could be more easily visualized in these terms. Thus, for the symmetric Bragg case, only tie points on the hatched parts of Fig. 29 can be excited.

The nonexcitation of the tie point T_2 in the Bragg case differs from the nonexcitation of similar tie points high up on the α branch in the Laue case. There, since E_H becomes considerably greater than E_0, E_0 was quenched by assigning less and less of the incident energy, $E_0{}^i$ to it, as can be seen in Eq. (41). The partitioning of the incident amplitude is quite different in the Bragg case. Since there is only one excited tie point

$$\mathbf{E}_0{}^i=\mathbf{E}_{0_j}, \qquad \mathbf{E}_H{}^e=\mathbf{E}_{H_j}, \tag{102}$$

where j represents the single appropriate tie point. Thus the inside incident amplitude is the same as the outside incident amplitude, and the outside diffracted amplitude is identical with that of the inside diffracted field at the surface. The diffracted beam then is more truly a reflection; it is not generated by any flow reaching the surface and splitting up, as in the Laue case. Outside the range of total reflection, (the region between P_2 and P_3 in Fig. 29), an incident beam strikes the crystal, a flow into the crystal and a reflected beam are generated. The ratio, E_H/E_0, is the same in both of these effects. The internal flow eventually is completely absorbed, if the crystal is thick enough. Equation (24), for E_H/E_0, then gives the reflection coefficient, $|E_H{}^e/E_0{}^i|^2$. Multiplying the two expressions in Eq. (24) together, we have

$$\left(\frac{E_H}{E_0}\right)^2=\frac{\xi_0}{\xi_H}\frac{F_H}{F_{\bar{H}}}=|b|(\eta\pm(\eta^2-1)^{\frac{1}{2}})^2\frac{F_H}{F_{\bar{H}}}, \tag{103}$$

where we have used Eq. (31) in order to express ξ_0 and ξ_H in terms of η. Equation (103) is perfectly general, the only change in going from the Laue case, Eq. (35), to the Bragg case is to replace $(\eta^2+1)^{\frac{1}{2}}$ by $(\eta^2-1)^{\frac{1}{2}}$. For a centrosymmetric crystal $F_H=F_{\bar{H}}$, (which is often a good approximation in any case), and then the reflection coefficient becomes

$$\frac{|E_H{}^e|^2}{|E_0{}^i|^2}=\frac{|E_{H_j}|^2}{|E_{0_j}|^2}=|b||\eta\pm(\eta^2-1)^{\frac{1}{2}}|^2. \tag{104}$$

A. No Absorption

For the symmetric Bragg case, $b=-1$; and if there is no absorption η, [Eq. (32)], is real, and is given by:

$$\eta=(-\Delta\theta\sin 2\theta+\Gamma F_0)/|P|\Gamma F_H, \tag{105}$$

where F_0 and F_H are real.

If $\Delta\theta$ is large and negative, η is large and positive. The point is well down on the low-angle side on the α branch, and the negative sign in (104) gives us $|E_H|^2/|E_0|^2\Rightarrow 0$, i.e., no diffracted beam. Only the transmitted beam, E_0, exists. As η reduces to $+1$, $\Delta\theta$ going through zero and becoming positive, we have that $\Delta\theta\sin 2\theta=\Gamma F_0-|P|\Gamma F_H$, and that $|E_H|^2/|E_0|^2=1$. This corresponds to the incident point P_2, Fig. (29), which excites the diameter tie point on the α branch and is the beginning of total reflection [see Fig. (30)].

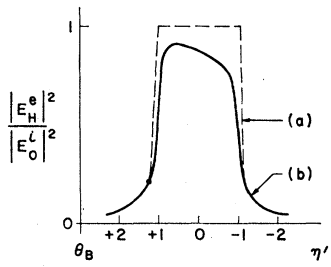

FIG. 30. Shape of the Bragg reflection from a perfect crystal, on an η' scale. The upper dotted curve is for zero absorption (Darwin curve) and the lower curve is with absorption (Darwin–Prins curve).

[26] A. Authier, J. Phys. Rad. **23**, 961 (1962).

The **S** vector, now, is along the atomic planes and also along the physical surface.

If one visualizes the incident plane wave as bounded by slits, then when this beam enters the crystal and discontinuously changes its flow direction to be more parallel to the surface, the cross section of the flow inside the crystal steadily reduces to zero as **S** becomes parallel to the surface. Thus at the beginning of total reflection, the cross section of the flow in the crystal is zero. There is, however, an exponential damping of the fields with depth in the crystal; an extinction at right angles to the flow direction, which is equivalent to the usual skin-depth concept, in the region of total reflection. We consider this further in 3.1.

At $\eta=-1$,

$$\Delta\theta \sin 2\theta=\Gamma F_0+ \mid P \mid \Gamma F_H, \qquad \mid E_H \mid^2/\mid E_0 \mid^2$$

is still unity, and we are at the diameter point on the β branch. Thus, now with the positive sign in Eq. (104), as $\Delta\theta$ increases, η becomes increasingly larger and negative, until $\mid E_H \mid^2/\mid E_0 \mid^2$ goes to zero again. We have just traced out the sides of the Darwin reflection curve, as shown in Fig. 30 upper curve.

Equation (104), for the reflection coefficient, continues to give unity for all values of η between $+1$ and -1. Thus, even though there are no tie points on the dispersion surface, Eq. (31) for ξ_0 and ξ_H in terms of the boundary conditions, still leads to valid descriptions of the fields in the crystal. The "solution surfaces," as discussed in 3.2, which reflect the boundary conditions, thus overlay the dispersion surfaces, which are a function of crystal structure and relative absorption. Thus we have in Eq. (104) a perfectly general expression for the shape of a Bragg peak on the η scale. Since, in general, η is a function of absorption, we have an "automatic" way of including absorption effects on Bragg peaks. Before moving on to the case with absorption, we might note that the center of the Darwin curve, which occurs at $\eta=0$, occurs at a $\Delta\theta \sin 2\theta=\Gamma F_0$, where F_0 is real, it can be seen that this angular displacement of peak position is due to an index of refraction effect.

B. With Absorption

If we assume, as in previous sections, that F_H''/F_H' is small enough compared with unity to neglect second-order terms in this ratio, then, for η, from Eq. (32), for the symmetric Bragg case ($b=-1$), we have

$$\eta'=(-\Delta\theta \sin 2\theta+\Gamma F_0')/\mid P \mid \Gamma F_H',$$

$$\eta''=-(F_H''/F_H')(\eta'-1/\mid P \mid \epsilon), \qquad (106)$$

where ϵ again is F_H''/F_0''.

The Darwin–Prins curve can be obtained directly from Eq. (104) using the complex η defined in the above equations. A typical curve is shown in Fig. 30 curve (b). From Eq. (106) we see that η' is essentially the same parameter that was used in 3.1A in discussing the Darwin curve. Thus the general features are similar. We note also that η'' is a linear function of η', with a small slope and with an intercept at $\eta'=1/\mid P \mid \epsilon$. Since $\eta'>0$ for $\eta''=0$, the Darwin–Prins curve matches the Darwin curve only at a point close to the low-angle slope of the peak. It is less than the Darwin curve at all other points. Aside from a general lowering of the reflection curve, the effect of absorption is to enchance the reduction of the diffracted intensity at the high-angle side of the range of "total" reflection, producing an asymmetric reflection curve. Some physical insight as to the reason for the asymmetry is brought out when we discuss the fields in Sec. 3.2. The only subtle variable in the calculation of the values of (104), with absorption, is ϵ. F_0'' can be determined directly from the linear absorption coefficient, but F_H'' is still of concern.

In Appendix C we go into a detailed discussion of the evaluation of (104). However, we notice that for the weaker reflections, i.e., as F_H' becomes smaller, the range of total reflection gets smaller. The dispersion surface hyperbolas come closer together and closer to the Q point. Also, for $\eta'=0$, which still is closely the "center" of the curve, we have that $\eta''=F_0''/\mid P \mid F_H'$. Since the greater η'' at this point, the greater the deviation from total reflection, we see that the ratio of the absorption to the strength of the reflection (i.e., F_0''/F_H') determines whether the peak needs to be described by the dynamical theory or the kinematical (mosaic) theory.

As opposed to the symmetric case with no absorption, there is never total reflection since $\mid E_H \mid^2/\mid E_0 \mid^2<1$, and so there must always be some energy flow into the crystal. This follows from energy conservation. In other words, energy never flows parallel to the crystal surface when an absorption process is allowed, with any penetration of the fields into the surface. We can see this formally from Eqs. (66) and (67) which, when combined, give:

$$\tan\Delta=\frac{\mid E_H \mid^2/\mid E_0 \mid^2-1}{\mid E_H \mid^2/\mid E_0 \mid^2+1}\tan\theta, \qquad (107)$$

where Δ is the angle of flow with respect to the atomic planes. Since $\mid E_H \mid^2/\mid E_0 \mid^2$, by Eq. (104) is always less than unity, Δ is never zero. Thus, although we may think of approaching the diameter points in Fig. 29, the effect of the boundary conditions on the field amplitudes at the crystal surface prevents the region near the diameter points from being excited. The effect of absorption is to force a small flow into the crystal and so the "solution-surface" leaves the dispersion surface at the appropriate value of Δ. The important thing in the Laue case was the attenuation of the flows, and small variations of E_H/E_0 due to boundary conditions were not too significant. In the Bragg case, the amplitude ratio at the surface is critical.

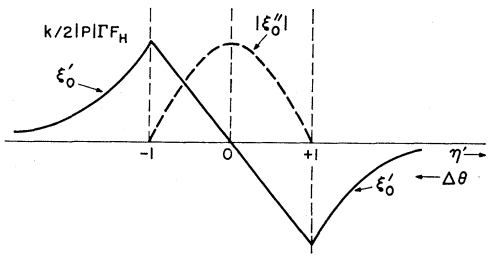

FIG. 31. Plot of real part ξ_0', and imaginary part ξ_0'', of ξ_0 as a function of η' for the no-absorption case and symmetric Bragg conditions. The curved parts of ξ_0' correspond to points on the dispersion surface. The linear portion represents points between the diameter points of the dispersion sheets. This "solution surface" thus departs from the dispersion surface. The values of ξ_0'' give the extinction depth, or skin depth, for the penetration of radiation during total reflection.

3.1 PRIMARY EXTINCTION

In order to get a feeling for the penetration of the fields during the angular range over which "total" reflection is occurring, we consider the symmetric Bragg case with no absorption, and a centrosymmetric crystal ($F_{\bar{H}}=F_H$). From Eq. (31) we have for ξ_0 with $b=-1$

$$\xi_0=\tfrac{1}{2}k\mid P\mid \Gamma F_H[\eta\pm(\eta^2-1)^{\frac{1}{2}}], \qquad (108)$$

in which all parameters on the right are real because of no absorption. ξ_0 is real outside the total reflection range, $\mid\eta\mid>1$, and within the range $(-1<\eta<+1)$, has the real and imaginary parts:

$$\xi_0'=\tfrac{1}{2}k\mid P\mid \Gamma F_H\eta,$$
$$\xi_0=\tfrac{1}{2}k\mid P\mid \Gamma F_H(1-\eta^2)^{\frac{1}{2}}. \qquad (109)$$

In Fig. 31 we show a plot of ξ_0' and ξ_0'' as a function of η. (Note that increasing η means decreasing glancing angle $\Delta\theta$ so that the α branch is on the right.) Within the range of total reflection ξ_0' varies linearly with $\Delta\theta$. The imaginary part is zero outside the range and varies parabolically inside having its greatest magnitude in the center of the Darwin curve. The curve in Fig. 31 can be thought of as a "solution surface" which overlays the dispersion surface in Fig. 29, but provides a connection between the diameter points.

From Eq. (23) we can relate ξ_0'' to attenuation of the wave field and determine the extinction factor which describes the skin depth of the probing field. From Eq. (23) with $F_0''=0$ we have

$$\xi_0''=-K_0''\sin\theta, \qquad (110)$$

and the extinction factor for intensity is then, combining (109) and (110),

$$\exp(-4\pi\mathbf{K}_0''\cdot\mathbf{r})$$
$$=\exp\{[-2\pi k\mid P\mid \Gamma F_H(1-\eta^2)^{\frac{1}{2}}/\sin\theta]z\}, \qquad (111)$$

where z is depth in the crystal. At the edges of the total reflection range ($\eta=\pm1$) the extinction factor is unity and is maximum at the center of the range $\eta=0$. The average value of the extinction factor over the range is

$$\exp[(-\tfrac{1}{2}\pi^2k\mid P\mid \Gamma F_H/\sin\theta)z]. \qquad (112)$$

[Average value of $(1-\eta^2)^{\frac{1}{2}}$ in range, $-1<\eta<+1$, is $\frac{1}{4}\pi$.]

In the usual case, this attenuation is many times greater than that produced by normal photoelectric absorption so that within the total reflection range, only a thin surface layer contributes to the diffraction. It is for this reason that the integrated intensity for a crystal with absorption does not differ greatly from the Darwin value where absorption has been neglected.

The ratio ξ_0''/ξ_0' is not small in the region of total reflection and the approximations leading to Eq. (57) are not valid. Thus the energy flow is no longer perpendicular to the ξ_0' curve. However, the situation shown in Fig. 17 is valid and the flow direction is given by $\mid\mathbf{E}_H\mid^2\mathbf{s}_H+\mid\mathbf{E}_0\mid^2\mathbf{s}_0$. When absorption is present, $\mid\mathbf{E}_H\mid<\mid\mathbf{E}_0\mid$ and a flow is forced into the crystal. With absorption, the curves shown in Fig. 31 also deviate from the dispersion surface in the region of the diameter points, and the points which would normally predict flow along the surface are not excited.

3.2 WAVE FIELDS IN CRYSTAL

As discussed in Sec. 2.10, for full reflections the α branch tie points produce minimum field intensity at the atom sites, while the β branch tie points have a maximum. The structure of the fields is still given by

$$R=\mid 1+(E_H/E_0)\exp(2\pi i\mathbf{H}\cdot\mathbf{r})\mid^2, \qquad (113)$$

where the strength of the maximum or minimum is given by E_H/E_0. Since the tie points on the α branch correspond to the low-angle side of the Bragg peak and the tie points on the β branch to the high-angle side, we would expect that the high-angle side suffers greater absorption.

If E_H/E_0 is actually evaluated in the range of total reflection for the nonabsorbing crystal as a function of depth in the crystal, von Laue[27] has shown that a wave field with nodal planes is formed throughout this range. Since $\mid E_H/E_0\mid=1$ in this range, Eq. (113) is a sine wave with a period equal to the d spacing giving an intensity variation as in Fig. 3. The nodes are situated in the atom planes at the beginning (the low-angle side) of the total reflection range, and as the glancing angle increases, the nodal plane moves linearly with angle, until the antinodes are at the atoms at the high-angle end of the range.

The quantity R, proportional to the electric field intensity at an atom, *near the surface*, is plotted as the solid curve in Fig. 32 as a function of the Bragg angle η'. For a full symmetrical Bragg reflection with no absorption, at low glancing angles, the tie point is on the hatched portion of the α branch (Fig. 29), and the intensity and direction of energy flow at the atoms is

[27] M. v. Laue, Ann. Physik, **23**, 705 (1935); or Ref. 5, p. 431.

that of the incident beam. As the reflecting region is approached, a weak diffracted beam appears, and the interaction of these two beams reduces the intensity at the atoms. The direction of energy flow in the crystal alters towards parallelism with the Bragg planes. As the tie point moves up the α branch to the diameter point, the intensity at the atoms reduces to zero (as $E_H \rightarrow E_0$) and total reflection takes place. As the total reflection range is crossed, the field intensity at the atoms increases from zero to four times its value when no diffraction is taking place. That is, an antinode is at the atoms at the high-angle end of the range. As the angle increases, the tie point moves up the β branch and the intensity at the atoms is always higher than the value for no diffraction.

For atoms somewhat below the surface, the intensity is the same as at the surface (again we neglect photoelectric absorption) outside the total reflection range. Within the range, however, the extinction factor discussed in the previous section comes into play, and the fields are attenuated at right angles to the flow. The dotted curve in Fig. 32 gives the field at an atom plane somewhat deeper in the crystal.

We now consider the corresponding situation when the crystal is absorbing. As we approach total reflection from the low-angle side, the nodal features appear and the effective photoelectric absorption coefficient becomes less than its normal value. It approaches a value the order of $\mu_0(1-P\epsilon)$ near the beginning of total reflection. Since, for full reflections, ϵ can be close to unity, the absorption is low, as in the Borrmann effect. However, since the energy flow is fairly parallel to the surface, there is no great depth of penetration, but there is a lateral penetration with respect to the point of incidence. This is not a very pronounced effect, from power considerations based on the cross section of the beams, but Borrmann[28,29] and Authier[20] have observed this weak anomalous beam by allowing the incident beam to fall near the edge of the crystal and recording the radiation leaving the side face.

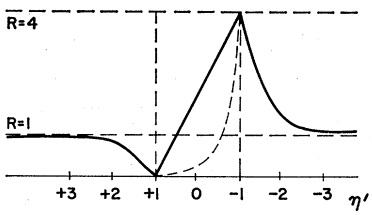

FIG. 32. Field intensity at an atom for a full reflection with no absorption in the Bragg case as a function of η'. The nodes at the atoms, α branch ($\eta=+1$), move linearly with glancing angle, until antinodes are at the atoms, β branch ($\eta=-1$). The solid curve is for surface atoms, the dashed curve is for atoms deeper in the crystal. The marked lowering of intensity in the total reflection region is due to extinction.

[28] G. Borrmann, Naturwiss. **38**, 330 (1951).
[29] G. Borrmann, G. Hildebrant, H. Wagner, Z. Phys. **142**, 406 (1955).

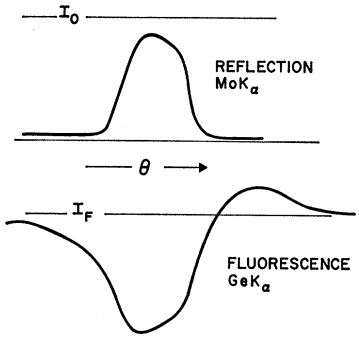

FIG. 33. Fluorescence measured during a rotation through a Bragg peak, used as a measure of the field strengths shown in Fig. 32. See text for discussion.

As the Bragg angle is swept through the now not-quite-totally reflecting range, the x-ray intensity at the atoms increases in this probing, attenuated field, and at the end of the range, the linear absorption coefficient has changed from very nearly zero to $\mu_0(1+P\epsilon)$, or very nearly *twice* the normal value. Thus at the high-angle end, a higher than normal absorption takes place at the atoms. Since more energy is absorbed, less is diffracted, and the reflection curve is asymmetric, with less diffracted intensity on the high-angle side.

A rather direct verification of the nodal picture described above was given by Batterman[30] who used the secondary fluorescence emission as a probe of electric field strength (and absorption) at the atom. This technique is conceptually similar to the work of Knowles,[31] who used a nuclear neutron-induced γ-ray emission to study the distribution of neutrons in a perfect crystal while neutron diffraction was occurring. In the x-ray case, Mo K_α radiation is sufficiently energetic to excite the K fluorescence of Ge, which, itself is of sufficiently short wavelength to readily escape from the crystal and be easily detected. Thus, if the Ge K_α fluorescence radiation is measured while a perfect crystal of Ge, exposed to a beam of Mo K_α radiation is slowly rotated through a strong Bragg reflection, the field at the atoms can, essentially, be determined. In the experimental curves in Fig. 33, the upper curve is the Bragg reflection of the Mo K_α radiation, while the lower curve is the Ge K fluorescence. The reflected beam shows the asymmetry of the Darwin–Prins curve, which is due to absorption. The features of the fluorescence curve correlate with the structure of fields within the crystal, as discussed above. Far off the reflection, further off than shown in the figure, the background fluorescence I_F, the horizontal solid line in Fig. 33, is produced when all of the primary beam is absorbed within the crystal. As we move to a given diffracted intensity on the low-angle side of the peak, corresponding to a tie point on the α branch, field

[30] B. W. Batterman, Appl. Phys. Letters **1**, 1962; Phys. Rev. (to be published).
[31] J. W. Knowles, Acta Cryst. **9**, 61 (1956).

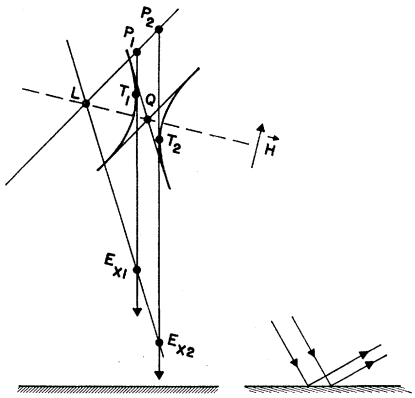

FIG. 34. Asymmetric Bragg reflection. Note that in this case the angular width with respect to the incident beam, P_1P_2, is less than the angular width in the diffracted beam $E_{x1}E_{x2}$. At the same time, the cross section of the diffracted beam is less than that of the incident beam.

intensity is shunted away from the atoms and so the primary beam penetrates more deeply before it is absorbed. The self-absorption of this deep-generated fluorescence radiation in getting back out of the crystal causes the drop in the measured fluorescence. For a corresponding diffracted intensity on the high-angle side of the peak, the same amount of fluorescence radiation is generated, but now it is all generated very near to the surface because of the high fields at the atoms, and so it experiences little self-absorption in leaving the crystal. This produces a measured fluorescence which is even more intense than that observed when all the energy is absorbed with the crystal well off the diffracting condition, i.e., I_F. This enhancement of the fluorescence due to surface generation is shown in Fig. 33. The large dip, and asymmetry, in the central region of the fluorescence curve is in effect a mirror image of the diffracted beam, since the predominant change in the fluorescence is due to the fact that energy is prevented from entering the crystal and is diverted instead into the diffracted beam. The quantitative comparison of the fluorescence generated with that predicted using the nodal patterns given by Eq. (113), with corrections for self absorption in leaving the crystal, is very good.

A final point with respect to the Bragg case, for asymmetrically cut crystals, is illustrated in Fig. 34. The left-hand side of this figure shows the dispersion sheets and, with the physical surface cut so as to be more perpendicular to the incident beam, we see that the α branch tie point at the onset of total reflection (T_1) has moved up the dispersion curve; $\mathbf{S}_1$, however, is still parallel to the crystal surface. The important feature is that the angular range of total reflection, the entrance points P_1 to P_2, is now less than that for the symmetric case, whereas the angular range in the diffracted beam, the exit points E_{X1} to E_{X2}, is now greater than that for the symmetric case. Thus the half-width of the reflection with respect to the incident beam is reduced, but more divergence exists in the diffracted beam. The physical situation shown in the right-hand side of Fig. 34 is the reverse, where we see that a broad incident beam is condensed to a narrow diffracted beam. The asymmetrically cut crystal, used in this orientation, thus accepts less divergence from a broad incident beam and gives more cross-fire in a narrowed diffracted beam with respect to the behavior of a similar symmetrically cut crystal. These interesting condensing and collimation and power gathering effects of asymmetrically cut perfect crystals used in Bragg diffraction have been pointed out by Renninger[32] and Kohra[33] and have been used by them to experimentally measure a single unconvoluted Darwin–Prins curve.

The reflection coefficient, $|E_H|^2/|E_0|^2$, for tie point T_1, may be greater than unity. In fact, for very small absorption, it becomes unity on the low-angle side of the peak, for an entrance point which would select the diameter tie point. Thus the diffracted field amplitude may be greater than the incident amplitude; this is consistent with the change in beam cross section as shown in the right-hand side of Fig. 34, where, if there is total reflection, the reduced cross section must be accompanied by an increase in field strength so that incident and diffracted power are the same.

4.0 SPECIAL TOPICS

The concepts developed in the general theory with respect to energy flows, standing waves, absorption and integrated intensity have been confirmed by a number of experiments.[29,34–37] We consider briefly certain points which have proved of special interest.

If we consider the absorption terms in detail for a particular symmetric Laue transmission case, say the (220) reflection (a full reflection) in Ge with Cu K_α radiation, for a crystal slab 1 mm thick, then $\mu_0=350$ cm^{-1}, $2\theta=45°$, $\epsilon=0.95$ and we have:

Normal absorption: $e^{-\mu_0 t_0/\gamma_0}=e^{-350(0.1/0.924)}=e^{-38}$

σ polarization, α branch: $e^{-38(1-0.95)}=e^{-1.9}$
π polarization, α branch: $e^{-38[1-(0.707)(0.95)]}=e^{-12.5}$
π polarization, β branch: $e^{-38[1+(0.707)(0.95)]}=e^{-63.5}$
σ polarization, β branch: $e^{-38(1+0.95)}=e^{-74}$.

It is quite obvious from the above that only radiation of σ polarization, α branch will get through the crystal. This implies of course, that the Borrmann effect can be used as an x-ray polarizer. Since the above calculations refer to the forward-diffracted beam also, the polarizer-monochromator can be inserted in an x-ray beam without appreciably changing its line of action and if the crystal is rotated about this line, the

[32] M. Renninger, Z. Naturforsch. **16a**, 1110 (1961).
[33] K. Kohra, J. Phys. Soc. Japan **17**, 589 (1962).
[34] G. Borrmann, Z. Phys. **127**, 297 (1950).
[35] G. Schwarz and G. L. Rogosa, Phys. Rev. **95**, 950 (1954); G. Brogren and D. Adell, Arkiv Fysik **8**, 97 (1954).
[36] G. Borrmann, Z. Krist. **106**, 109 (1954).
[37] W. H. Zachariasen, Proc. Natl. Acad Sci. U. S. **38**, 378 (1952).

E vector in the beam can be rotated to any desired angle. These polarization effects have been verified by Cole *et al.*[38]

The anomalous absorption effects predicted by the general theory for x rays should also hold for other types of waves such as neutrons or electrons. Dynamical effects are the rule in electron diffraction. This is because the number of atomic planes necessary for perfect crystal diffraction is much smaller than in the x-ray case since the scattering amplitude per plane is very high for electrons. (Electron diffractionists would say that the extinction distance, which is proportional to the reciprocal of the scattering amplitude per plane, is very much smaller for electrons than for x rays.) Anomalous transmission effects are much more difficult to observe because the absorbing power is more uniformly distributed between the planes. Recently, however,[39–41] electron diffraction effects have been observed which can be traced directly to the difference in absorption between the two types of wave fields. In an experiment which is the electron analogy to the fluorescence experiment described in Sec. 3.2, Duncumb[41] has observed enhanced x-ray emission from extinction contours indicating the presence of the antinodal wave field.

For the case of neutrons the dynamical effects have been verified. Knowles' experiment[31] (which was suggested by Ewald) which we have also mentioned in Sec. 3.2, detects the presence of one of the wave fields through an incoherent scattering. In this case, he chose a crystal for which there is a nuclear reaction (γ-ray emission) between the neutrons and nucleus of one of the matrix atoms. During diffraction, the standing wave pattern reduced the neutron intensity at the nucleus and a corresponding reduction in γ-ray output was observed.

The presence of the Borrmann effect is indicative of crystal perfection; the absence of the effect in full strength should be a useful measure of crystal defects. Hunter[42] began to explore these ideas by observing the Borrmann effects in elastically strained slabs of single-crystal Ge. This work was continued, and a theory of the transmission through strained crystals, was worked out by Polder and Penning[43] and further experimental work was performed by Okkerse and Penning.[44]

A recent series of papers has been published dealing with dynamical diffraction in slightly deformed crystals. Howie and Whelan[45] have developed a theory for electron diffraction by a kinematic "column approximation" which allows for the inclusion of displaced atoms. Two papers by Kato[46] deal with the same problem from the x-ray viewpoint.

Photographs by Borrmann[47] and others made using the anomalous transmission have revealed dislocations and other elastically strained regions in crystals. The strained regions undergo enhanced absorption and cast shadows in the anomalously transmitted and diffracted beams. Patel and Batterman[48] have used anomalous transmission to detect the presence of 1 part in 10^6 dissolved oxygen in highly perfect silicon. By appropriate heat treatment, the precipitation of the oxygen strained the lattice enough to completely destroy any anomalous transmission. By proper solution heat treatment, the original anomalous transmission could be regained.

In the special case of a bar cut for symmetrical Laue diffraction elastically bent so as to "fan out" the atomic planes from front to back, no change in Borrmann effect for a perfect crystal should take place. This is due to the fact that the changing d spacing through the thickness of the bar and the changing Bragg angle that results, is just compensated for by the changing angle of incidence as the radiation penetrates into the crystal. However, the exit Bragg angle is different from the entrance Bragg angle, and this change, although small, was measured by Cole and Brock[49] and affords the possibility of producing slight "focusing" of an x-ray beam.

5.0 SUMMARY

The radiation field inside a periodic scattering and absorbing medium is a remarkably structured entity. This can be shown in a straightforward way by solving Maxwell's equations in a medium with a periodic dielectric constant, taking into account the conservation of momentum for waves scattered by waves (Bragg's Law). When nodal patterns in the time-averaged field coincide with density concentrations in the medium, startling results are obtained with respect to absorption, and other physical phenomena which depend upon field strengths. Many of these effects can be observed in x-ray, electron, and neutron diffraction when sufficiently perfect crystals are available.

Note added in proof. R. W. James has recently published and extended treatment in *Solid State Physics*, edited by F. Seitz and D. Turnbull (Academic Press Inc., New York, 1963), Vol. 15.

ACKNOWLEDGMENTS

This paper was undertaken at the suggestion of Professor B. E. Warren and we wish to acknowledge his interest and encouragement in the development of

[38] H. Cole, F. W. Chambers, C. Wood, J. Appl. Phys. **32**, 1942 (1961).
[39] M Hashimoto, A. Howie, and M. Whelan, Proc. Roy. Soc. (London) **A269**, 80 (1960).
[40] P. B. Hirsch, A. Howie, M. Whelan, Phil. Mag. **7**, 2095 (1962).
[41] P. Duncumb, Phil. Mag. **7**, 2101 (1962).
[42] L. P. Hunter, J. Appl. Phys. **30**, 874 (1959).
[43] P. Penning and D. Polder, Philips Res. Rept. **16**, 419 (1961).
[44] B. Okkerse and P. Penning, Philips Res. Rept. **18**, 82 (1963).
[45] A. Howie and M. J. Whelan, Proc. Roy. Soc. (London) **A263**, 217 (1961).
[46] N. Kato, Acta Cryst. **16**, 276 and 282 (1963).
[47] G. Borrmann, W. Hartwig, and H. Irmler, Z. Naturforsch **13a**, 423 (1958).
[48] J. R. Patel and B. W. Batterman, J. Appl. Phys. **34**, 2716 (1963).
[49] H. Cole and G. E. Brock, Phys. Rev. **116**, 868 (1959).

this review. The authors benefited greatly from discussions with Professor P. P. Ewald and from his critical comments on the manuscript.

APPENDIX A: WAVES SATISFYING BRAGG'S LAW AND MAXWELL'S EQUATIONS

The assumed solution for the wavefield in the crystal which satisfies Bragg's law and Maxwell's equations is taken as a sum of plane waves. The field vectors are then written in the form

$$\mathbf{A}=\exp(2\pi i\nu t)\sum_H \mathbf{A}_H \exp(-2\pi i\mathbf{K}_H\cdot\mathbf{r}), \quad \text{(A1)}$$

where $\mathbf{A}$ stands for $\mathcal{E}$, $\mathfrak{D}$, or $\mathfrak{IC}$. Note that if (A1) and (14) are combined, we have

$$\mathbf{A}=[\sum_H \mathbf{A}_H \exp(-2\pi i\mathbf{H}\cdot\mathbf{r})]\exp(-2\pi i\mathbf{K}_0\cdot\mathbf{r})\exp(2\pi i\nu t)$$

which is, in form, a Bloch function, the form known to be correct for wave solutions in a periodic medium. It is a wave of wave vector $\mathbf{K}_0$ and amplitude expressible as a Fourier series. Taking the curl of (A1) and writing it explicitly in terms of $\mathcal{E}$, we have

$$\nabla\times\mathcal{E}=-(2\pi i)\exp(2\pi i\nu t)\sum_H(\mathbf{K}_H\times\mathbf{E}_H)\times\exp(-2\pi i\mathbf{K}_H\cdot\mathbf{r}). \quad \text{(A2)}$$

And taking the time derivative of (A1), expressing the result in terms of $\mathfrak{IC}$, we have

$$\partial\mathfrak{IC}/\partial t=(2\pi i)\nu\exp(2\pi i\nu t)\sum_H\mathfrak{IC}_H\exp(-2\pi i\mathbf{K}_H\cdot\mathbf{r}). \quad \text{(A3)}$$

Inserting (A2) and (A3) in Maxwell's equation (13a) results in an equality which must hold at all points and at all times, and thus must be separately true for each term in the summation (each Fourier component). We obtain, then, the condition that

$$\mathbf{K}_H\times\mathbf{E}_H=\nu\mu_0\mathbf{H}_H. \quad \text{(A4)}$$

Similarly, from the second of Maxwell's equations, (13b), and the appropriate forms of (A1), we have that

$$\mathbf{K}_H\times\mathbf{H}_H=-\nu\mathbf{D}_H. \quad \text{(A5)}$$

Except for the very small imaginary parts of the wave vectors, Eq. (A4) states that $\mathbf{H}_H$ is perpendicular to $\mathbf{K}_H$, and Eq. (A5) then implies that $\mathbf{K}_H$, $\mathbf{H}_H$, and $\mathbf{D}_H$ form a mutually orthogonal set. $\mathbf{E}_H$, although in the plane of $\mathbf{K}_H$ and $\mathbf{D}_H$, is not necessarily along $\mathbf{D}_H$, i.e., it may have a longitudinal component.

From the relation $\mathfrak{D}=\kappa\epsilon_0\mathcal{E}$, Eq. (7) for κ, and (A1) for the assumed form of $\mathfrak{D}$ and $\mathcal{E}$, we have for the relation between $\mathfrak{D}$ and $\mathcal{E}$, that

$$\sum_H\mathfrak{D}_H\exp(-2\pi i\mathbf{K}_H\cdot\mathbf{r})=\epsilon_0[1-\Gamma\sum_{H'}F_{H'}\times\exp(-2\pi i\mathbf{H}'\cdot\mathbf{r})]\sum_H\mathbf{E}_H\exp(-2\pi i\mathbf{K}_H\cdot\mathbf{r}), \quad \text{(A6)}$$

where the index H' is used to distinguish it from H. After appropriate changes in indices of summation and using the fact that $\mathbf{K}_{H'}+\mathbf{H}=\mathbf{K}_{H'+H}$ [from (14)], the infinite double sum on the right side of (A6) can be rewritten to give

$$\sum_H\mathfrak{D}_H\exp(-2\pi i\mathbf{K}_H\cdot\mathbf{r})=\epsilon_0\sum_H\mathbf{E}_H\exp(-2\pi i\mathbf{K}_H\cdot\mathbf{r})-\epsilon_0\Gamma\sum_H(\sum_P F_{H-P}\mathbf{E}_P)\exp(-2\pi i\mathbf{K}_H\cdot\mathbf{r}). \quad \text{(A7)}$$

Again, since this relationship must hold for all $\mathbf{r}$ it must hold for each Fourier component, and we have

$$\mathfrak{D}_H=\epsilon_0\mathbf{E}_H-\epsilon_0\Gamma\sum_P F_{H-P}\mathbf{E}_P=\epsilon_0(1-\Gamma F_0)\mathbf{E}_H-\epsilon_0\Gamma\sum_{P\neq H}F_{H-P}\mathbf{E}_P. \quad \text{(A8)}$$

$\mathfrak{D}_H$ is thus predominantly $\epsilon_0\kappa_0\mathbf{E}_H$, but modified slightly by small contributions from the other Fourier components of the electric field.

By taking the cross product of $\mathbf{K}_H$ with each side of (A4), and substituting in (A5), we obtain

$$\mathbf{K}_H\times(\mathbf{K}_H\times\mathbf{E}_H)=\nu\mu_0(\mathbf{K}_H\times\mathbf{H}_H)=-\nu^2\mu_0\mathbf{D}_H. \quad \text{(A9)}$$

If we now substitute from (A8), we obtain

$$\mathbf{K}_H\times(\mathbf{K}_H\times\mathbf{E}_H)=-\nu^2\mu_0\epsilon_0(\mathbf{E}_H-\Gamma\sum_P F_{H-P}\mathbf{E}_P), \quad \text{(A10)}$$

where, in making the substitution, we have neglected time derivatives of F_H in taking $\partial\mathfrak{D}/\partial t$. Since $\mu_0\epsilon_0=1/c^2$ and $\nu^2/c^2=k^2$, (A10) can be written as

$$\mathbf{K}_H\times(\mathbf{K}_H\times\mathbf{E}_H)+k^2\mathbf{E}_H-k^2\Gamma\sum_P F_{H-P}\mathbf{E}_P=0. \quad \text{(A11)}$$

Using the vector identity for a triple cross product

$$\mathbf{K}_H\times(\mathbf{K}_H\times\mathbf{E}_H)=-(\mathbf{K}_H\cdot\mathbf{K}_H)\mathbf{E}_H+(\mathbf{K}_H\cdot\mathbf{E}_H)\mathbf{K}_H$$

we have

$$[k^2(1-\Gamma F_0)-(\mathbf{K}_H\cdot\mathbf{K}_H)]\mathbf{E}_H-k^2\Gamma\sum_{P\neq H}F_{H-P}\mathbf{E}_P+(\mathbf{K}_H\cdot\mathbf{E}_H)\mathbf{K}_H=0. \quad \text{(A12)}$$

This is the fundamental set of equations describing the field inside the crystal. For each amplitude $\mathbf{E}_H$, this is a complex vector equation. The set of equations must hold then for the real and imaginary parts, and for each component of the vectors, separately. The real and imaginary parts need not be separated until the end; however, we need to discuss the different components of $\mathbf{E}_H$ separately.

We only consider the case where one reciprocal lattice point is near enough to the Ewald sphere to give any appreciable diffraction. That is, let all the field amplitudes be negligibly small except for two, $\mathbf{E}_0$ and $\mathbf{E}_H$. We were not free to make this restriction to just two waves earlier, since then the terms in the infinite double sum (A6) could not have been converted to the form (A7). Physically, all waves exist in the crystal,

but we assume that only two are of appreciable amplitude. The wave vectors $\mathbf{K}_0$ and $\mathbf{K}_H$ of the two waves define the plane of incidence. We then discuss the components of $\mathbf{E}_0$ and $\mathbf{E}_H$ in terms of the components which are normal to this plane, the σ polarization state, and those that are parallel to this plane, the π polarization state.

For the σ polarization state, Eq. (A12) becomes

$$\begin{aligned}&\text{(a)}\quad [k^2(1-\Gamma F_0)-(\mathbf{K}_0\cdot\mathbf{K}_0)]E_0{}^\sigma-k^2\Gamma F_{\bar{H}}E_H{}^\sigma=0,\\ &\text{(b)}\quad -k^2\Gamma F_H E_0{}^\sigma+[k^2(1-\Gamma F_0)-(\mathbf{K}_H\cdot\mathbf{K}_H)]E_H{}^\sigma=0.\end{aligned}\tag{A13}$$

This pair of equations has a nontrivial solution for the ratio $E_H{}^\sigma/E_0{}^\sigma$ only if its determinant is zero. However, before investigating the restrictions imposed by this condition, let us consider the π polarization state.

The field vectors $\mathbf{E}_0$ and $\mathbf{E}_H$ each have two components in the plane of incidence: a longitudinal component along their respective wave vectors, and a component at right angles to their wave vectors. The longitudinal components can be seen to be negligible by the following: If $\mathbf{D}_H$ is dotted into Eq. (A12) and (A8) substituted, we see that

$$\epsilon_0\mathbf{E}_H\cdot\mathbf{D}_H=[(\mathbf{K}_H\cdot\mathbf{K}_H)/k^2)]\mathbf{D}_H\cdot\mathbf{D}_H.$$

Since the dielectric constant differs from unity by one part in 10^5, $\mathbf{K}_H\cdot\mathbf{K}_H/k^2$ differs from unity by this order, so that the component of $\epsilon_0\mathbf{E}_H$ not along $\mathbf{D}_H$ is of this order. Secondly, if $\mathbf{K}_H$ is dotted into Eq. (A12), we have

$$\mathbf{K}_H\cdot\mathbf{E}_H(1-\Gamma F_0)=\Gamma\sum_{P\neq H}F_{H-P}(\mathbf{K}_H\cdot\mathbf{E}_P)$$

which again, since $\gamma F\sim10^{-5}$, implies that the component of $\mathbf{E}_H$ along $\mathbf{K}_H$ may be neglected.

Also, this last condition implies, from (A8), that $\nabla\cdot\mathfrak{D}=0$, rather than $\nabla\cdot\mathfrak{D}=\rho(r)$. This is consistent with the assumed high-frequency behavior, where the positive charge does not play a role, and so the positive charge may be distributed in the same manner as the negative charge, leading to zero net-charge density.

Neglecting the longitudinal components of $\mathbf{E}$, the remaining π components lie in the plane of incidence and are perpendicular to their respective wave vectors. Taking the angle between the directions of $\mathbf{K}_0$ and $\mathbf{K}_H$ to be 2θ we can now write a pair of equations like (A13) for the π components, namely,

$$\begin{aligned}&\text{(a)}\quad [k^2(1-\Gamma F_0)-(\mathbf{K}_0\cdot\mathbf{K}_0)]E_0{}^\pi\\ &\qquad\qquad -k^2(\cos 2\theta)\Gamma F_{\bar{H}}E_H{}^\pi=0,\\ &\text{(b)}\quad -k^2(\cos 2\theta)\Gamma F_H E_0{}^\pi+[k^2(1-\Gamma F_0)\\ &\qquad\qquad -(\mathbf{K}_H\cdot\mathbf{K}_H)]E_H{}^\pi=0.\end{aligned}\tag{A14}$$

Letting

$$P=1\quad\text{or}\quad\cos 2\theta.\tag{A15}$$

The determinant of either (A13) or (A14) may be written as

$$\begin{vmatrix} k^2(1-\Gamma_0)-\mathbf{K}_0\cdot\mathbf{K}_0 & -k^2P\Gamma F_{\bar{H}} \\ -k^2P\Gamma F_H & k^2(1-\Gamma F_0)-\mathbf{K}_H\cdot\mathbf{K}_H \end{vmatrix}\tag{A16}$$

which, when set to zero, gives the permitted wave vectors.

APPENDIX B: BOUNDARY CONDITIONS

We wish to match a set of plane waves outside a plane surface to a set inside where there is no change in amplitude or frequency in crossing the surface. For a single plane wave crossing the surface under these conditions we have only to satisfy a condition on the wave vectors outside $\mathbf{k}_i$, and inside, $\mathbf{k}_p$. From the expressions for a plane wave, we have the condition that:

$$\exp(-2\pi i\mathbf{k}_i\cdot\boldsymbol{\tau})=\exp(-2\pi i\mathbf{k}_p\cdot\boldsymbol{\tau}),\tag{B1}$$

where the origin has been chosen in the surface and $\boldsymbol{\tau}$ is a vector in the surface. To satisfy (B1) at every point on the surface (every value of $\boldsymbol{\tau}$), we must have that $\mathbf{k}_i\cdot\boldsymbol{\tau}\equiv\mathbf{k}_p\cdot\boldsymbol{\tau}$ which restricts $\mathbf{k}_i$ and $\mathbf{k}_p$ to:

$$\mathbf{k}_i=\mathbf{k}_p+a\mathbf{n},\tag{B2}$$

where $\mathbf{n}$ is a unit vector along the surface normal, and a is determined by other considerations. That is, the wave vectors of related waves can only differ by a vector along the surface normal, or, in other words, their tangential components must be equal. Physically, this condition assures the continuity of phase fronts in crossing a surface.

For a set of plane waves on each side of the boundary, (B1) becomes

$$\sum_i\mathbf{E}_i\exp(-2\pi i\mathbf{k}_i\cdot\boldsymbol{\tau})=\sum_p\mathbf{E}_p\exp(-2\pi i\mathbf{k}_p\cdot\boldsymbol{\tau}).\tag{B3}$$

Using the principle of superposition of waves, we need apply (B3) only to the waves that are physically related, or coupled. The sets that we are interested in are the ones which satisfy Bragg's Law. From one of these sets we divide the waves inside into two groups: those whose wave vectors end at the origin of the reciprocal lattice, the "inside incident" waves, and the "diffracted" waves related to these through Bragg's Law. Let the "inside incident" wave vectors be given by $\mathbf{K}_{0j}$ where j is a running index whose values may depend on how many reciprocal lattice points are on the sphere of reflection and how many such waves may be associated with each reciprocal lattice point. For convenience, however, we assume that only one lattice point is on the Ewald sphere. The "diffracted" waves, from Bragg's Law, are then described by the wave vectors $\mathbf{K}_{Hj}=\mathbf{K}_{0j}+\mathbf{H}$. We can sort out the related outside waves in the same way. Letting q be a running index, we can write any $\mathbf{k}_i$ as a $\mathbf{k}_{0q}$, an "incident" or "transmitted" wave, or as $\mathbf{k}_{0q}+\mathbf{H}'$, a "diffracted"

wave. $\mathbf{H}$ and $\mathbf{H}'$ differ because of the index of refraction. We can now write (B3) as

$$\sum_q \exp(-2\pi i\mathbf{k}_{0q}\cdot\boldsymbol{\tau})[\mathbf{E}_{0q}{}^i+\mathbf{E}_{Hq}{}^i\exp(-2\pi i\mathbf{H}'\cdot\boldsymbol{\tau})] = \sum_j \exp(-2\pi i\mathbf{K}_{0j}\cdot\boldsymbol{\tau})[\mathbf{E}_{0j}+\mathbf{E}_{Hj}\exp(-2\pi i\mathbf{H}\cdot\boldsymbol{\tau})]. \tag{B4}$$

Because the reciprocal lattice vectors are nonzero constants, (B4) is separately true for each value of H (each Fourier term). Thus

$$\sum_q \mathbf{E}_{0q}{}^i\exp(-2\pi i\mathbf{k}_{0q}\cdot\boldsymbol{\tau}) = \sum_j \mathbf{E}_{0j}\exp(-2\pi i\mathbf{K}_{0j}\cdot\boldsymbol{\tau}) \tag{B5}$$

with corresponding expressions for each $\mathbf{E}_H$. Since the field amplitudes are nonzero constants, (B5) requires that the tangential components of all these "incident" wave vectors, inside and outside, independently of the "diffracted" waves, must be equal. If, for example, we consider a single outside incident wave $k_0{}^i$, the other wave vectors can be written as

$$\mathbf{k}_0{}^i=\mathbf{K}_{0j}+a_{0j}\mathbf{n}. \tag{B6}$$

And from (B4), we have that

$$\mathbf{H}'=\mathbf{H}+C_H\mathbf{n}. \tag{B7}$$

Corresponding relationships to (B6) exist between the tangential components of the outside "diffracted" wave vectors and the inside "diffracted" wave vectors.

With these relationships between the wave vectors, we have from (B5) and (B4) that

$$\sum_q \mathbf{E}_{0q}{}^i=\sum_j \mathbf{E}_{0j}, \tag{B8}$$

$$\sum_q \mathbf{E}_{Hq}{}^i=\sum_j \mathbf{E}_{Hj}. \tag{B9}$$

These last conditions say simply that the "inside incident" field amplitudes add up to the "outside incident" field amplitudes and that the "inside diffracted" amplitudes add up to the "outside diffracted" field amplitudes, for each active reflection $\mathbf{H}$. (B8) also applies equally well to the "transmitted" beams leaving an exit surface.

APPENDIX C: NUMERICAL EVALUATION OF INTEGRATED INTENSITIES

1. The Laue Case

For the symmetric Laue case, the intensities of the diffracted and forward diffracted beams are obtained from the sum of the contributions from the two wave fields (± sign) in Eqs. (89a) and (89b), giving:

$$\frac{I_H{}^e}{I_0}=\frac{1}{2}\frac{\exp(-\mu_0 t)}{1+(\eta')^2}\cosh\frac{\mu_0 t\,|\,P\,|\,\epsilon}{[1+(\eta')^2]^{\frac{1}{2}}}, \tag{C1}$$

$$\frac{I_0{}^e}{I_0}=\frac{1}{2}\frac{\exp(-\mu_0 t)}{1+(\eta')^2}\cosh\left(\frac{\mu_0 t\,|\,P\,|\,\epsilon}{[1+(\eta')^2]^{\frac{1}{2}}}\pm X\right), \tag{C2}$$

where $\cosh X=1+2(\eta')^2$, $t=t_0/\gamma_0$, and X has the same sign as η'. The integrated intensity R^θ on the θ scale is related to the value on the η' scale, $(R^{\eta'})$ by (90)

$$\rho^\theta=\frac{N\lambda^2(e^2/mc^2)\,|\,F_{H'}\,||\,P\,|}{\pi\sin 2\theta}\rho^{\eta'} \tag{C3}$$

and

$$\rho_H{}^{\eta'}=\exp(-\mu_0 t)\cosh B\int_0^\infty \frac{\cosh\{B/[1+(\eta')^2]^{\frac{1}{2}}\}}{[1+(\eta')^2]\cosh B}\,d\eta' \tag{C4a}$$

$$\rho_0{}^{\eta'}=\exp(-\mu_0 t)\cosh B\int_0^\infty\left\{\left(\frac{1+2(\eta')^2}{1+(\eta'')^2}\right)\times\frac{\cosh\{B[1+(\eta')^2]^{\frac{1}{2}}\}}{\cosh B}-\frac{2}{\cosh B}\right\}d\eta', \tag{C4b}$$

where $B=\mu_0 t\,|\,P\,|\,\epsilon$, and the term $2/\cosh B$ in (C4b) subtracts the background transmission present when the crystal is off the diffracting position.

For large values of B, Kato[50] has derived asymptotic expansions of the integrals as

$$\rho_H{}^{\eta'}\approx\exp[-\mu_0 t(1-|\,P\,|\,\epsilon)]\left(\frac{\pi}{8B}\right)^{\frac{1}{2}}\times\left(1+\frac{1}{8B}+\frac{9}{128B^2}+\frac{0.0732}{B^3}+\cdots\right) \tag{C5a}$$

$$\rho_0{}^{\eta'}=\exp[-\mu_0 t(1-|\,P\,|\,\epsilon)]\left(\frac{\pi}{8B}\right)^{\frac{1}{2}}\times\left(1+\frac{17}{8B}+\frac{5.32}{B^2}+\frac{18.59}{B^3}+\cdots\right). \tag{C5b}$$

The equations for the diffracted beam (C5a) is accurate to better than 1% for $B\geq 3$. Equation (C5b) for the transmitted beam is in error about 3% at $B=6$ and is progressively better, the higher the B value. For large values of B, Kato's equations reduce to Eq. (101). A tabulation of the integrals in (C4a) and (C4b), evaluated with a computer is given in Ref. 20 for values of B from 0 to 30. The table can be interpolated to give accurate results in the low range of B where the asymptotic formulas break down.

Note that Eqs. (C4a) and (C4b) are for a given state of polarization so that the integrated intensity depends upon the degree of polarization of the primary beam. If $I_0{}^\sigma$ and $I_0{}^\pi$ are the intensities of each polarization in the primary beam, then the integrated intensity is

$$\rho_{\sigma+\pi}{}^\theta=(I_0{}^\sigma\rho_\sigma+I_0{}^\pi\rho_\pi)/(I_0{}^\sigma+I_0{}^\pi). \tag{C6}$$

The important parameter ϵ needed to calculate the intensity is discussed in Sec. 3 of Appendix C.

[50] N. Kato, J. Phys. Soc. Japan **10**, 46 (1955).

2. The Bragg Case

The calculation of integrated intensity for the Bragg case is more involved than in the Laue case. In principle, the intensity can be calculated directly from the complex form given in Eq. (104), choosing the sign in such a way as to keep the reflectivity less than unity. Another form of this expression has been given by Miller,[51] which eliminates complex variables and the sign ambiguity. Although Miller's expression is more complicated, it provides an easier form to carry out the integration. For a centrosymmetric structure and reflection condition $b=-1$ (surface parallel to diffracting planes) we have

$$(\mathbf{E}_H^e/\mathbf{E}_0^e)^2=G(\eta)-[G^2(\eta)-1]^{\frac{1}{2}}, \qquad \text{(C7)}$$

where

$$G(\eta)=\frac{\eta^2+X^2+\{[\eta^2-(1+Y^2-Z^2]^2+[2X(\eta+Z)]^2\}^{\frac{1}{2}}}{1+B^2} \qquad \text{(C8)}$$

and

$$X=F_0''/|P|F_H', \quad Y=F_H''/F_H', \quad Z=|P|F_H''/F_0''. \qquad \text{(C9)}$$

The integrated intensity ρ_H^θ, for polarization P is

$$\rho_H^\theta=\frac{\lambda^2(e^2/mc^2)N|F_H'||P|}{\pi\sin 2\theta}\int\left(\frac{E_H^e}{E_0^e}\right)^2 d\eta. \qquad \text{(C10)}$$

The integral in (C10) reduces to $\frac{8}{3}$ when absorption is zero ($F_0''=F_H''=0$) giving Darwin's result.

The parameters X, Y, and Z can be obtained as follows: F_H' is derived from the structure and the calculated free-atom form factors. For greater accuracy, one would include the Hönl correction to the real part of the scattering factor. Thermal motion is included through a Debye–Waller factor on the scattering amplitudes

$$f'(2\theta)=f_0'(2\theta)\exp[-M(2\theta)],$$

where $f_0'(2\theta)$ is the free-atom form factor and $M(2\theta)$ that portion of the Debye–Waller[52] factor depending on the mean square vibrational amplitude. F_0'' is obtained from the linear absorption coefficient according to Eq. (11). The only subtlety is the quantity F_H'' which involves the angular dependence of the imaginary part of the scattering factor with its temperature dependence. This is discussed in more detail in Sec. 3 in terms of $\epsilon=F_H''/F_0''$. For the reflection case we are considering here, a simplifying assumption holds quite accurately; namely, that there is no angular dependence to the imaginary part of the atomic scattering factor $f_0''(2\theta)$. In the particular case of germanium reflections, Batterman[53] has shown by direct evaluation of (C10) the accuracy of this assumption. The thermal factor is accounted for as before so that $f_H''=f_0''\exp(-M)$ and f_0'' is obtained from Eq. (11) through the tabulated atomic absorption factors.

The reason the integrated intensity is not sensitive to ϵ can be readily seen physically. In the Bragg case, there exists a region of nearly total reflection. This means that because of extinction there is very little penetration into the crystal, and that true photoelectric absorption is a relatively small perturbation on the diffracted intensity (see Sec. 3.1).

Hirsch and Ramachandran[6] have developed an empirical formula for $\rho_H^{\eta'}$

$$\rho_H^{\eta'}=\frac{\pi[1+(F_H''/F_H')^2]}{4\{\exp[-(1+(F_H''/F_H')^2)(|g|+C)]+|g|\}}, \qquad \text{(C11)}$$

where

$$g=\frac{1-b}{2k|(|b|)^{\frac{1}{2}}|}\frac{F_0''}{|F_H|}[1+(F_H''/F_H')^2]^{\frac{1}{2}},$$

$$C=\log_e(32/3\pi).$$

Expression (C11) is accurate to 2% and allows calculation for the nonsymmetric case where $b\neq-1$.

Detailed consideration of integrated intensities in the Bragg case, for noncentrosymmetric crystals near an absorption edge has been given by Cole and Stemple.[54] They have used the change of integrated intensity as one crosses an absorption edge to determine the polarity of a gallium-arsenide crystal.

3. Evaluation of ϵ

Recent experimental work by Okkerse,[21] Hildebrandt and Wagenfeld,[55] and quantum mechanical calculations of Wagenfeld[23] have shed considerable light on the significance of ϵ. From the treatment in Sec. 2.10B3, we see that ϵ is related to the distribution of absorbing power in the atom and the vibrational amplitude in the lattice. Okkerse's and Hildebrandt's experimental results for germanium indicate that the correct temperature dependence is the same as for the Bragg case, namely, $\exp(-M)$; i.e.,

$$\epsilon=\epsilon_0\exp(-M).$$

The intrinsic value of ϵ_0, like the form factor, must be evaluated for each element. The added complication is that since absorption is involved, ϵ_0 for a given element is wavelength dependent. A truly accurate value for ϵ_0 can only be obtained from a quantum mechanical calculation such as Wagenfeld's[23] for germanium.

There are however, reasonably good approximations that can be made which would be sufficiently accurate for the Bragg case since the intensity is quite insensi-

[51] F. Miller, Phys. Rev. **47**, 209 (1935).
[52] B. W. Batterman, Phys. Rev. **127**, 686 (1962).
[53] B. W. Batterman, J. Appl. Phys. **30**, 509 (1959).
[54] H. Cole and N. R. Stemple, J. Appl. Phys. **33**, 2227 (1962).
[55] G. Hildebrandt and H. Wagenfeld. Paper presented at Sixth International Congress of the International Union of Crystallography, Rome, Italy (September 1963).

TABLE I. Wagenfeld's[a] calculated value of ϵ_0 and ϵ ($\theta=291°K$) for germanium with Cu K_α and Mo K_α radiations.

	Cu K_α		Mo K_α	
hkl	ϵ_0	ϵ	ϵ_0	ϵ
220	0.989	0.959	0.998	0.964
400	0.978	0.913	0.997	0.931
422	0.968	0.872	0.995	0.896
440	0.957	0.834	0.994	0.867
444	0.936	0.762	0.990	0.806

[a] See Ref. 23.

tive to ϵ. For the thick crystal Laue case where the anomalous transmission effect predominates, ($\mu_0 t>2$) the approximation to be described below can produce sufficient uncertainty in ϵ_0 to cause errors in the calculated intensity greater than that of the experiment and serves only as a first approximation.

ϵ_0, in general, departs very slightly from unity—much less than one would expect from the form factor of those electrons involved in the absorption. For low-order reflections from germanium, for example, most of the deviation of ϵ from unity is due to the Debye–Waller factor. Table I gives Wagenfeld's results for ϵ_0 and the total ϵ, using a Debye temperature of 291°K. For germanium a fairly reasonable approximation would be to let $\epsilon_0=1.0$ so that $\epsilon=\exp(-M)$. Okkerse pointed out an empirical relationship between the values of ϵ_0 as a function of order of reflection. He found that the deviation of ϵ_0 from unity follows closely a linear dependence with $1/d^2$ [or $(\sin\theta/\lambda)^2$]. Thus,

$$\frac{1-\epsilon_0(hkl)}{1-\epsilon_0(h'k'l')}=\frac{d^2(h'k'l')}{d^2(hkl)}.$$

The calculated values of ϵ_0 in Table I closely follow this dependence. If one has an experimental value for ϵ_0 for a low-order reflection, the value for a higher order can be obtained using this relationship.

NOMENCLATURE

λ	x-ray wavelength
d	interplanar crystal spacing
θ_B, θ	exact Bragg angle, general glancing angle to planes
I_0, I_D, I_T	x-ray intensity in primary, diffracted and transmitted directions
$\mathbf{k}_0{}^i, \mathbf{K}$	wave vector of vacuum-incident wave, and wave in crystal
μ_0	linear photoelectric-absorption coefficient
t_0, t	crystal thickness of parallel plate, thickness in incident direction
$\rho(\mathbf{r})$	electron density in lattice at position vector $\mathbf{r}$
$\mathbf{H}$	reciprocal lattice vector of Miller indices h, k, l; $\mid H \mid = 1/d$
$F_H=F_H'+iF_H''$	structure factor for the *hkl* reflection (generally complex)
f_n	atomic scattering factor for nth atom in unit cell
$r_e=(e^2/4\pi\epsilon_0 mc^2)$	classical electron radius
κ	dielectric constant
$\Gamma=r_e\lambda^2/\pi V$	proportionality constant between Fourier coefficients of charge density and dielectric constant.
V	unit cell volume
$\mathbf{E}_H$	$\mathbf{H}$th component of electric-field amplitude in crystal
$P(=1 \text{ or } \cos 2\theta)$	polarization factor
ξ_0, ξ_H	parameters of the dispersion surface. Difference in magnitudes of wave vector permitted in the crystal and that corrected for the average index of refraction
$\mathbf{n}$	unit inward surface normal
qk	magnitude of vector along $\mathbf{n}$ connecting $k_0{}^i$ and $\mathbf{K}_0$
γ_0, γ_H	direction cosines of incident and diffracted beams with respect $\mathbf{n}$
$b=\gamma_0/\gamma_H$	ratio of direction cosines, $=-1$ for symmetric Bragg case and $=+1$ for symmetric Laue case.
$\eta=\eta'+i\eta''$	A generalized coordinate related to glancing angle. η' is proportional to $\Delta\theta$
$\mathbf{S}_i$	Poynting's vector for field i
Δ	angle between $\mathbf{S}_i$ and atomic planes
$P=\tan\Delta/\tan\theta$	
$\mathcal{R}_H, \mathcal{I}_H$	real and imaginary part of $F_H F_{\bar{H}}$
ϵ	generally the ratio of the imaginary part F_H'' to the imaginary part, F_0''
α	polarizability of medium

Equation List (Numbers refer to equations in text)

Charge density

$$\rho(r)=V^{-1}\sum_H F_H \exp(-2\pi i\mathbf{H}\cdot\mathbf{r}) \quad (1)$$

Structure factor

$$F_H=\sum_n f_n \exp(2\pi i\mathbf{H}\cdot\mathbf{r}_n) \quad (2)$$

Dielectric constant

$$\kappa(r)=1-\Gamma\sum_H F_H \exp(-2\pi i\mathbf{H}\cdot\mathbf{r}) \quad (7)$$

Absorption coefficient

$$\mu_0=(2\pi/\lambda)\Gamma F_0'' \quad (11)$$

Dispersion surface

$$\xi_0\xi_H=\tfrac{1}{4}k^2P^2\Gamma^2F_HF_{\bar{H}} \quad (21)$$

Dispersion surface parameter

$$\xi_0' = K_0' - k(1 - \tfrac{1}{2}\Gamma F_0') \tag{23}$$
$$\xi_0'' = -K_0''\gamma_0 + \tfrac{1}{2}k\Gamma F_0''$$

Field-amplitude ratios for tie point of coordinate ξ_0 on dispersion surface

$$\frac{E_H}{E_0} = -\frac{2\xi_0}{kP\Gamma F_{\bar{H}}} \tag{24}$$

Dispersion-surface parameters in terms of incident conditions

$$\xi_0 = \tfrac{1}{2}k \mid P \mid\mid b \mid^{\frac{1}{2}} \Gamma[F_H F_{\bar{H}}]^{\frac{1}{2}}[\eta \pm (\eta^2 + b/\mid b \mid)^{\frac{1}{2}}],$$
$$\xi_H = \tfrac{1}{2}k \mid P \mid (\Gamma/\mid b \mid^{\frac{1}{2}})[F_H F_{\bar{H}}]^{\frac{1}{2}}[\eta \pm (\eta^2 + b/\mid b \mid)^{\frac{1}{2}}]^{-1} \tag{31}$$

$$\eta \equiv \frac{b\Delta\theta \sin 2\theta + \tfrac{1}{2}\Gamma F_0(1-b)}{\Gamma \mid P \mid\mid b \mid^{\frac{1}{2}}[F_H F_{\bar{H}}]^{\frac{1}{2}}} \tag{32}$$

Massive Condensations in Interstellar Matter and Stellar Associations

JOSEPH F. BIRD

Applied Physics Laboratory, The Johns Hopkins University, Silver Spring, Maryland

CONTENTS

SUMMARY

The very massive, expanding H I clouds and high-velocity "runaway" stars that accompany expanding associations of young stars have led to the suggestion that stellar associations originate in the nuclear explosion of massive condensations. To assess this idea, we develop a theory of the evolution of massive gravitational condensations (without the usual fragmentation assumption). Since the work is exploratory, some crudity in the calculations is tolerated for the sake of including the many forces (gravity, rotation, gas and radiation pressures, magnetism, turbulence) and processes (rotation braking, radiation, ionization, dissociation, transmutation, etc.) encountered on the long path from cold, dilute interstellar matter to hot, dense stellar material. The theory is couched mainly in terms of two parameters, the condensation mass M and a coefficient of angular momentum loss κ_J. Generous ranges of the parameters are considered, and for representative values the evolutionary history is calculated.

It is seen that the condensation probably forms in the cool interior of a very massive H I cloud. After an early era of free fall, secular contraction at a rate fixed by κ_J ensues. Ultimately, thermonuclear energy release halts the contraction and forces a secular reexpansion, during which the condensation suffers an unfamiliar form of instability and explodes. In many cases the nature of the explosion is such as to explain the most spectacular of stellar association phenomena. Thus, the concept of explosive birth of stellar associations is lent theoretical support and some interesting aspects of star formation are revealed. Possible implications for other stellar or galactic catastrophes are indicated.

The first part of this paper surveys other works and draws heavily on them, particularly to estimate M and κ_J. This review material should also serve as a brief introduction to the problems of star formation.

I. INTRODUCTION

Blue giant stars have main-sequence lives as short as 10^6 yr, and are ordinarily found in spiral arms amid clouds of dust and gas (see, e.g., Spitzer 1963, in press;